Erasmus MC
Universitair Medisch Centrum Rotterdam

ICIN

Thoraxcentre

The Ninth European Symposium on Ultrasound Contrast Imaging

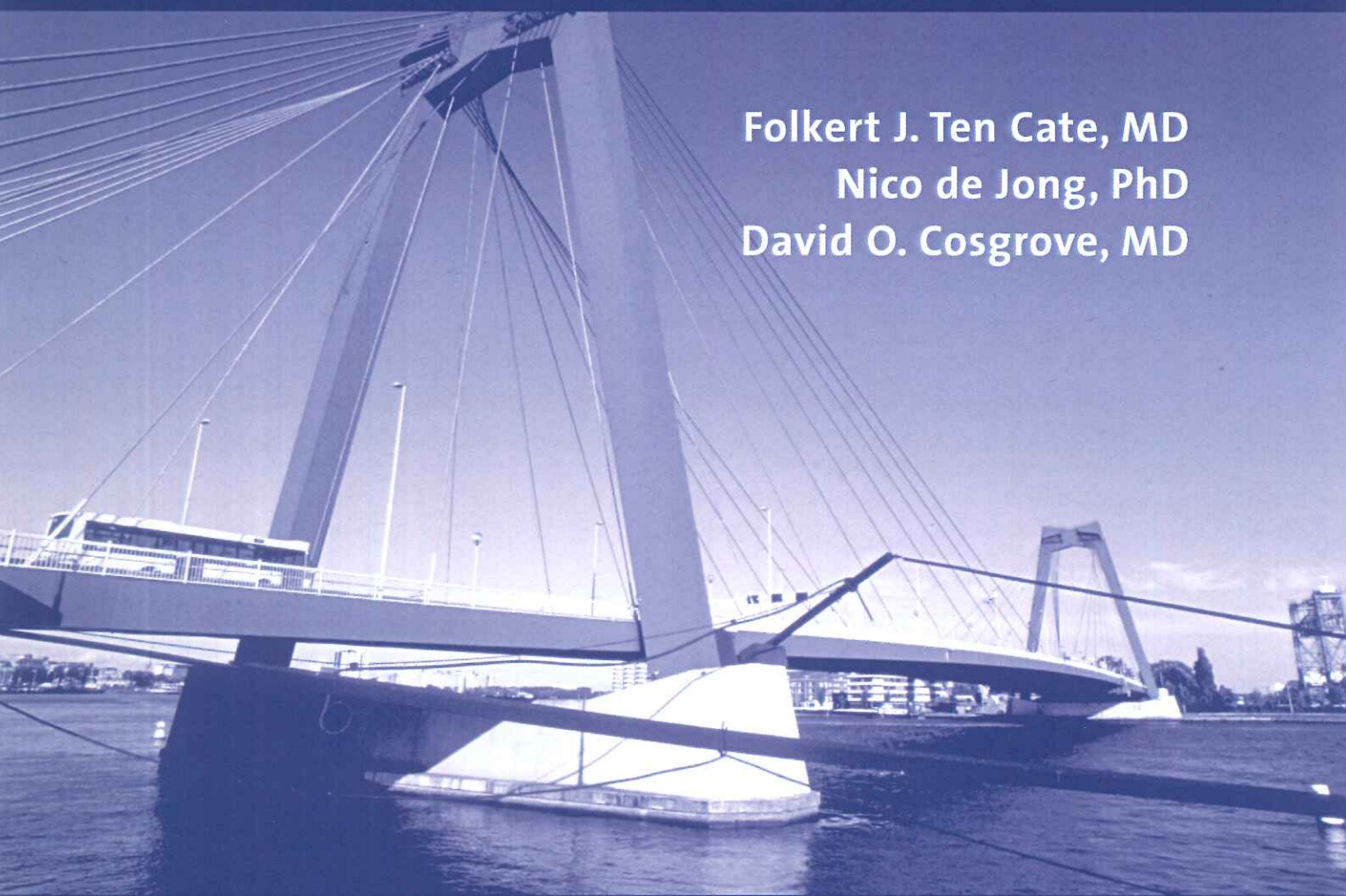

Folkert J. Ten Cate, MD
Nico de Jong, PhD
David O. Cosgrove, MD

Abstract book

January 22-23, 2004, Rotterdam, The Netherlands

9th EUROPEAN SYMPOSIUM ON ULTRASOUND CONTRAST IMAGING
22 -23 JANUARY 2004, Rotterdam, The Netherlands

WEDNESDAY, 21 January 2004

10.00 – 16.00	**Practical Contrast Imaging Course**	**Erasmus MC**
18.00 - 20.00	**Registration - Welcome Drinks - Posters**	**Hilton Hotel**

THURSDAY, 22 January 2004

08.00 - 09.00	**Registration**	
09:00 - 09:05	**Opening address by Professor Wiek van Gilst, director ICIN**	
09.05 - 10.35	**CLINICAL APPLICATIONS**	*Chairpersons: Folkert ten Cate and Peter Burns*
Mark Monaghan	New technologies for contrast echo real time 3D echocardiography	1
K. Schlottmann	Characterisation of tumors of the eye by high frequency contrast harmonic imaging with BR1	3
Grigorios Korosoglou	Real-time Myocardial Perfusion Imaging in the Evaluation of Patients with Chest Pain. Added value to clinical and biochemical markers	4
E.Korsten/M.Mischi	Contrast Ultrasound Quantification of Ejection Fraction &Pulmonary Blood Volume	6
Jean-Michel Correas	Clinical application : Ultrasound contrast imaging in radiology	9
Discussion		
10.35 - 11.00	**Intermission**	
11.00 - 12.30	**TECHNOLOGY I**	*Chairpersons: Michel Versluis and James Macioch*
Peter Burns	Listening	11
Nico de Jong	and looking to breaking bubbles	
Mike Averkiou	Pulsing schemes for the detection of nonlinear echoes from contrast microbubbles	17
Charlie Church	Current models; Are they useful?	25
Larry Crum	Recent Studies of the Physics of Ultrasound Contrast Agents and their Therapeutic Biological Applications	26
Discussion		
12.30 – 14.00	**Lunch**	
14.00 - 15.30	**RADIOLOGY**	*Chairpersons: David Cosgrove and Mike Averkiou*
Martin Blomley	Functional imaging in Radiology	27
Thomas Albrecht	Focal liver lesions:what we know, what we don't know, what we want for the future.	29
Thomas Porter	Non-Invasive Detection of CarotidArtery Endothelial Dysfunction Due to Hyper-triglyceridemia With High Frequency Real Time Low Mechanical Index Imaging of Retained Microbubbles	31
Wilko Wilkening	Ultrasound contrast perfusion imaging in acute stroke patients	32
Naohisa Kamiyama	Micro Flow Imaging and Arrival Time Parametric Imaging of the liver	34
Discussion		
15.30 – 16.00	**Intermission**	
16.00 – 17.30	**DRUG DELIVERY**	*Chairpersons: Steven Feinstein and Thomas Porter*
Jonathan Lindner	Gene and drug delivery with ultrasound contrast agent	36
Carmel Moran	Targetted microbubbles for atherosclerotic plaque	38
Sophie Mehier	Sonoporation: A first approach of cellular mechanisms	39
Alexander Klibanov	Targeting of microbubbles: *in vitro* flow chamber studies	41
Rene Musters:	3D Live-cell imaging of molecular and cellular aspects of local drug and gene delivery through ultrasound microbubbles	43
Discussion		
18.30 - 22.30	**SOCIAL EVENT "Launching Solid Spheres" (incl. Dinner buffet)**	94

FRIDAY, 23 January 2004

07.30 - 08.00 **Registration**

07.30 - 09.00 **POSTER DISCUSSION**.....*Moderators: Folkert. ten Cate and Nico de Jong*

09.00 - 10.30 **TECHNOLOGY II**.....*Chairpersons:Nico de Jong and Thomas Albrecht*

Discussion

10.30 - 11.00 **Intermission**

Announcement of the winner of the poster-price sponsored by the Dutch Foundation for Ultrasound Society in Medicine & Biology (SUGB)

NEW TECHNOLOGIES for CONTRAST ECHO: REAL-TIME 3D ECHOCARDIOGRAPHY

Dr Mark J Monaghan, Dr Stam Kapetenakis

King's College Hospital, London, UK

Background: Real-time three-dimensional echocardiography (RT3DE) is a new modality. As with 2D echo, endocardial delineation is limited in a substantial proportion of patients. The use of echo contrast has not been previously evaluated in RT3DE and may enhance endocardial border detection.
Methods: 50 patients (60% male, 62.5 ± 11 years). RT3DE was performed with the Sonos 7500 and the X4 transducer. Contrast images were acquired with continuous infusion of Sonovue®. Average acquisition time was 6 sec. 3D datasets were cropped to produce 4, 2 and 3 chamber views and a short axis view of the LV. Two cropping methods – thin and thick - produced 800 digital loops. 3 observers reviewed these for image quality and endocardial delineation. The Endocardial Border Definition Index (EBDI) was defined as total score for all segments reviewed divided by that number of segments.
Results: With contrast, there was significant improvement in image quality. More loops had adequate (59% of contrast images vs. 36.25%) or excellent (28.2% of contrast images vs. 8.5%) quality. Significantly fewer loops were uninterpretable when enhanced with contrast (0.75% of contrast images vs. 18.3%). There was a significant improvement in EBDI when images were enhanced with contrast (1.87±0.288 for contrast images vs. 1.09±0.55 – $p < 0.001$) regardless of cropping.
Conclusion: Contrast enhanced RT3DE is feasible and provides rapid, high quality acquisition of 3D images. This technology will be especially valuable during Stress Echo.

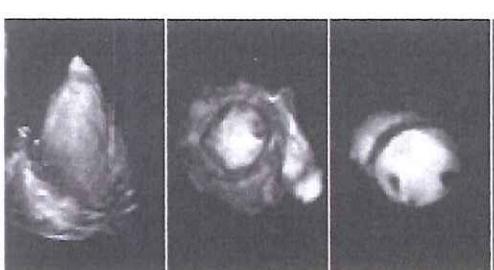

3D Contrast Echo. Left: LV opacification. Middle: Thick SAX. Right: Thin SAX

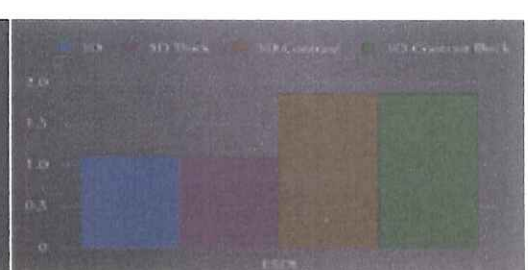

EBDI for both cropping methods shows significant improvement with contrast ($p < 0.001$)

3D Contrast
(FVA, Thick and Thin Slices)

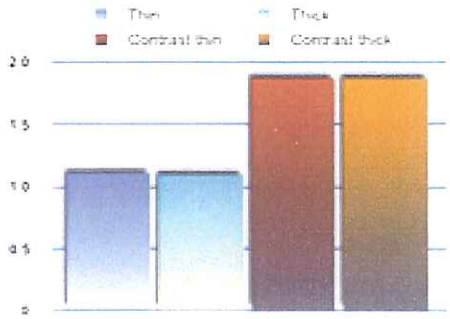

EBDI

CHARACTERISATION OF TUMORS OF THE EYE BY HIGH FREQUENCY CONTRAST HARMONIC IMAGING WITH BR1

K. Schlottmann[1], B. Fuchs[2], M. Demmler[2], V.-P. Gabel[2], J. Schölmerich[1]

[1]Department of Internal Medicine 1, Interdisciplinary Dept. of Ultrasound,
[2]Department of Ophthalmology
University Hospital Regensburg, Germany

Background: Determination of the vascularization and perfusion of choroid tumors has important diagnostic and therapeutic implications, especially after focal irradiation of choroid melanomas. In daily routine the vascularization and blood supply of choroid tumors is determined qualitatively by A-mode or by color-Doppler ultrasound (US). However, small vessels and capillaries cannot be visualized due to physical restrictions such as low perfusion velocity and low vessel diameters. We investigated whether small vessels and perfusion can be detected by contrast harmonic imaging (CHI) after i.v.-application of the ultrasound contrast agent BR1 (Sonovue, Bracco) and how perfusion is changed by focal irradiation of choroid melanomas.

Patients and Methods: 13 Patients with solid choroid tumors (9 melanomas and 4 metastases) underwent standard A-, B-mode and Doppler US of the eye, followed by i.v. injection of 4.8 ml BR1 (Sonovue, Bracco) and a high frequency US with a 7.5 MHz wide band linear transducer (Siemens, Sonoline Elegra) with CHI at low mechanical index (low-MI).

Results: On A-mode US signs indicative of blood vessels were detected in 12 solid tumors while color Doppler revealed only 6 tumors with signs of perfusion. CHI with BR1 resulted in more precise information about contrast enhancement and blood supply. While unirradiated choroid melanomas showed strong arterial inflow of the contrast agent, most irradiated melanomas were perfused less pronounced with one exception which was also heavily hyperperfused. However, there was still detectable blood supply in almost all irradiated melanomas. The metasases were clearly less perfused than melanomas. Fluid or non-solid lesions did not show any microbubbles traversing.

Conclusion: This is the first report about the use of low-MI CHI in the eye. CHI with BR1 can clearly discriminate vascularized from non-vascularized tumors. The irradiation efficiency, which, until now could only be evaluated by regular measurement of the size of the irradiated choroid tumors, seems to be much better evaluable by contrast ultrasound. Furthermore, in contrast to metastases, melanomas are heavily perfused. These tumors can be evaluated by CHI, even when the choroid cannot be seen on fundoscopy.CHI offers an opportunity for improved management of untreated and irradiated choroid tumors.

REAL TIME MYOCARDIAL PERFUSION IMAGING IN THE EVALUATION OF PATIENTS WITH CHEST PAIN. ADDED VALUE TO CLINICAL AND BIOCHEMICAL MARKERS

Grigorios Korosoglou, Nina Labadze, Alexander Hansen, Christiane Selter, Evangelos Giannitsis, Helmut Kuecherer

University of Heidelberg, Heidelberg, Germany

Background: In patients with acute coronary syndrome (ACS) rapid risk stratification is crucial. Real-time myocardial contrast echocardiography (MCE) provides information on myocardial perfusion and contractile function. We investigated whether MCE can accurately identify patients with ACS presenting to the emergency department.

Methods: Consecutive patients (n = 100) presenting with first occurrence of chest pain were included in our study. Exclusion criteria were ST-elevation on ECG, history of CAD and previous myocardial infarction. MCE images were analyzed visually and quantitatively, measuring peak signal intensity (A) and slope of signal intensity rise (β) in 16 myocardial segments. Perfusion defect size was measured by planimetry.

Results: Thirty-seven of 100 patients had final diagnosis of ACS. Of these 37 patients, 23 had abnormal ECG, 19 had elevated Troponin T (>0.03 μg/l) on admission, 25 had elevated TnT at 4 h follow-up and 33 had abnormal MCE. MCE was significantly more sensitive (89%) than ECG (62%), initial (51%) and follow-up TnT (68%). Multivariate logistic regression analysis showed that MCE was the strongest predictor of ACS adding value to conventional diagnostic tests. The perfusion defect size in patients with ACS correlated with TnT levels at 96 h follow-up ($r = 0.73$, $p < 0.001$, Figure).

Conclusions: Our data suggest that MCE can accurately identify patients with ACS. This information may support immediate risk stratification of patients with chest pain in the emergency department.

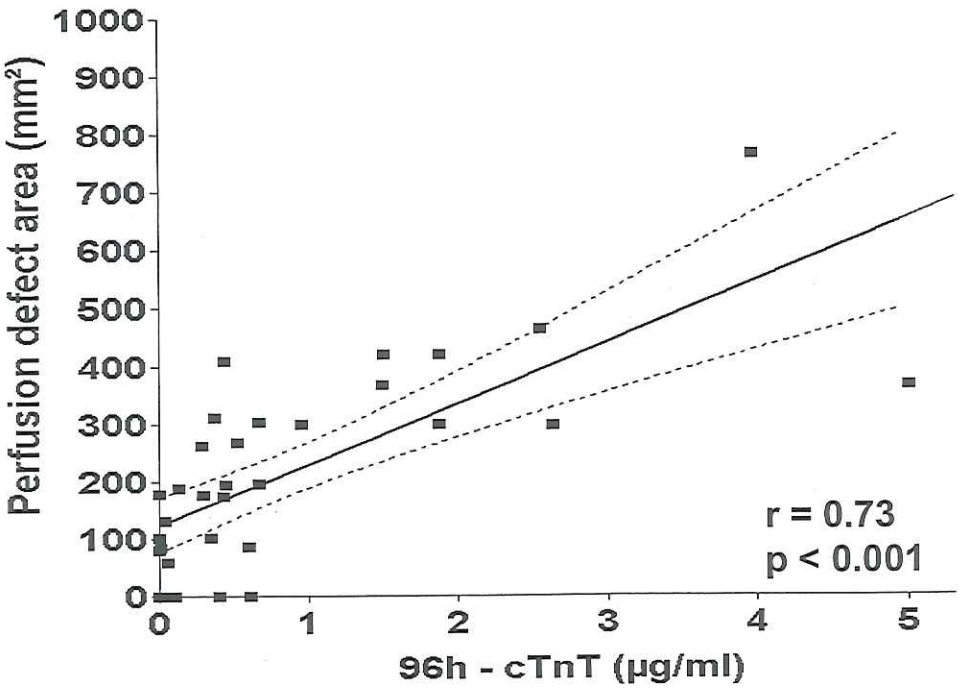

Figure: The initial perfusion defect size correlated with myocardial damage at 96 h follow-up

Contrast Ultrasound Quantification of Ejection Fraction and Pulmonary Blood Volume

M. Mischi[1], A.H.M. Jansen[2], A.A.C.M. Kalker[1], H.H.M. Korsten[1;3]

1- Technical University Eindhoven (The Netherlands) 2- Dept. of Cardiology and
3- Dept. of Anestesiology and Intesive-Care of the Chatharina Hospital Eindhoven (The Netherlands)

Despite the technological development, the assessment of diagnostic clinical parameters such as Ejection Fraction (EF) and Pulmonary Blood Volume (PBV) remains a difficult challenge. An accurate measurement of PBV requires the employment of very invasive indicator dilution techniques (dye- or thermo-dilution), which require catheterization. The Left Ventricle (LV) EF can be approximately estimated by use of 2-D or 3-D image segmentation algorithms combined with Simpson integration, however, there is no method for the assessment of the Right Ventricle (RV) EF.

In this study we show that the combined use of Ultrasound Contrast Agents (UCA) [1] and indicator dilution principles can result in a method that permits the simultaneous measurement of RVEF, LVEF, and PBV. 0.25mg of SonoVue® [3] diluted in 5ml of saline are injected in a peripheral vein and detected by an ultrasound transducer.

The analysis of the video or acoustic intensity of the B-mode output of ultrasound scanners allows the measurement of UCA Indicator Dilution Curves (IDCs) [4][5][6]. Several cardiac views permit the measurement of different IDCs from different sites. The Cardiac Output (CO) is multiplied times the contrast Mean Transit Time (MTT) to estimate the blood volume between two detection sites [5][6].
CO can be assessed non-invasively either by the RV IDC analysis (before the bubble loss in the lungs) [4], or by Aortic time-integration echo-Doppler, or by lithium dilution.
For the PBV assessment, two IDCs can be measured in the RV and the Left Atrium (LA) as shown in Fig. (1). The resulting IDCs are shown in Fig. (2).

If an IDC is also measured in the LV, than the LV IDC can be used together with the RV IDC for the measurement of LV and RV EF respectively.

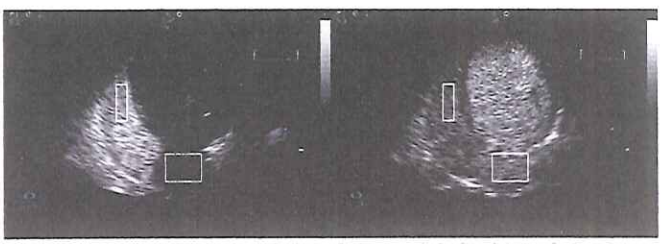

Fig. 1 – Opacification of the right and left side of the heart after a SonoVue® 0.25mg bolus injection. Two regions of interest are placed on the RV and the LA for the PBV assessment.

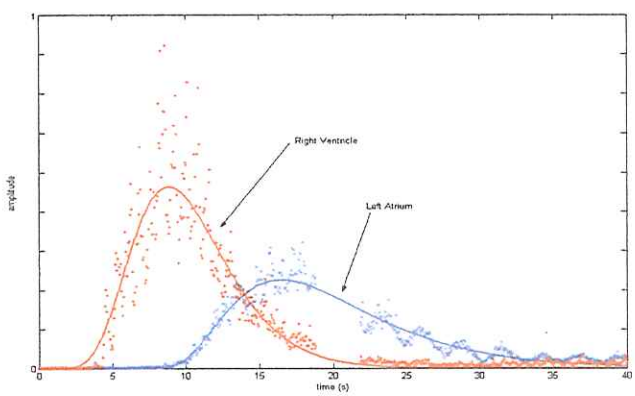

Fig. 2 – IDC derived from two regions of interest in the RV and the LA.

Due to the small contrast dose and the low Mechanical Index (MI=0.1), the relation between acoustic backscatter and contrast concentration is linear [4][9].

The measured IDCs are fitted and interpreted by the Local Density Random Walk (LDRW) model as given in Eq. (1), since it is a statistical description of diffusion with drift and gives the best IDC fit in terms of mean square error [2][7][8][10][4].

$$C(t)=\left(\frac{M}{Q}\right)\sqrt{\frac{\lambda}{2\pi\mu t}}\,e^{\lambda-\frac{\lambda}{2}\left(\frac{t}{\mu}+\frac{\mu}{t}\right)} \qquad (1)$$

$C(t)$ is the IDC, M is the injected mass of contrast, Q is the volumetric flow of the carrier fluid, μ is the time that elapses at the carrier velocity to cover the distance between injection and detection site, and λ represents the skewness of the curve.

The use of a model is necessary to overcome the low signal-to-noise ratios (SNR) and contrast recirculation issues. A specific fast and accurate least-square fitting algorithm is adopted [4]. MTT, RV EF, and LV EF are derived from the fitted model.

The MTT is equal to the parameter μ of the fitted LDRW model.

The EF assessment can be derived from the fitted model too, resulting in an increase of accuracy with respect to the usual technique, which considers the contrast concentration C at two subsequent systoles as given in Eq. (2).

$$EF = 1 - \frac{C_{n+1}}{C_n} \tag{2}$$

In fact, this approach assumes a sudden injection of the complete contrast bolus in the ventricle, which is washed out by the cardiac action.

If the contrast is peripherally injected, such a hypothesis is true only after infinite time, i.e., when no more contrast enters the ventricle. The IDC fitting for large time values fails due to the extremely low SNR. The problem is overcome if the limit of the LDRW model fit for t going to infinite is considered. The result, which represents the EF when the contrast is injected all at once in the ventricle, is given as in Eq. (3), where Δt is heart beat period.

$$EF = 1 - \frac{C_{n+1}}{C_n} = \lim_{t\to\infty}\left\{1 - \sqrt{\frac{t_n}{t_{n+1}}}e^{\frac{\lambda}{2}\left[\left(\frac{t_n}{\mu}-\frac{\mu}{t_n}\right)-\left(\frac{t_{n+1}}{\mu}-\frac{\mu}{t_{n+1}}\right)\right]}\right\}$$

$$\Rightarrow EF = 1 - e^{-\frac{\lambda\Delta t}{2\mu}} \tag{3}$$

The volume measurement is validated by in-vitro experimentation [5]. A Sonos 5500 ultrasound scanner is used to detect SonoVue® contrast agent IDCs. The scanner is set in power modulation mode at 1.9MHz. The results in Fig. (3) show very accurate volume measurements with a determination coefficient larger than 0.999. The standard deviation is smaller than 1.8% of the volume for a wide range of flows (from 1L/min to 5L/min).

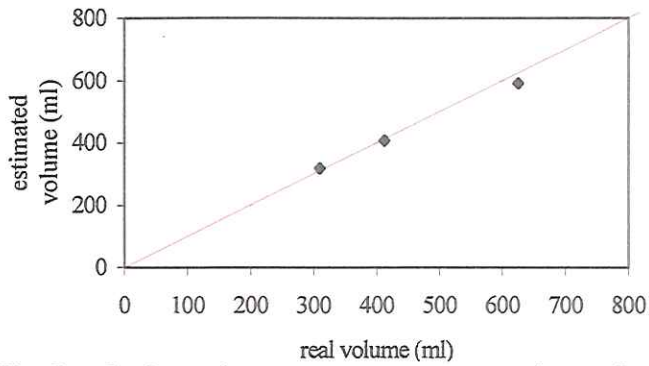

Fig. 3 – In-vitro volume measurements averaged over five flows from 1L/min to 5L/min.

The EF measurement is validated in patients. A small bolus of 0.25mg of SonoVue® is injected in an arm vein and detected in the LV by a trans-thoracic ultrasound transducer. The ultrasound scanner setting is the same as for the in-vitro volume measurements. The results are compared to those obtained by bi-plane Simpson integration. The results show a clear correlation between the two measurements with a correlation coefficient equal to 0.97 (see Fig. (4)).

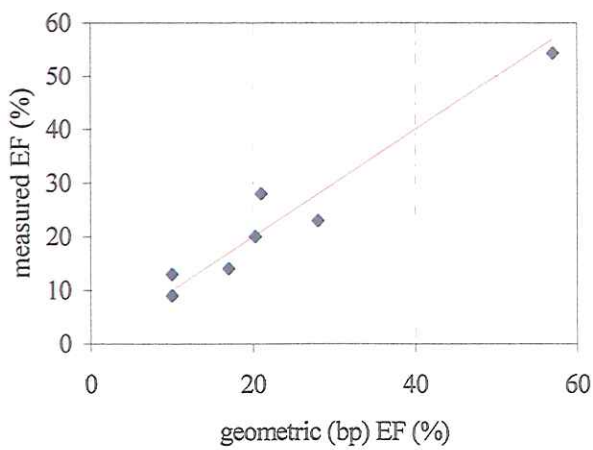

Fig. 4 – In-vivo LV EF measurements compared to bi-plane Simpson integration.

Also the PBV assessment system has been tested in patients with promising results. CO is measured by aortic echo-Doppler.

In conclusion, the simultaneous assessment of PBV, LVEF, and RVEF can be performed with minimal invasiveness by use of UCA.

This approach may be a real asset in cardiology, anesthesiology, and intensive care, since it allows the measurement of important diagnostic parameters that cannot be measured without use of very invasive techniques. It also permits studying the relation between blood volumes and cardiac diseases.

The major focus of this study is on the application of the system for resynchronization therapy. The set of parameters that can be assessed allows a better monitoring of the cardiac functionality before and after bi-ventricular pacing. Moreover, the novel information about pulmonary and intra-thoracic blood volumes could allow distinguishing between responders and non-responders to the resynchronization therapy.

Therefore, further research will focus on patient monitoring before and after bi-ventricular pacing by means of the presented technique. A more extensive in-vivo validation for volume and EF measurements will be object of future research too.

ACKNOWLEDGMENT

The authors like to thank the perfusionists and the operating room staff of the Catharina Hospital Eindhoven, and in particular Monique van den Yssel-Hessels and Susan van den Elzen for their valuable support with the in-vitro experimentation.

REFERENCES

[1] H. Becher, P.N. Burns, "Handbook of contrast Echography," Springer 2000

[2] J.M. Bogaard, S.J. Smith, A. Versprille, M.E. Wise, F. Hagemeijer, "Physiological interpretation of skewness of indicator-dilution curves;theoretical considerations and pratical application," Basic. Res. Cardiol., vol. 79, pp. 479-493, 1984

[3] J.M. Gorce, M. Arditi, M. Schneider, "Influence of bubble size distribution on echogenecity of ultrasound contrast agents: a study of SonoVue," Invest Radiol, vol. 35, no. 11, pp. 661-671, 2000

[4] M. Mischi, A.C.C.M. Kalker, H.H.M. Korsten, "Videodensitometric Methods for Cardiac Output measurements," Eurasip Journal on Applied Signal Processing, vol. 2003, no. 5, April 2003

[5] M. Mischi, A.H.M. Jansen, A.A.C.M. Kalker, H.H.M. Korsten, "Intra-Thoracic Blood Volume Assessment by Dilution of Ultrasound Contrast Agents," IEEE-UFFC Proceedings on the IEEE International Ultrasonics Symposium, Honolulu (Hawaii), 5-8 Oct. 2003

[6] M. Mischi, A.A.C.M. Kalker, H.H.M. Korsten, "Blood Volume Measurements by Videodensitometric Analysis of Ultrasound-Contrast-Agent Dilution Curves," IEEE-EMBS Proceedings on the 25th Annual International Conference of the IEEE Engineering in Medicine and Biology Society, Cancun (Mexico), 17-21 Sept. 2003

[7] K.H. Norwich, "Molecular dynamics in biosystems," Pergamon Press, 1977

[8] C.W. Sheppard "Basic principles of tracer methods: introduction to mathematical tracer kinetics," Wiley, 1962

[9] V. Uhlendorf, "Physics of ultrasound contrast imaging: scattering in the linear range," IEEE Trans. on ultrasonics, ferroelectrics, and frequency control, vol. 41, no. 1, pp. 70-79, Jan. 1994

[10] M.E. Wise, "Tracer dilution curves in cardiology and random walk and lognormal distributions," Acta Phisiol. Pharmacol. Neerl., vol 14, pp. 175-204, 1966

CLINICAL APPLICATION: ULTRASOUND CONTRAST IMAGING IN RADIOLOGY

JM Correas, O Hélénon

Department of Adult Radiology, Necker University Hospital, Paris, France

Despite the introduction of perfluorocarbon gas microbubbles and new imaging techniques, the development of ultrasound contrast agents (USCA) in the routine ultrasound (US) clinical practice is still restrained. One question remains: can USCAs be used as iodinated contrast agents for CT or Gadolinium chelates for MR applications in the near future? On the other hand, a significant increase in the USCA market is needed to justify further investment from companies. It is time for this new imaging technique to reach a large number of non expert ultrasound practitioners. The limiting factors have been underestimated by the overall community involved in USCA development and use.

The clinical role of contrast-enhanced sonography (CE-US) must be clearly identified. The first major limitation results from the role devoted to US, mostly recognized as a first step imaging modality in the assessment of many diseases. Thus, US should be widely available to offer a reasonable compromise between clinical ef

ficacy, inter-operator variability, invasiveness and cost. The concept of technically limited examinations is accepted and the referring to a more expensive or invasive imaging modality (such as CT and MRI) is generally accepted, even when no significant abnormal findings are found. CE-US introduces a completely different approach. CE-US becomes a more specialized modality that can compete with CT or MRI, and be used in some difficult cases that remain unclear at CT or MRI. Such a change in the role of CE-US should be validated by multicenter studies, and must become accepted not only by the community of radiologists and sonographers, but also by referring physicians and patients. The acceptance of this new imaging practice also requires a new and appropriate reimbursement fee, above the one of a Doppler US examination. To date, this specific fee still does not exist in most European countries and represents another strong limitation, as specific contrast software represents an additional cost for the acquisition of an ultrasound system. The clinical indications should be extended and validated using up-to-date imaging techniques. The complex protocols required by most agencies for drug approval are slowing down the development of new compounds. As technology evolves more rapidly, a clear inadequacy appears when a new drug is launched to the market with validated clinical indications performed using obsolete US imaging modality. The contrast semeiology does not differ too much from that of CT or MRI and is not a clear limitation. It has become widely accepted, at least for focal liver lesions.

Another limitation level results from technological issues. CE-US imaging modalities continuously evolve, and technology varies from system to system. The detection of the microbubbles remains difficult in deep attenuating conditions. Sometimes, the same technological approach leads to different trademark names depending on different manufacturers. Non expert US radiologists or sonographers

might be confused with this complex language. Strong improvements have been made in the past decade to make the use of specific USCA modalities easier. However, some critical features are still missing. CE-US examination should become easier to export to CD, with both dynamic loops and critical frames. The review of side by side pre and post contrast cineloops and the availability of simple quantitative tools can improve the diagnostic capability. Appropriate codec are necessary to compress the video loops, and improve storage. These compressed loops should also be compatible with PACS.

University teaching departments should concentrate on the diffusion of this new modality. However, most of these limitations will remain at least for 2004.

LOOKING AT AND LISTENING TO BREAKING BUBBLES: A CORRELATIVE OPTICAL ACOUSTIC STUDY OF SOME EXPERIMENTAL POLYMER/AIR AGENTS

Peter N. Burns Raffi Karshafian, Peter Bevan
University of Toronto. Toronto, Canada

Nico de Jong, Ayache Bouakaz, Chien Ting Chin, Michel Versluis
Erasmus Medical Centre, Rotterdam and University of Twente, The Netherlands

Glenn Tickner
Point Biomedical, San Carlos, CA

It is well known that Ultrasound contrast agents are destroyed by ultrasound if the MI exceeds a certain threshold. This threshold depends on the agent but lies typically between MI of 0.1 and 0.5. In the early years fragility of the agent to ultrasound was considered as undesirably, but today several researchers have shown that destruction of the agent can be beneficial. Examples are destruction / repurfusion imaging and drug and gene delivery. Roughly, there are currently two types of agents available. The first one is comprised of agents with soft shells, like Sonovue, Optison and Definity. The shell encapsulating the agent influences the acoustic behaviour, but only to a limited extent, e.g., the shell increases the resonance frequency by a factor 1-4 in addition to an increase in the friction. In the second type of agents, the bubbles are encapsulated with hard shells, like Quantison and Polymer agents, and the one used in this study. These agents show hardly any vibrations at low MIs, but for high MIs their behaviour is comparable with a free bubble. The hypothesis is that for high MI the encapsulation of the bubble "breaks" and that the gas escapes in a form of a free gas bubble. This will cause a sudden increase in the acoustic response, which will last until the released bubble has been dissolved into the surrounding medium. Because of that bubble disruption remains the basis of the most sensitive method for detecting perfusion with contrast agents, and is an essential component of hemodynamic quantitation with contrast. Until recently, however, our understanding the behaviour of bubbles under a disrupting pulse of ultrasound was derived entirely from a combination of acoustic studies and single bubble models. Reconciling these sources is fraught with problems: theoretical models offer no analytic view of disruption events and are replete with free variables. The experimental studies, on the other hand, generally expose bubbles of an unknown distribution of sizes in a volume cell to a range of ultrasound pressures determined by their unknown position in an ultrasound field.

High speed optical imaging, with its ability to measure the behaviour of a single bubble during a disruption event, adds a new dimension to the experimental tools available. In this study, we examine the disruption characteristics of a number of experimental air/polymer agents (Point Biomedical Inc, San Carlos CA), using both the response to a rapid sequence of acoustic pulses and high speed optical photography with the Brandaris system immediately following disruption.

1. Contrast Agents

The contrast agents used had the same mean diameter (4 μm) and contained the same gas, but varying shell thickness. All agents were prepared and handled in the same way, following the procedure specified by Point Biomedical. First, the agent was suspended at room temperature with 10ml of de-ionized water and swirled gently by hand until all ingredients were suspended. This suspension was further diluted for the subsequent acoustic experiments by adding 0.2ml to 1000ml de-ionized water. The agent was gently swirled before withdrawing it for each experiment. All acoustic measurements were performed within 8 hours of preparing the agent.

2. Acoustic measurements

Figure 1 shows the experimental setup. A computer controlled 1 Giga sample/sec arbitrary waveform generator produced Gaussian enveloped detection pulses with a centre frequency of 2.0MHz and a pulse length of six wavelengths. It also produced disruption pulses with an eight-cycle tone burst at a centre frequency of 2.0 MHz. These were then amplified by an ENI 240L 50dB power amplifier, calibrated into a 50W load. Separate transmit (MATEC 2.25 MHz) and receive (MATEC 3.5 MHz) transducers were used. Acoustic values were measured directly by a broadband membrane hydrophone and digital oscilloscope with a traceable calibration to the NBS standard. A hydrophone system was also used to determine the focal zone location and geometry of each transducer. These were then placed in a water tank in a custom made jig that maintained the beams of the transmitting and receiving transducers so that they crossed at right angles in their respective focal zones. In this location was placed a small flow cell with mylar windows for acoustic transparency. Contrast agent was then flowed from a reservoir above the flow cell and discharged below it. The acoustically active volume, situated in the approximate centre of the cell, was about $3mm^3$. The distance between the transmitting transducer and the sample volume was about 62mm, and the distance between the receiving transducer and the sample volume was about 42mm. De-ionized water, in gas equilibrium with room air, was used at room temperature. The receive transducer was connected to a programmable digital oscilloscope (leCroy Inc), connected to PC. Exposure and acquisition sequences were controlled centrally by means of Labview modules, which stored the RF data to disk for later analysis.

The time-course of the acoustic response to disruption pulses was assessed by applying a series of very low MI pulses to a diluted suspension of these agents: a low MI pre-disruption detection pulse, a high MI disruption pulse, followed by a series of seven low MI detection pulses at millisecond intervals after disruption. The peak negative pressure of the disruption pulse was 0, -480kPa, -1.13 and 1.95MPa at 2.0MHz. Acoustic values were measured directly by the broadband membrane hydrophone. The detection pulses had a peak negative pressure of -30kPa, which was sufficiently small as not to affect the integrity of any of the agents.

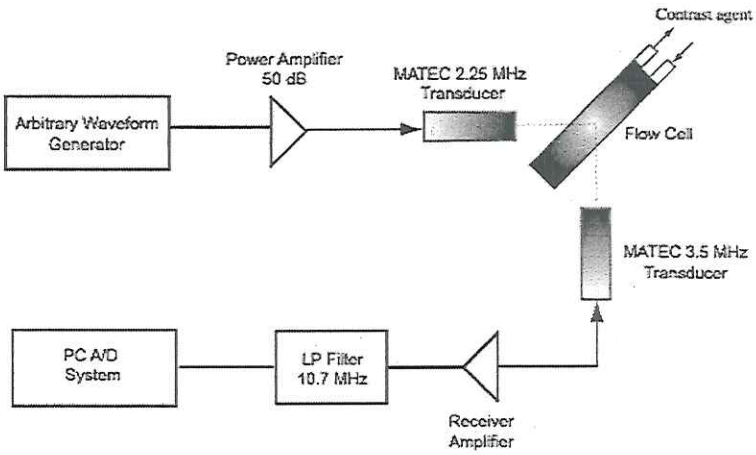

Figure 1: Experimental setup used to measure the time course acoustic response of ultrasound contrast agents.

The diluted suspension of the contrast agent was allowed to flow initially for two minutes to fill the flow cell. Between measurements, the diluted agent was allowed to flow for 30 seconds in order to completely refresh the bubbles with the chamber. Flow was then stopped for 60 seconds. A sequence of 8 detection and 1 disruption pulse was sent, constituting a single measurement. Each measurement was repeated fourteen times. The sequence of pulses transmitted consisted of a pre-disruption detection pulse (at –0.5ms), a disruption pulse (at 0ms), and a series of detection pulses at 1, 10, 20, 30, 50, 100, 200ms (Figure 2).

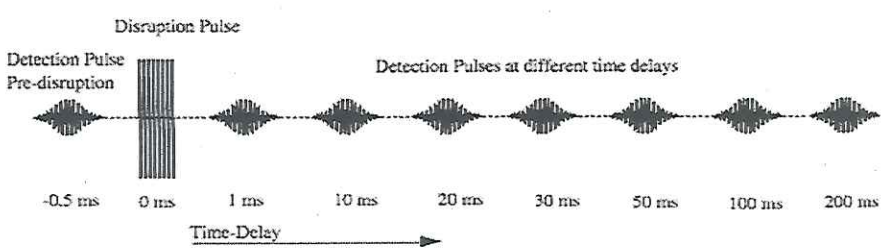

Figure 2: The sequence of pulses (pre-disruption detection pulse, a disruption pulse, and seven detection pulses) used to measure the time course acoustic response of the contrast agents.

3. Optical measurements

The experimental setup is shown in fig. 3. The electrical gated signal (8 cycles, 1.7MHz) was generated by a waveform generator. The signal was amplified by a 60-dB linear power amplifier (A-500, ENI, NY, NY), and the amplitude could be adjusted by an attenuator from 0 to 120 dB in steps of 1 dB. In this way, the required amplitude could be controlled accordingly. The peak negative acoustic pressures were measured separately using a calibrated hydrophone (Precision Acoustics, Dorset, UK). The amplified electrical signal is directed to the transducer (Panametrics, Waltham, MA) focused at

75 mm. The transducer was mounted in a Perspex block, under an angle of 45° relative to the top of the block. A synthetic Cuprophan® capillary fibre with an outer diameter of 200 µm was placed horizontally in the focus of the transducer. The contrast agent could freely flow through the fibre. The flow was turned on to move fresh bubbles into the region of interest and then stopped. The bubble under investigation should remain in view for several hundred milliseconds or longer. A microscope was positioned above the Perspex block, and projected images of the contrast agent bubbles with a magnification of 120 times on the Brandaris 128.

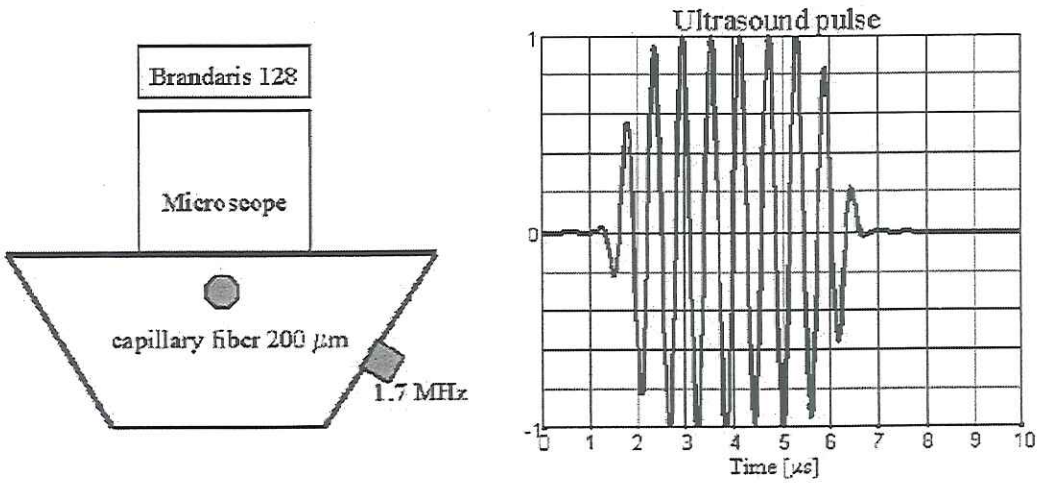

Figure 3. Optical setup.

The frame rate used ranged from 10 to 18 MHz corresponding to an optical scanning duration between 7 and 12.8µs for a total of 128 frames. The transmit frequency was 1.7 MHz with 8 cycles corresponding to 4.7µs of ultrasound scanning. Therefore optical observation was always longer than the ultrasound irradiation. The first optical recording (first few frame) was always positioned before ultrasound insonification starts, so that the initial bubble size could be estimated. Typically 7 to 16 frames were recorded before ultrasound was launched.

Results and conclusions

A typical example of gas escaping from its encapsulation and forming a new free bubble is shown in the figure below. Image on the left shows the optical recording before US insonification and on the right during high MI ultrasound exposure. It is observed that in this image the encapsulation of one sphere is "broken" and the gas is in process of escaping.

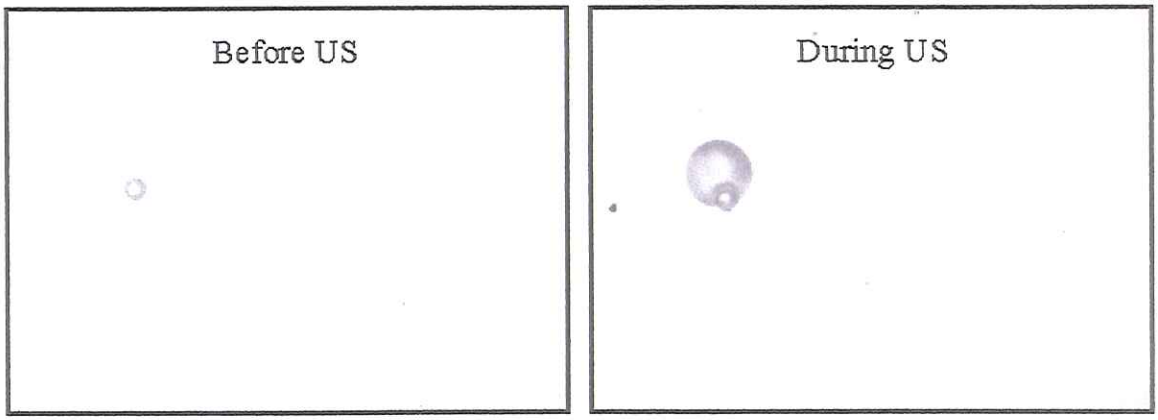

Brandaris observation of a hard-shelled contrast bubble demonstrating the release of gas and formation of a new free bubble upon US exposure.
US: 1.7MHz, 8cycles, MI=1.3, Optic=15.10^6 fps

The following observations were made with the acoustic and optical experiments:

1. Low MI behaviour.

Acoustic: At low MI, these bubbles behave as low elasticity, linear scatterers. The low, non-disruption scattering cross section decreases with increasing shell thickness.

Optical: At low applied acoustic pressure, hardly any oscillations are induced at this mechanical index for all the different agents tested.

2. Disruption threshold behaviour.

Acoustic: At high MI, a disruption threshold is seen with each agent, increasing with shell thickness

Optical: Bubbles "break" immediately upon arrival of the 1st US cycle and their gas is released thereafter.

3. Transient increase following disruption.

Acoustic: A transient increase in integrated scattered power is observed following a disruption pulse at the four peak negative pressures tested

Optical: After disruption the bubble shows gas escaping and forming "new" and probably free bubbles that expand and compress vigorously during subsequent cycles.

4. Post-threshold decay with common time-constant.

Acoustic: When the disruption peak negative pressure is above the threshold level for a particular agent, the subsequent decay of the echo level is very similar for all agents

Optical: After release of the free gas bubbles, their gradual disappearance follows over time.

Final conclusions

These experiments represent preliminary, independent correlation between the acoustic response of a bubble population following a disruption pulse and the physical behaviour of individual bubbles observed optically with a time resolution of less than 1μs. Specific measurements made here are relevant for the optimisation of imaging methods to detect disrupting bubbles.

Pulsing schemes for the detection of nonlinear echoes from contrast microbubbles

Michalakis Averkiou, Matthew Bruce, Seth Jensen, Patrick Rafter,
Tony Brock-Fisher, and Jeffry Powers
Philips Medical Systems, Bothell, Washington, USA

1 Introduction

Ultrasound contrast agents are used in cardiology for the assessment of myocardial perfusion and in radiology for the detection and characterization of tumors. One widely used approach of imaging contrast agents is to use a low Mechanical Index (MI) nonlinear imaging technique to avoid bubble destruction and image both the macro– and micro–circulation in real-time. Various pulsing schemes are employed for the detection of nonlinear echoes from contrast microbubbles. The objective of this paper is to evaluate the various pulsing schemes for low MI imaging of contrast microbubbles and better understand their similarities and differences. The pulsing schemes considered are pulse inversion, power modulation, and their combination. Emphasis is placed on identifying whether nonlinearity due to propagation in tissue may be discriminated from nonlinearity due to scattering from bubbles. Bubble destruction (use of high MI) and tissue motion were not considered in this work. The evaluation of the different pulsing schemes was performed with numerical simulations from well established theoretical models and experimental data from microbubbles in a tissue phantom.

The pulsing schemes used in this work are described first. Then, the theoretical models for the simulations are discussed and the experimental set-up is described. The numerical and experimental results are finally presented and discussed, followed by conclusions.

2 Pulsing schemes

The pulsing schemes investigated are shown here. Only whole and half amplitudes with phases of zero or π were considered. The various transmit amplitude states A_t used are $1, -1, 0.5, -0.5$. The specific sequences considered in terms of A_t and A_r (receive amplitude) are:

1. Pulse Inversion: PI, [A_t(1, -1), A_r(1, 1)]. Since we do not consider tissue motion in this work, this sequence is equivalent to [A_t(1, -1, 1), A_r(0.5, 1, 0.5)], also referred to as PPI. The same observation applies to the rest of the 2–pulse sequences mentioned below.

2. Amplitude (or power) modulation: PM, [A_t(0.5, 1), A_r (2, -1)].

3. 2–state amplitude modulated pulse inversion: PMPI2, [A_t(0.5, -1), A_r(2, 1)].

4. 3–state amplitude modulated pulse inversion: PMPI3, [A_t(0.5, -1, 1, -1, 0.5), A_r(-8, -1, 6, -1, -8)]. Since no motion is considered here, this sequence is equivalent to [A_t: (0.5, -1, 1), A_r(-8, -1, 3)].

5. 4–state amplitude modulated pulse inversion: PMPI4, [A_t(0.5, -1, 1, -0.5), A_r(-2, -1, 1, 2)].

Every pulsing scheme was evaluated for nonlinear propagation in tissue and nonlinear scattering from resonant microbubbles. The receive amplitudes, A_r, were scaled so that the summation of their absolute values equal one: $\sum |A_r| = 1$.

3 Theoretical models and experimental set-up

All simulations considered two specific scenarios: (a) nonlinear propagation in typical tissue parameters for THI images, and (b) nonlinear scattering from typical contrast microbubbles. One of the purposes of the simulations is to compare the nonlinear behavior of wave propagation of diffracting sound beams with that of scattering of ultrasound from microbubbles.

For nonlinear propagation in tissue, a time-domain numerical solution of the KZK equation is used. The source is assumed to be circular as this assumption does not affect the general trends of nonlinear propagation in tissue (Averkiou, IEEE-Ultrasonics 2000). The KZK equation accounts for diffraction (directive beam and focusing gain), absorption (thermoviscous), and medium nonlinearity ($\Gamma = 1 + B/2A$). The KZK equation is used to calculate the pulse shape (distortion) and spectrum after nonlinear propagation to the focus.

For the pulsing schemes considered here, tone bursts are generated with the equation,

$$f(\tau) = exp\left[-(\tau/N_{cyc}\pi)^{2m}\right] sin[\tau + \phi]\,, \tag{1}$$

where m is proportional to the envelope slope and N_{cyc} is proportional to the number of cycles and τ is the retarded time $\tau = \omega_0(t - z/c_0)$. Here we use $N_{cyc} = 3$ (3 cycles between the 1/e points of the envelope) and $m = 2$ (squared Gaussian). The rest of the parameters needed for the KZK model are $A = 0.43$ (dimensionless absorption parameter), $N = 0.24$ (dimensionless nonlinearity parameter), and $G = 3.95$ (linear focusing gain $G = ka^2/2d$). (Averkiou, IEEE-Ultrasonics 2000)

For nonlinear scattering from contrast microbubbles, the Gilmore equation is used. It is solved with a 4-5 Runge–Kutta scheme. The Gilmore equation models a free bubble. It has been shown in literature that at a simple level the shell only affects the overall bubble resonance behavior. For the purposes of this work the assumption of free bubbles is considered to be adequate. The same tone burst is used in the bubble simulations as the one described for tissue propagation. Initial bubble radius was $R_0 = 1.25\mu$m (roughly at resonance), but radii of $R_0 = 0.5\mu$m (below resonance) and $R_0 = 2.0\mu$m (above resonance) were also considered (not shown here). The frequency used was $f = 2$ MHz, and the medium surface tension and viscosity were $\sigma = 0.0725$ N/m and $\mu = 0.003$ P, respectively.

In the experiments, an HDI-5000 was used to transmit the various pulsing sequences. The pulses closely approximated those used in the theoretical simulations. The center frequency was 1.7 MHz and all scanning was performed at MIs of 0.09 or less. A tissue phantom that included a wall-less tube of 8 mm diameter was used to hold stationary (non-flowing) contrast microbubbles (Optison) and was scanned with the various pulsing sequences. RF-data was collected for further analysis.

4 Results

There are four unique pulses with amplitudes of 1, -1, 0.5, and -0.5, that are used in the sequences considered. Those four pulses are either propagated to the focus with the KZK equation or used as the acoustic input in the Gilmore equation to calculate the bubble wall velocity. In Fig. 1, the waveforms and spectra of the four pulses after nonlinear propagation (with the KZK) to the focus are shown. The transmit amplitude term A_t is shown for every pulse. With these four conditions all pulsing schemes can be implemented. The y-axis is in dimensionless pressure ($P = p/p_0$) and the x-axis is in retarded time ($\tau = \omega_0 * t'$, $t' = t - z/c_0$) for the waveforms. For the spectra, the y-axis is in dB, and the x-axis in

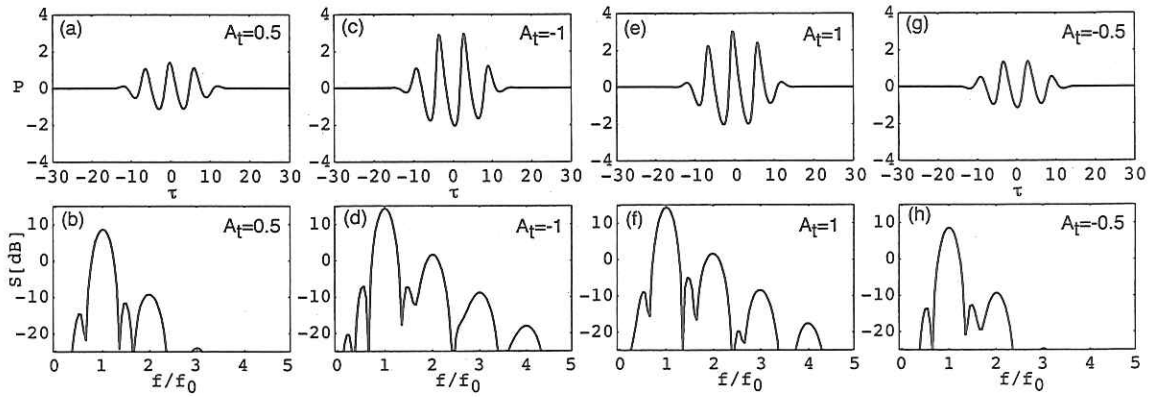

Figure 1: Waveforms and spectra after nonlinear propagation in tissue to the focus for the 4 amplitude and phase conditions considered in the various pulsing schemes.

normalized frequency ($f_n = f/f_0$), where 1 is the fundamental, 2 the second harmonic, etc. The spectra Fig. 1(b) and (h) are almost identical as the only difference between them is a π phase term. The same applies for the spectra of Fig. 1(d) and (f).

Pulse inversion is shown in Fig. 2(a)-(b). It is the result of adding the waveforms in Fig. 1(c) and (e). As noted earlier, the receive weights A_r are normalized such that the sum of their absolute values equals one. The resulting spectrum Fig. 2(b) has only the even harmonic components (2^{nd} and 4^{th} harmonic components. The second and fourth harmonic components seen in the PI spectrum are *identical* with those shown in the spectra of either state (1 or -1) shown in Fig. 1(d) or (f).

Tissue results for PM are shown in Fig. 2(c)-(d). From the spectrum we see the resulting pulse has energy present in all harmonic components (1,2,3,4). The energy shown in the spectrum is clearly the result of nonlinear activity as it would be absent if a linear case was considered where the resulting pulse would be zero. By comparing Figs. 2(a) and (c) we see that PI has a greater amplitude than PM. However, this may also be due to the normalization procedure or due to the fact that PI uses two full amplitude pulses.

PMPI2 is considered in Fig. 2(e)-(f). The resulting waveform in Fig. 2(e) is very similar to the PI waveform Fig. 2(a) and is comprised of mostly second harmonic as seen in the spectrum Fig. 2(f). However, in Fig. 2(f) we also see both fundamental and third harmonic components not present in PI Fig. 2(b). Finally, the amplitude of PMPI2 is twice that of PM but it is still half as much as that of PI.

PMPI4 is shown and in Fig. 2(g)-(h) and PMPI3 in Fig. 2(i)-(j). We note that both of these schemes have energy in the fundamental and third harmonic bands. In addition, they both result in pulses of low amplitude. The spectrum Fig. 2(j) shows two main components present, fundamental and third harmonic just like PMPI4, but a small amount of second harmonic is also present. Both sequences (PMPI3, and PMPI4) have small overall amplitude. A comparison of the nonlinear energy in either of the two spectra with one of the original transmitted pulses (0.5, 1, -0.5, -1) in Fig. 1, reveals that not all nonlinear energy of any of the harmonic components is present in the processed pulse.

In Fig. 3 the four unique pulses (echoes) and their spectra after nonlinear scattering from microbubbles (that are used in the pulsing schemes) are shown. The left column shows the individual bubble responses to various amplitudes (bubble wall velocity U in m/s which is proportional to bubble echoes), and the right column their respective spectra. In a similar fashion with the tissue results in the previous section, a half and full state with their inverts are considered, and the amplitude parameter A_t is denoted in each waveform. In comparing the spectra in Fig. 1 with those in Fig. 3 we see that the bubble second harmonic relative to the fundamental is higher than the tissue propagation results. This is expected as

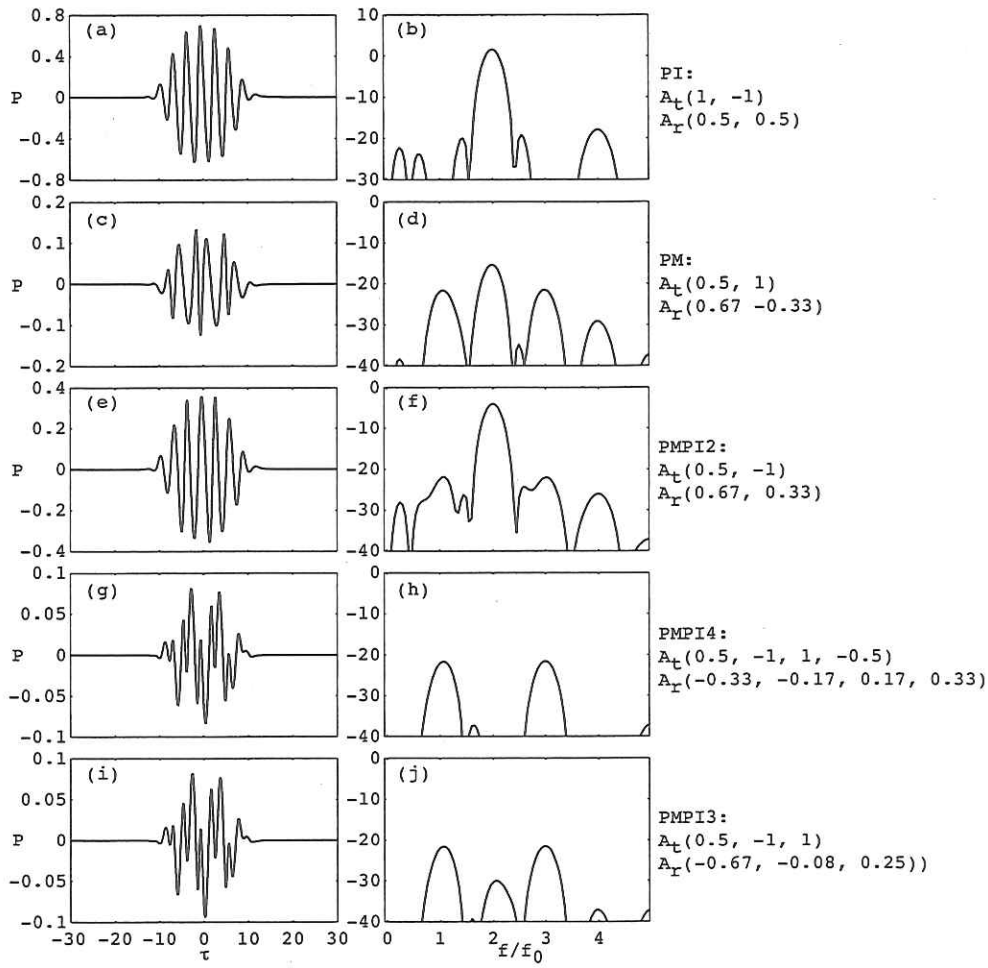

Figure 2: Nonlinear tissue components with various pulsing schemes. (a)-(b) PI, (c)-(d) PM, (e)-(f) PMPI2, (g)-(h) PMPI4, (i)-(j) PMPI3.

the bubble nonlinearity is higher than the tissue nonlinearity.

Pulsing schemes are shown in Fig. 4. In Fig. 4(a) and (b) results for PI are shown. They are similar to the tissue results Fig. 2(a)-(b), where only even harmonic components are preserved. Nonlinearity generated by tissue propagation and microbubble scattering exhibit similar amplitude spectral content.

PM is considered in Fig. 4(c)-(d). The results here are also similar with the tissue results. All harmonic components are present, with the fundamental being reduced and lower than the second and third. The amplitude of PM is lower than that of PI as also seen in the tissue results above.

PMPI2 is shown in Fig. 4(e)-(f). The overall results are very similar with those for tissue. In the spectrum Fig. 4(f) we see a dominant second harmonic component, but also present are the fundamental and third harmonics reduced in amplitude. Comparing PI and PMPI2 we see many similarities. They both succeed in extracting second harmonic with PI having a slight edge in the overall signal level (PI amplitude is twice that of PMPI2). We note these are conclusions based only on the specific examples considered here.

PMPI4 is considered in Fig. 4(g)-(h). As we see in the spectrum Fig. 4(h) the fundamental and third harmonic are present, with the second harmonic totally absent. This result is again similar to the tissue

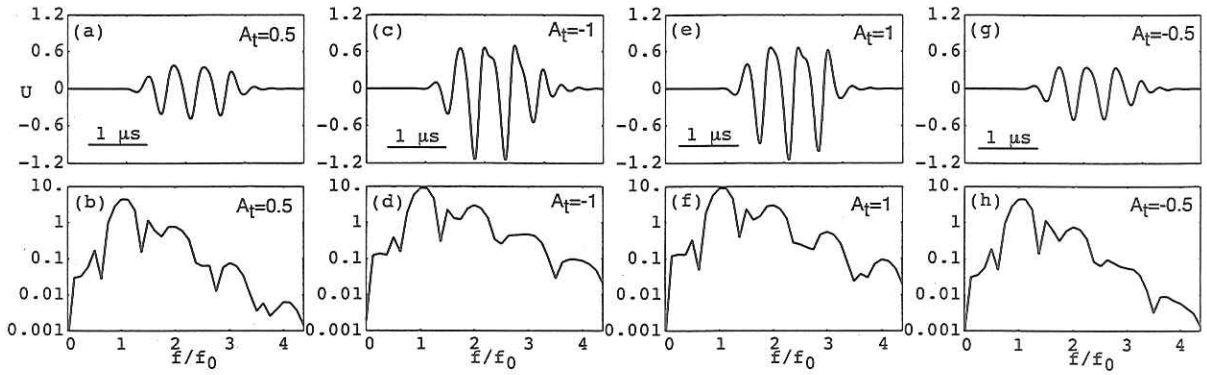

Figure 3: Nonlinear echoes from microbubbles and their spectra for the 4 amplitude conditions considered in the various pulsing schemes.

result for the same sequence in Fig. 2(h).

Finally, PMPI3 is considered in Fig. 4(i)-(j). In the spectrum (j) we clearly see fundamental and third harmonic components, but also some small amount of second harmonic. This is the only difference between PMPI4 and PMPI3. Overall, these two pulsing schemes are approximately equivalent and the resulting time domain waveforms are almost identical.

Experimental results are shown in Fig. 5. All data is taken from a ray intersecting the phantom tube. In Fig. 5(a)-(b) the RF data from the echoes from the first pulse of a PI sequence and its spectrum is shown. The beginning and end of the tube is clearly seen. In Fig. 5(c)-(d) RF data from the echoes of the second pulse (the full amplitude pulse) of a PMPI2 sequence and its spectrum are shown. The data is taken from different frames, but effort was made to choose frames with comparable amplitudes. In Fig. 5(e)-(f) and Fig. 5(g)-(h) the results of PI and PMPI2 processing are shown, respectively. They are very equivalent in terms of overall dynamic range (25 dB). Additionally, from further analysis of similar data (not shown here), it was found that the tissue fundamental cancellation was 30-36 dB for PPI and 20-23 dB for PMPI2. Also, the bubble signal to clutter ratio was 25 dB for PPI and 20 dB for PMPI2.

5 Discussion

An important observation is the striking similarity in terms of frequency content between the results for tissue nonlinearities and bubble nonlinearities. The general trends in Fig. 2 are identical to those in Fig. 4. It may be deduced from this observation that none of these techniques can identify what part of the nonlinear component is tissue versus what part is bubbles. The one clear feature for discriminating between tissue and bubbles remains their difference in nonlinearity (bubbles are much more nonlinear than tissue). This is the main property that has been exploited in the past with low MI techniques. At very low MI ($MI \leq 0.1$), the nonlinear tissue response (nonlinear propagation) is much lower than that of microbubbles.

In comparing the various pulsing schemes we can see that PI gives the maximum amount of nonlinearity at the even harmonics and the PI-processed pulse has the highest amplitude. It is the only scheme where the second and fourth harmonic components are extracted directly from the original spectrum in *full* content. The rest of the schemes at best extract only a large portion of the nonlinear activity. PI uses two identical inputs that only differ in phase and *isolates* the even harmonic components. With PI we get the total amount of nonlinearity present in those components (even harmonics). In addition, for low

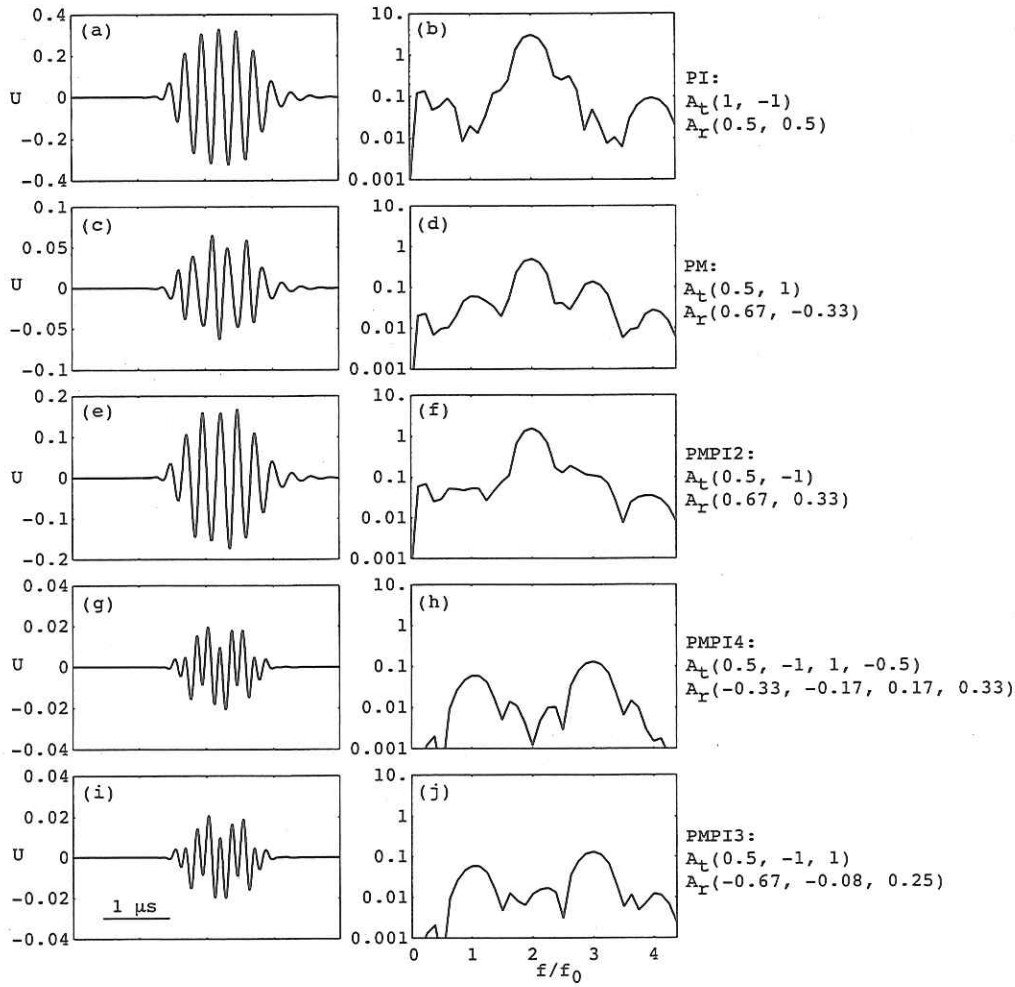

Figure 4: Nonlinear echoes with various pulsing schemes. (a)-(b) PI, (c)-(d) PM, (e)-(f) PMPI2, (g)-(h) PMPI4, (i)-(j) PMPI3.

nonlinearity (quassilinear case) where only fundamental and second harmonics are present, the second harmonic is the total amount of nonlinear energy. With pulsing schemes where different amplitudes are used (PM), we are forced to look at the *differential* nonlinearity between the 2 or more states of input. In the limiting case where one pulse is at full amplitude and the other is almost at zero (or zero nonlinearity), their difference would then result in the *total* nonlinearity. With two or more states at full and half amplitudes the resulting pulse will have less nonlinear energy than the full amplitude result ($A_t = 1$).

PI is very close to PMPI2. Their amplitudes differ by 6 dB. However, PMPI2 has also a small "nonlinear" fundamental component and some third that may possibly be utilized in a beneficial way especially when considering the transducer bandwidth characteristics and frequency dependent tissue attenuation.

PM is the technique with the most components present (1,2,3,4). The largest component of PM is the second harmonic. Amplitudes other than full and half may also be considered in the future. PM may be used as a technique for "nonlinear" fundamental extraction but PMPI3 and PMPI4 do a better job of that, by removing or considerably reducing the 2^{nd} harmonic, at the expense of reduced frame rate due

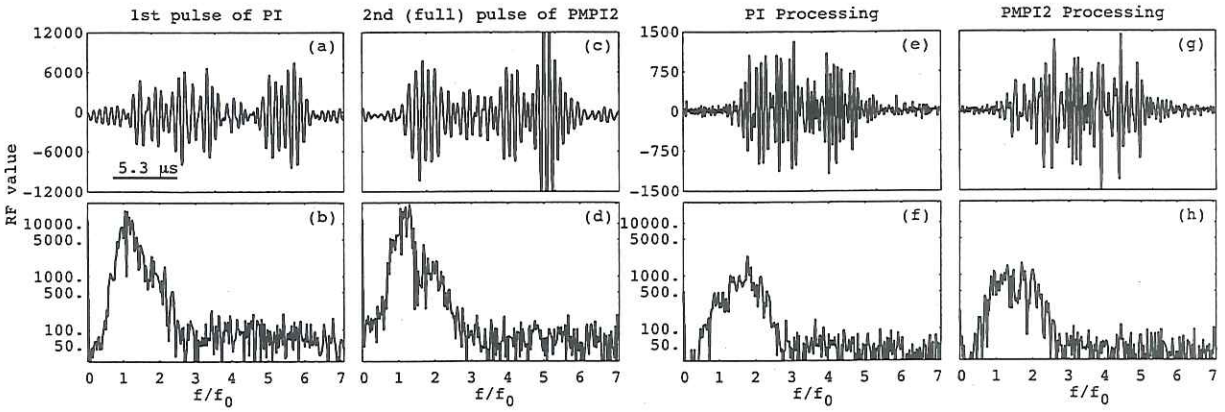

Figure 5: Experimental results. (a)-(b) The first line of a PPI sequence and its spectrum, (c)-(d) the second (full amplitude) line of a PMPI2 sequence, (e)-(f) result of PPI processing, (g)-(h) result of PMPI2 processing

to the higher ensemble length.

PMPI3 and PMPI4 isolate the fundamental and third harmonic components. Their only difference is that PMPI3 has also a small amount of second harmonic. It should be noted that the amount of "nonlinear" fundamental in PMPI3 and PMPI4 is almost identical to PM. Finally, both PMPI3 and PMPI4 result in a very small overall signal (about 20 dB lower than PI). This result depends on the scaling scheme. PMPI4 is effectively equivalent to the difference between 2 "*inverse*" PI schemes at two distinct levels [see Fig. 6(a)]. By "*inverse*" PI here we mean $[A_t(1, -1), A_r(1, -1)]$, which results in the odd harmonic components. By re-examining Figs. 2 and 4 (g-h) we can now better understand where

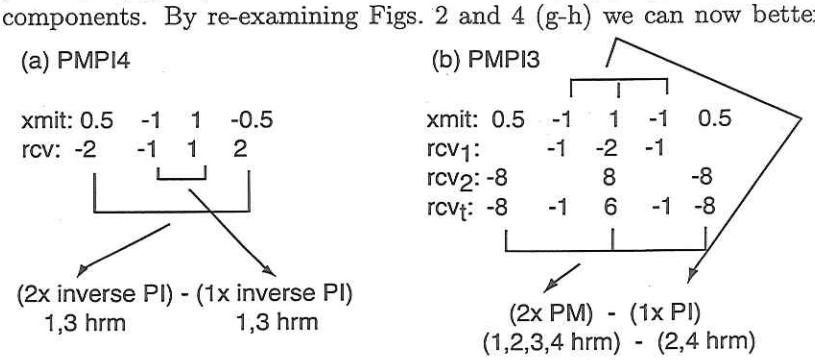

Figure 6: (a) Explanation of PMPI4. This scheme is effectively the difference between two inverse PI schemes, where only odd harmonic components are retained. (b) Explanation of PMPI3. This scheme is effectively the difference between PM and PI.

the spectral components shown originate. They are the odd harmonic components that result from 2 individual PI schemes at different levels. As seen in those figures, the fifth harmonic is also present (barely seen at the corner of the box). The "nonlinear" fundamental component is almost the same as the third harmonic component in the cases considered (and less than the second).

The"nonlinear" fundamental is the result of using two unequal amplitudes. The nonlinear systems discussed here do not generate any nonlinear energy in the fundamental band. What is seen in the fundamental band is the differences in the fundamental (linear) component between the two states which is the result of the system nonlinearity. This fundamental component is always less than the second

harmonic component.

Now we turn our attention to PMPI3 and attempt to further explain that scheme. It is the combination of PI and PM as shown in Fig. 6(b). By re-examining Figs. 2 and 4 (i)-(j) we now see the components shown are the result of subtracting PI from PM. Since PM has components in all bands (1,2,3,4) and PI only at the even harmonics (2,4), the end result is a waveform with mostly fundamental and third harmonic component. A small amount of second harmonic component is also observed. This is due to the fact that in PM we use two different states of nonlinearity and the end result is their difference whereas in PI the end result contains all second harmonic. Effectively, the second harmonic component left in PMPI3 is the amount of second harmonic present in PI in excess of PM.

From the analysis of PMPI3 and PMPI4, we conclude that these pulsing schemes are indeed combinations of PI and PM. It is also noted that all of the techniques described in this paper may be implemented in a preferred way to extract a desired signal component for real-time low MI imaging.

Another important observation from the experimental data is the actual overall dynamic range of the echoes. In Fig. 5 (f)-(h) the resulting signal after PI and PMPI2 processing has about 25 dB dynamic range. This is very typical of what is observed in abdominal and cardiac images at these low MIs.

6 Conclusions

The pulsing schemes considered here do a great job of isolating the nonlinear response of either tissue or bubbles. They extract different parts of the nonlinear spectrum and reject all linear response. The maximum amount of nonlinear energy is equal to the energy present in the harmonics (2 and above) in the full amplitude case. The toughest challenge in contrast imaging is the small dynamic range of the low MI images. Typical microbubble signals for low MI imaging exhibit only about 25 dB SNR depending on bubble concentration and attenuation. Tissue and bubble nonlinearities may not be differentiated with the pulsing schemes considered here. The higher effective nonlinearity of bubbles over tissue remains the main discriminating factor between tissue and bubbles. PI is the most sensitive technique for second harmonic imaging. PM is the best technique for "nonlinear" fundamental imaging. PMPI3 and PMPI4 techniques are useful when there is interest in observing the third harmonic component and the "nonlinear" fundamental. Some of the schemes investigated are combinations of PI and PM. The transducer bandwidth, clinical application, contrast agent used, and frequency dependent attenuation are some of the factors that influence the choice and effectiveness of the pulsing schemes. The analysis presented here indicated that they are all comparable in extracting nonlinear components from bubble echoes under low MI imaging conditions.

CURRENT BUBBLE MODELS, ARE THEY USEFUL?

Charles C. Church

National Center for Physical Acoustics, University of Mississippi, University, MS USA

Theoretical study of bubble activity is generally considered to have begun with the work of Lord Rayleigh in his investigation of the erosion of high-speed ship propellers, a process that has since become known as hydrodynamic cavitation. Rayleigh's original 1917 model for free bubbles was improved by several workers, including Plesset, Noltingk, Neppiras, and Poritsky, with the resulting formulation being known as the RPNNP equation, or more often as the Rayleigh-Plesset equation. The Rayleigh-Plesset equation provides the simplest complete description of the response of a gas bubble to an acoustic field. Research into the acoustic response of a bubble having a layer of surface-active molecules at the gas-liquid interface began much more recently, notably with the work of Glazman, who accounted for the dilational elasticity of a thin adsorbed film. Theoretical work on albumin-encapsulated microspheres began nearly fifteen years ago when Albunex®, the first agent approved for clinical use in the US, was still in development. Since that time, the number of potential ultrasound contrast agents has grown considerably. These agents utilize a variety of both shell materials (e.g., proteins, synthetic polymers, surfactants, lipids) and encapsulated gases (e.g., air, sulfur hexafluoride, perfluorocarbons). The shell may be very thick or vanishingly thin. It is clear that a thorough understanding of the interaction between ultrasound pulses and contrast microbubbles is essential for the successful clinical application of a particular agent. However, can this understanding be obtained through use of theoretical models alone? The nature of various contrast agents will be discussed, and appropriate models for each will be described. The basis of each of these models is the theory for a free bubble "supplemented" by the effect of the encapsulating shell. The differences among the models lie primarily in their treatment of the encapsulating layer and, to some extent, the surrounding medium. In this talk, models developed by de Jong et al., Church, Ye, Allen et al., Khismatullin et al., and others will be reviewed. Comparisons among models will include predictions of clinically significant acoustic responses (resonance frequency, scattering strength, nonlinearity, etc.). Strengths and weaknesses of the various approaches will be discussed, and suggestions for future work will be offered.

RECENT STUDIES OF THE PHYSICS OF ULTRASOUND CONTRAST AGENTS AND THEIR THERAPEUTIC BIOLOGICAL APPLICATIONS

Lawrence Crum[1], Michael Bailey[1], Andy Brayman[1], Jingfeng Guan[1], Joo Ha Hwang[1], Vera Khokhlova[2], Thomas Matula[1], Carol Miao[3], Juan Tu[1], Oleg Sapozhnikov[2], and Shahram Vaezy[1]

[1]Center for Industrial and Medical Ultrasound, Applied Physics Laboratory, 1013 NE 40th St, Seattle, WA 98105 USA

[2]Department of Acoustics, Faculty of Physics, M. V. Lomosov Moscow State University, Leninskie Gory, Moscow 119992, RUSSIA

[3]Department of Pediatrics and Medicine, Box 356320, University of Washington, Seattle, WA 98195 USA

Ultrasound contrast agents serve an important role in medical imaging due to their enhanced backscatter; however, as stabilized microbubbles, they also serve as nucleation sites for cavitation that can be induced by the applied ultrasound field. Under even moderate ultrasound exposure conditions, the stabilizing shell can be disrupted and a free gas bubble released which can undergo large amplitude pulsations. Using both acoustic and optical probes, we have examined the shell disruption and the subsequent dynamics of the released gas bubble. Under certain conditions, the gas rapidly dissolves and loses its effectiveness; however, under different conditions, inertial cavitation is induced and the potential generated for tissue damage and other bioeffects. In some cases, these bioeffects are desirable; *e.g.*, we have examined the enhancement of transfection by exposure of the murine liver *in vivo* to cavitation fields during simultaneous presentation of plasmid DNA and ultrasound contrast agent. In other cases, the increased absorption of ultrasound has enabled us to induce more rapid coagulative necrosis of undesirable tissues as well as the more rapid induction of hemostasis in a bleeding vessel. A description of our techniques for acoustic and optical probing of contrast agents shall be given as well as some specific examples of our utilization of these agents as cavitation nuclei.

FUNCTIONAL IMAGING IN RADIOLOGY

Martin Blomley, Adrian Lim, Thomas Bryant, Anand Rattansingh, David Cosgrove, Nayna Patel, Cliona Cunningham, Demosthenes Kokkonos, Madeleine Lynch, Rob Eckersley, Simon Taylor-Robinson, David Cosgrove

Imaging Sciences Department, Hammersmith Hospital, Faculty of Medicine, Imperial College, London W12 0HS

This presentation will argue the case that most promising clinical applications of microbubbles are in fact functional imaging methods. These include:

Transit time methods in larger vessels

It is relatively easy to measure temporal indices after a microbubble injection, such as arrival time, especially with newer agents such as SonoVue. With organs that have single and easily identifiable input and output vessels, true arteriovenous transit time can be easily measured. With organs with more complex blood flow, such as the liver, transit times between vessels such as the hepatic artery and hepatic veins can be measured. Even when using a simple index, such as the arrival time in a hepatic vein after intravenous injection, very useful data can be obtained. "Early" enhancement is consistently seen in cirrhosis and significant liver fibrosis, diffuse liver disease can be graded, and the method shows promise in detecting very early or "micrometastatic" disease in colorectal cancer. Another promising application is assessing the response to interferon therapy in diffuse liver disease. We are currently investigating the method in assessing the response to therapy in colorectal cancer metastases. An advantage over parenchymal methods is that whole organs or portions of organs can be easily studied, not just a scan plane.

Parenchymal measurements in the microcirculation

The newer microbubble methods show parenchymal enhancement of tissues well, and the uptake of microbubbles can be measured to produce time enhancement curves. The method lends itself well particularly well to the production of parametric images, and the utility of these are being investigated. The initial uptake after bolus injection can be studied, but by deliberately disrupting microbubbles and allowing refilling, more precise control over the "input function" is possible. There is encouraging evidence that indices such as microcirculatory flow speed, fractional vascular volume, and indices proportional to true perfusion can be measured using these reperfusion kinetic approaches. A limitation, however, is tha it is hard to study more than one scan plane at a time.

Targeted microbubbles

Even with simple "passively targeted" liver specific microbubbles, the pattern of uptake in focal lesions gives useful information. For example, many benign liver lesions show uptake while malignancies, especially metastases, show reduced uptake. The benefit of this has been shown in a recent multicentre study. If Actively targeted microbubbles open many possibilities for more precise functional information.

Methods that demonstrate communication between body cavities or vessels:

These include one of the earliest uses of microbubbles, namely for shunt detection, which relies on injecting bubbles that will not go through the intact pulmonary circulation for demonstration of right to left cardiopulmonary shunts. Another application is demonstrating communication between or within body cavities, such as in urinary reflux studies or the assessment of transport in peritoneal fluid.

Other functional methods of assessing vascular morphology

These include the analysis of vascular enhancement in many focal liver lesions (such as haemangiomas which show a pathognomic pattern of peripheral vascular enhancement and centripetal infilling). Another new development is a novel methods of displaying relatively small vessels in a mass such as a breast carcinoma (MVI, Philips Medical Systems) which can be used to build a map of the vascular pattern within a lesion. Many carcinomas show marked vascular irregularity. We are evaluating the utility of the method in assessing the response to neo-adjuvant therapy.

FOCAL LIVER LESIONS: WHAT WE KNOW, WHAT WE DON'T KNOW, WHAT WE WANT FOR THE FUTURE

Thomas Albrecht

Klinik und Poliklinik für Radiologie und Nuklearmedizin -Campus Benjamin Franklin -Charité - Universitätsmedizin Berlin - Freie Universität Berlin und Humboldt-Universität zu Berlin - Hindenburgdamm 30 - 12200 Berlin – Germany - thomas.albrecht@charite.de

Imaging of focal liver lesions is by far the most important application of ultrasound contrast agents in Radiology. The recent technological improvements of non-linear imaging modes and the advent of perfluor-based agents such as SonoVue (Bracco) have lead to significant progress in this field in the last few years. Contrast enhanced ultrasound (CEUS) of the liver is now routine clinical practice in many European centres. It performs outstandingly well in characterising focal liver lesions. The rate of correctly diagnosed lesions is in the order of 90% and differentiation between benign and malignant is possible in almost all cases. CEUS is thus superior to CT and at least as good as MRI in this application. Detection of metastases is also substantially improved by the use of microbubbles. The sensitivity of CEUS in the detection of hepatic metastases is very similar to that of contrast enhnamced spiral CT, its specificity is higher.

Detection of HCC with CEUS is more difficult. In principle, detection of HCC can be done either in the arterial phase (looking for hyperenhancing lesion), or in the delayed phase, (looking for hypoenhancing lesions). The former is limited by the very short temporal window, the latter by the unpredictable delayed enhancement characteristics of HCC., especially when non-liver-specific mircrobubbles are used. We don't know what determines the delayed phase contrast behaviour of HCC; there is speculation that it may be dependent on tumour differentiation, but this remains to be proven. We also don't know what the benefit of the use of microbubbles for detection of HCC is, studies on this topic are lacking. This is particularly relevant with regards to HCC screening.

Another poorly understood area is the fate of the microbubbles in the liver. Two mechanisms determining the duration and distribution of enhancement exist: sinusoidal pooling and phagocytosis. While these mechanisms have been proven for some of the agents, this is not the case for others. Another intriguing observation is heterogeneous late enhancement of the liver. This very obvious in approximately 1% of patients where it produces a very peculiar pappern, which should not be confused with disease. More subtle forms occur in far more, if not all patients.The like mechanism is the formation of large bubbles, possibly in the bowel wall, with subsequent trapping in the liver.

Liver specific agents have some important advantages over non-specific agents, especially with regards to detection of HCC and metastases. The ideal contrast agent for liver imaging would be a

liver-specific perfluor agent, which combines the advantages of liver-specificity with the ability to perform low MI real time imaging.

Unfortunately, no such agent is available to date, although two of them have entered clinical development (Sonazoid, Amersham Medical and BR14, Bracco). Our limited experience with these agents has been very encouraging. These agents would likely make the biggest difference in detection of HCC, which is currently a substantial limitation of CEUS and a clinical problem of ever increasing importance. With regards to imaging techniques, the recent developments have brought substantial progress. Techniques combining amplitude modulation and phase inversion (CPS, Acuson Siemens) have resolved the problem of sensitivity. However dynamic range needs further improvement. In general, it remains to be seen if colour overlay techniques such as CPS or VRI (Toshiba) will be preferred over B-mode techniques. The latter have the advantage of a greater dynamic range but do not provide sufficient tissue information at low MI. Penetration continues to be another unresolved problem in patients with diffuse liver disease and sometimes in very deep lesions and/or obese patients.

NON-INVASIVE DETECTION OF CAROTIDARTERY ENDOTHELIAL DYSFUNCTION DUE TO HYPERTRIGLYCERIDEMIA WITH HIGH FREQUENCY REAL TIME LOW MECHANICAL INDEX IMAGING OF RETAINED MICROBUBBLES

Jeane Mike Tsutsui, Feng Xie, Stanley J. Radio, Patrick Phillips, James Chomas, John Lof, Thomas R. Porter

University of Nebraska Medical Center, Omaha, NE

Endothelial dysfunction (ED) occurs with hyperlipidemia, even before the development of atherosclerotic plaque. Intravenous (IV) albumin-coated microbubbles (MB) normally pass freely through the large and small vessels, but are retained in regions where ED exists. New low mechanical index (MI) pulse sequence schemes (PSS) permit the detection of these MB without destroying them. We hypothesized that ED due to hyperlipidemia could be observed in large vessels by imaging retained MB with high frequency PSS. **Methods:** Carotid arteries (CA) from 4 pigs were imaged transcutaneously before and after a 125 milliliters of 20% intralipid infusion. A 7 MHz linear array transducer using a low MI real time PSS (Contrast Pulse Sequence, Siemens Acuson Sequoia) imaged both CA following IV injections of albumin coated MB (PESDA). Retained MB were defined as MB adherent to the arterial wall which persisted late after injection. Endothelial acoustic intensity (AI) was quantified after clearance of free flowing MB. CA responses to acetylcholine (ACH) were also measured. **Results:** CA responses to10^{-7} and 10^{-6} Molar ACH demonstrated vasoconstriction after intralipid infusion, and triglyceride levels increased significantly ($p<0.05$). Retained MB following IV PESDA could be seen after intralipid infusion (Figure) and endothelial AI increased by 1.3 ±1.8 units ($p<0.0001$).

Conclusions. These data indicate that early ED can be non-invasively detected and quantified using a real time PSS following IV albumin-coated MB.

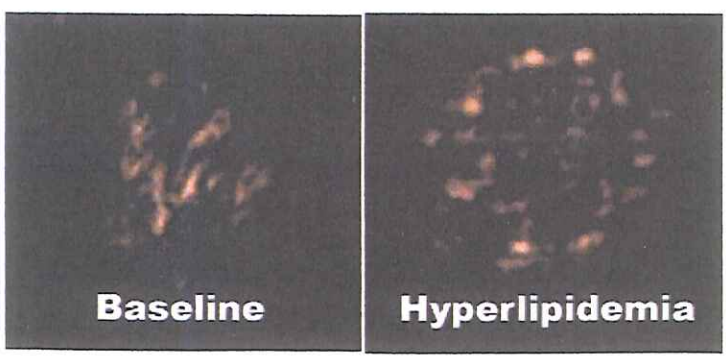

ULTRASOUND CONTRAST PERFUSION IMAGING IN ACUTE STROKE PATIENTS

W. Wilkening[1,3,4], J. Eyding[2,3,4], C. Krogias[2,3,4], S. Meves[2,3,4], Th. Postert[4,5], H. Ermert[1,3,4]

[1]Institute of High Frequency Engineering and [2]Department of Neurology, Ruhr-University Bochum, Germany
[3]www.kmr-bochum.de, [4]www.umeds.org

[5]Department of Neurology, St. Vincenz-Krankenhaus, Paderborn, Germany

INTRODUCTION

Transcranial imaging is especially challenging because of the high attenuation and defocussing effect of the temporal bone window [1, 2]. Nevertheless, destructive contrast agent imaging is possible, and it provides images with sufficient signal-to-noise ratio for qualitative perfusion imaging. Earlier clinical results of our group were obtained using destructive imaging approaches with more than 2 pulses (e.g. 6-10) per beam line [3, 4]. Such techniques are very sensitive and offer a very good contrast between contrast agent and tissue. Recent clinical evaluations have shown that a combination of Sonovue® as a state-of-the-art contrast agent and THI (high MI pulse/phase inversion on a Siemens Sonoline® Elegra) outperforms the earlier approaches, although the residual tissue signal makes local baseline subtraction necessary. The dynamic range for contrast agent detection of pulse inversion, which detects nonlinearity and destruction, turns out to be higher than of purely destruction-based imaging techniques, and sensitivity is less of an issue when using newer contrast agents.

In an ongoing study we were able to show that qualitative perfusion imaging in acute stroke patients is feasible, where both brain hemispheres can be assessed from one side (bilateral approach), i.e. in one examination with a single bolus injection of contrast agent. Imaging the contralateral (distant) hemisphere is of great value for brain perfusion imaging, since the sector format of the image covers the hemisphere almost completely (i.e. including cortical structures). There is no near field artifact (i.e. phased arrays do not allow contrast specific imaging within the first 2 – 3 cm) which makes evaluation of "ipsilateral" cortical structures impossible. However, other parenchymal structures of the ipsilateral half (e.g. lentiform nucleus, thalamus) of the image can still serve to compare the affected to the unaffected brain hemisphere of a stroke patient [5].

METHODS

Stroke patients who present to the stroke unit within 12 hours after symptom onset are included in the current study. Ultrasound scanning is performed from the assumedly healthy side so that the infarcted area falls into the contralateral part of the imaging plane. A Siemens Sonoline® Elegra equipped with a 2.5 MHz phased array driven at 2.0 MHz is used to acquire a sector of 90° and 150 mm depth in phase inversion harmonic imaging (PIHI) mode at an MI > 1, which may actually be lower inside the brain. Imaging at a frame rate of 0.5 Hz starts immediately after injection of 2.5 ml of Sonovue®followed by 10 ml of Saline. The total data acquisition takes approximately 90 s so that the peak intensity and decay can clearly be seen in the images.

Local time-intensity curves (TICs) are extracted form the image series. Following a model-based approach, which has been described earlier [6], the baseline intensity is automatically eliminated. Parametric images of the peak intensity and the time-to-peak intensity visualize the brain perfusion qualitatively or semi-quantitatively. TICs derived from various parenchymal or vessel regions (approximately 25 –100 mm^2) can be calculated to evaluate the perfusion condition more sensitively.

RESULTS

9/10 of the acute stroke patients included in the study so far could be examined following the bilateral PIHI approach, i.e. parametric images, like the one shown in Figure 1, depicted unperfused areas quite clearly. In 4 cases, where all acquired data has been analyzed, yet, follow-up CT scans confirmed the findings of the ultrasound examinations, i.e. the initial US examinations were able to predict size and localization of the eventual infarction. In one of these cases, the ultrasound examination did not find perfusion in the core region of the infarction, i.e. the model-based TIC processing algorithm could not fit the model to the measure TIC. In a border region of the infarction that eventually survived, a considerable delay in the time-to-peak-intensity was found (35.6 s, where "normal" TPIs are in the range of 22 s).

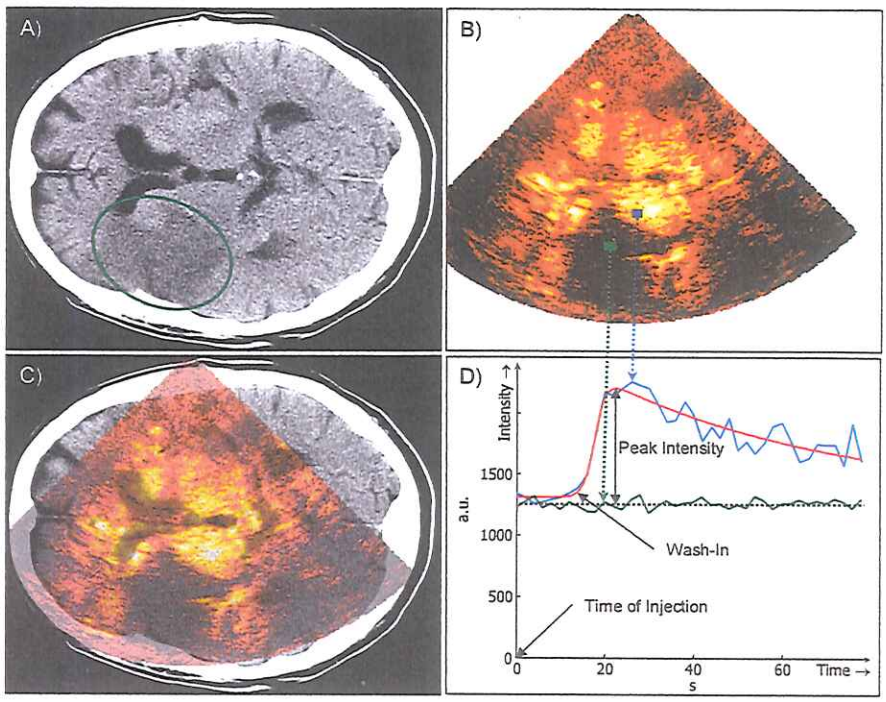

Figure 1: Brain perfusion images and TICs. A): Follop-up CT scan of a stroke patient showing the infracted tissue (green ellipse). B): Ultrasound perfusion image (peak intensity) showing the perfusion deficit in the acute phase. C): The overlay of A) and B) confirms the localization of the infarction. D) Time-intensity curves derived from perfused and unperfused ROIs.

CONCLUSIONS

The bilateral PIHI approach can be considered a significant advancement in ultrasonic brain perfusion imaging, since the affected brain hemisphere can be visualized completely, and direct intra individual comparisons between affected and unaffected hemispheres are possible, while the examination time is reduced. Early results suggest that differentiation between hypoperfusion and ischemia may be possible using the described algorithm which emphasizes the semi-quantitative character of the examination.

ACKNOWLEDGEMENT

The work is a project of the Ruhr Center of Competence for Medical Engineering (KMR Bochum), supported by the BMBF (Federal Ministry of Education and Research, Germany), grant 13N8079, and of UMEDS (Ultrasonographic Monitoring and Early Diagnosis of Stroke, 5th Framework Programme), supported by the European Union, QLG1-CT-015018).

REFERENCES

[1] Eyding J, Wilkening W, Postert T: Brain Perfusion and Ultrasonic Imaging Techniques. Eur J Ultrasound. 2002:16(1-2):91-104.

[2] Meyer K, Wiesmann M, Albers T, Seidel G: Harmonic imaging in acute stroke: detection of a cerebral perfusion deficit with ultrasound and perfusion MRI. J Neuroimaging. 2003;13:166-8.

[3] Postert T, Hoppe P, Federlein J, Helbeck S, Ermert H, Przuntek H, Büttner T, Wilkening W: Contrast agent specific imaging modes for the ultrasonic assessment of parenchymal cerebral echo contrast enhancement. J Cereb Blood Flow Metab. 2000;20:1709-1716.

[4] Holscher T, Postert T, Meves S, Thies T, Ermert H, Bogdahn U, Wilkening W. Assessment of brain perfusion with echo contrast specific imaging modes and Optison. Acad Radiol. 2002;9S2:S386-388.

[5] Eyding J, Krogias C, Wilkening W, Meves, S, Ermert H, Postert T. Parameters of cerebral perfusion in phase inversion harmonic imaging (PIHI) ultrasound examinations. Ultrasound Med Biol. 2003;29:1379-85.

[6] Wilkening W, Postert T, Federlein J, Kono Y, Mattrey R, Ermert H. Ultrasonic assessment of perfusion conditions in the brain and in the liver. 2000 IEEE Ultrasonics Symposium. Proceedings. International Symposium. Vol. 2, 2000: 1545-8.

MICRO FLOW IMAGING AND ARRIVAL TIME PARAMETRIC IMAGING OF THE LIVER

Naohisa Kamiyama[1], Hiroko Iijima[2] and Fuminori Moriyasu[2]

[1] Toshiba Medical Systems Co. (TMSC), Otawara, Japan

[2] Dept. of Gastroenterology & Hepatology, Tokyo Medical University. Tokyo, Japan

MICRO FLOW IMAGING

When ultrasound scan is performed at high transmission power, microbubbles in the scan volume are destroyed. Right after bursting, replenishment of the microbubbles into the scan volume is observed by using harmonic imaging mode at low transmission power (called flash-replenishment sequence (FRS)) [1]. Though there are a large number of blood vessels and the blood flow is rapid in the liver, the number of microbubbles in the small vessels is still small at the moment immediately after the burst-scan. The small vessels are therefore not visualized in the conventional contrast imaging.

When the number of microbubbles in the vessels is very small or flow is very slow, max-holding imaging that traces position of the moving bubbles are very efficient to visualize micro-vessels [2][3].

Micro flow imaging is a combination technique of FRS and a max-hold image processing [4]: The ultrasound system starts max-hold processing just after burst-scan following the FRS. The processing reconstructs micro-vessels in the liver then they are being covered with the inflow into the sinusoid (less than spatial resolution). FRS makes it possible to visualize micro-vessels repeatedly.

ARRIVAL TIME PARAMETRIC IMAGING

The two dimensional mapping of arrival time is the well-known concept: intensity in the B mode image is painted in different colors due to the time of appearance. We applied the parametric image to the FRS. The subjects were white house rabbits weighing 3 kg. Tracheal intubation was performed under general anesthesia for breath-holding. Replenishment imaging was obtained under infusion injection of the contrast agent. The duration to calculate arrival time was five to ten seconds.

Arrival time color mapping visualized small vessels as different colors separated from the perfusion, while the small vessels in the conventional gray-scale image at five second after burst-scan was covered with perfusion brightness.

The results suggest that the FRS method is a convenient and reliable new technique for visualization and quantification of micro vessel perfusion of the liver.

REFERENCES

[1] Kamiyama N: USP 5,694,937; 1997.

[2] Burns PN: Imaging methodology for new contrast agents, basic and clinical aspects. 4th International Symposium on Ultrasound Contrast Imaging (Proc.), 2002, p 28-30.

[3] Powers J, Jensen S, et al.: Microvascular imaging of the breast. The 8th European Symposium on Ultrasound Contrast Imaging (Proc), 2003, p 8.

[4] Moriyasu F, Kamiyama N, et al.: Ultrasound contrast imaging of hepatic microcirculation using a flash-replenishment sequence. RSNA2003 (Proc.), 2003, p.620.

GENE AND DRUG DELIVERY WITH ULTRASOUND CONTRAST AGENT

Jonathan R. Lindner, MD

University of Virginia Medical Center, Charlottesville, Virginia, USA

It has recently become possible to target microbubble contrast agents to disease-related cellular and molecular processes. Targeting has been possible by either changing the chemical constituents on the bubble shell, or by conjugating specific ligands to the surface of the microbubbles. Our lab has successful at imaging both inflammatory processes and angiogenesis by targeting endothelial cell adhesion molecules. In this talk we will discuss some recent advances in each of these fields and how they relate to improving therapy.

Microbubbles targeted to angiogenesis have been developed by conjugating the disintegrin echistatin, which binds to alpha-v beta-2 integrins, to the surface of lipid-shelled microbubbles. This agent has been shown to adhere to neovessels in matrigel models of angiogenesis and in glioblastomas in rats. We have recently used this agent in a rat hind-limb model of angiogenesis to image endogenous and therapeutic angiogenesis. Occlusion of the iliac artery in rats resulted in a reduction of resting flow, measured by MCE, to approximately one third of normal. The endogenous angiogenic response resulted in an increase in blood flow to just over half of normal by 14-28 days. This increase in blood flow was preceded by a peak in the signal from angiogenesis-targeted microbubbles at day 4-7, which was also the peak of alpha-v integrin expression on immunohistochemistry. In rats treated with slow-release FGF-2 after iliac occlusion, perfusion increased faster and to a greater degree than non-treated rats (reaching 75% of normal). In FGF-2-treated compared to non-treated rats, the signal from angiogenesis-targeted microbubbles at 4-7 days was greater. These data demonstrate that alpha-v beta-3-targeted microbubbles can provide data on the extent of endogenous and therapeutic angiogenic responses prior to any measurable changes in blood flow.

We have previously used microbubbles targeted to endothelial cell adhesion molecules and to leukocytes to study inflammatory responses to ischemia-reperfusion injury in the heart and kidney. More recently, we have developed microbubbles targeted to MAdCAM-1, which is selective for gastrointestinal inflammation, in order to diagnose and follow inflammatory bowel disease. Flow chamber studies have demonstrated selective adhesion of these targeted microbubbles to stimulated cells that express MAdCAM-1. Contrast imaging with MAdCAM-1-targeted microbubbles in SAMP1/YitFC mice which develop spontaneous Crohn's disease has demonstrated intense bowel and medial lymph node enhancement. Enhancement was very low for non-targeted microbubbles in these animals and for targeted microbubbles in control mice (AKR). These data demonstrate that assessment of inflammatory bowel disease may be possible with ultrasound and microbubbles targeted to MAdCAM-1. This method may be valuable in the clinical setting for early diagnosis and for

differentiating disease flares from chronic changes, for which there is no diagnostic technique currently available.

Finally, gene delivery and drug delivery are possible with custom microbubble carriers. There is now evidence that tissue deposition of these therapeutic agents is more efficient when microbubbles are apposed or in proximity to the vessel wall, which can be accomplished with targeting.

TARGETED MICROBUBBLES FOR ATHEROSCLEROTIC PLAQUE

CM Moran, J Ross, M Butler, WN McDicken*

Medical Physics and *Clinical and Surgical Sciences, University of Edinburgh, Scotland

Background: The size and composition of commercially available ultrasonic contrast microbubbles are such that when insonated at routinely used diagnostic frequencies (2-7MHz), the bubbles resonate and strongly scatter ultrasound. Recently there has been increasing interest in imaging and manipulating these microbubbles at higher frequencies (30-40MHz) for possible applications in targeting microbubble-encapsulated drugs to specific plaque sites in arteries and to image such sites using intravascular ultrasound.

Method: A lipid-encapsulated microbubble was developed in-house and sized using a Malvern Mastersizer 2000. The agent was diluted to various concentrations using saline and blood-mimicking fluid (BMF). Using a ClearView Ultra system, an Atlantis SR intravascular probe was inserted into each solution and one frame of unprocessed ultrasonic data was acquired. The data was downloaded onto a PC. A region-of-interest (ROI) of 128 data points and 9 ultrasonic lines was chosen. Over these ROIs, mean backscatter power was calculated and referenced to data collected from a water-air interface. The ability of the agent to be targeted to specific cells was assessed microscopically by labelling the microbubbles with an antibody (CD54) and then passing these microbubbles over endothelial cells grown on an agar interface.

A flow chamber was developed to enable both acoustical and optical images to be obtained of the cells under physiological flow conditions. Using Laser Doppler Anemometry (LDA) permitted a precise measurement of flow velocities and shear stresses exerted on the microbubbles attached to the surface of the cells.

Results: The level of backscatter from the in-house agent is comparable to commercial agents at 30MHz and is adequate for arterial plaque studies. When observed using a microscope and in the flow chamber, antibody-loaded microbubbles were observed firmly attached to cells. LDA provides quantitative information on the velocities and stresses experienced by the attached microbubbles.

SONOPORATION:
A FIRST APPROACH OF CELLULAR MECHANISMS

Sophie Mehier-Humbert[1], Thierry Bettinger[2], Feng Yan[2], Richard Guy[1]

[1]University of Geneva, School of Pharmacy and Biopharmacy, 30 Quai Ansermet, 1211 Geneva 4, Switzerland; [2]Bracco Research SA, Dpt of Novel Agents Research, 31 route de la Galaise, 1228 Plan-les-Ouates, Switzerland

Introduction: Sonoporation is a new promising method for gene therapy. Compared to other transfection techniques (viral or non-viral), it should allow introduction of genetic material into cells or tissues with high spatial and temporal control and minimal toxicity. Although many research efforts have recently been made, it seems that the development of this technique reaches a "steady state". This is mainly due to a lack of mechanistic comprehension of this relatively complex technology and also the limited work on the optimization of ultrasound contrast agents dedicated for this approach. For example, additives are present in some ultrasound contrast agent formulations but their interaction with cells has not been reported yet. In this lecture, we will give an overview of our preliminary results concerning sonoporation mechanisms, at the cell level.

Methods: Rat mammary adenocarcinoma cells (MAT B III) were sonoporated using a rotating tube exposure system in the presence of ultrasound contrast agent (UCA), at frequencies of 1.15 MHz (P- = 0.40 MPa) and 2.25 MHz (P- = 0.57 MPa) for 10 seconds. Cells were sonoporated with a fluorescent marker (FITC-Dextran 77 kDa) or a plasmid encoding for the Green Fluorescent Protein (GFP) or labelled with an intercalating agent (YOYO-1). Cell viability and kinetics of cell membrane resealing were assessed using propidium iodide fluorescent probe. The positive cells were quantified by flow cytometry and observed with a fluorescent microscope. Lipofection (Lipofectamine 2000) was also performed for comparison. Influence of additives on cell membrane fluidity was studied by measuring anisotropy using fluorescence polarization of 1,6-diphenyl-1, 3, 5-hexanetriene (DPH).

Results: As compared to lipofection that requires endocytosis, sonoporation allowed a rapid and direct transfer of naked DNA into the cell cytoplasm via ultrasound-induced pores in the plasma membrane. Consequently, the kinetics of protein expression were significantly faster for sonoporation than for lipofection. The duration of pore opening was very short (likely less than one second). In contrast, complete cell membrane resealing was a slow process, since only 22 to 33% of cells were impermeable to propidium iodide 4.5 hours after insonification in the presence of UCA. Surfactants, such as Pluronic® polymer F127, improved sonoporation (both transfection and cell viability) by fluidization of cell membranes that may facilitate transient pore formation and membrane resealing.

Conclusion: The results show that sonoporation is a powerful method to deliver relatively large molecules in the cytoplasm, with minimal cell damage. However, the transient state of "pore opening" will limit the actual amount of molecules delivered into cells. These results suggest that the development of new agents dedicated to sonoporation is warranted (i.e. loaded with active compound or use of targeted microbubbles). This should improve drug/gene delivery, by increasing the local concentration of molecules at the cell surface.

TARGETING OF MICROBUBBLES: IN VITRO FLOW CHAMBER STUDIES

A.L. Klibanov, J.J. Rychak, A.M. Takalkar, S. Kaul, J.R. Lindner, K. Ley

University of Virginia School of Medicine, Charlottesville VA 22908

In order to improve the design of targeted ultrasound contrast agents, a simple technique is needed to evaluate the ability of ligand-carrying microbubbles to attach to surfaces coated with molecular markers of disease. We have set up a parallel plate flow chamber system to evaluate microbubble targeting in the flowing aqueous medium *in vitro*. This parallel plate setup allows rapid experimental evaluation of the ability of ligand-carrying bubbles to attach to the respective target receptors immobilized on the surface of the 35mm Petri dishes, in a fully controlled setting.

Mouse P-selectin-Fc fusion protein was attached to the surface of polystyrene dishes by adsorption. Site surface densities of the attached protein were assessed using biotinylated anti-P-selectin RB40.34 monoclonal antibody, Eu-labeled streptavidin and time-resolved fluorescence detection. Targeted microbubbles were prepared from decafluorobutane gas stabilized with a monolayer of DSPC, biotin-PEG-DSPE and PEG stearate. Biotinylated RB40.34 antibody was attached to their surface via a streptavidin bridge. Free streptavidin and antibody were removed from the microbubble preparation by centrifugal flotation. Targeted microbubbles were diluted in phosphate-buffered saline and perfused through the flow chamber with the aid of an aspiration syringe pump.

Targeted microbubbles rapidly accumulated on the P-selectin target, as observed by video microscopy. Bubbles did not attach to the control surface without P-selectin. Microbubble accumulation at the target improved with the increase of the surface concentration of P-selectin (3 to 109 molecules/$\square m^2$ range). When the microbubble aqueous dispersion flow rate increased, targeting initially improved, because the number of microbubbles flowing through the target area increased, until a critical wall shear stress has been reached (>0.6 dyne/cm^2 for this system). Above critical shear, microbubble accumulation at the target became less efficient.

When microbubbles were allowed to attach to the target in a temporarily stopped flow, their ability to remain bound to the target surface under subsequently applied shear flow improved considerably: some bubbles were retained on the target despite shear stresses exceeding 80 dyne/cm^2. For each shear rate tested, retention was always greater at the surfaces with higher P-selectin site surface density.

By designing a new generation of targeted bubbles that carry targeting ligands on the extended surface folds, we have improved the ability of these bubbles to bind to P-selectin-coated target surface. In the parallel plate flow chamber tests, wrinkled bubbles demonstrated a statistically significant ($p<0.05$) improvement of the sustained attachment yield as compared with spherical bubbles. Targeted

bubbles, both spherical and wrinkled, retained the ability to scatter ultrasound and could be visualized with a regular medical ultrasound imaging system.

In conclusion, parallel plate flow chamber system serves as a simple inexpensive technique for *in vitro* evaluation of targeted ultrasound contrast materials.

3D LIVE-CELL IMAGING OF MOLECULAR AND CELLULAR ASPECTS OF LOCAL DRUG AND GENE DELIVERY THROUGH ULTRASOUND MICROBUBBLES

René J.P. Musters, Ph.D.

Laboratory for Physiology (ICaR-VU), VU University Medical Center (VUMC), Amsterdam, The Netherlands

Aim of the study – In this presentation a new approach to study molecular and cellular aspects of local drug and gene delivery through ultrasound microbubbles using 3D live-cell digital imaging microscopy (4D-DIM) is evaluated.

Background – Ultrasound contrast agents containing microbubbles have been proposed as a new vehicle for local delivery of drugs and genes. Although several studies have assessed the enhancement of drug and gene delivery by ultrasound microbubbles in animals showing promising results, the exact molecular and cellular mechanism(s) by which this process is enhanced remain(s) to be elucidated.

Methods – 4D DIM of microbubbles and cells was performed on a Marianas™ digital imaging microscopy workstation under full software control (3I, Denver, CO). Sonovue®, a phospholipid-coated ultrasound contrast agent was used. Three different fluorescent dyes were tested using equal concentrations: Oregon-green® 488 wheat germ agglutinine (WGA) conjugate; NBD-PE (N-(7-nitrobenz-2-oxa-1,3-diazol-4-yl)-1,2-dihexadecanoyl-*sn*-glycero-3-phosphoethanolamine, triethylammonium salt), a fluorescent phospholipid (WGA and NBD-PE from Molecular Probes); and a 73 kD rhodamine-dextran conjugate (Sigma). Furthermore, we tested binding of propidium iodide (PI)-labeled DNA to microbubbles.

Results – All fluorescent dyes were found to bind to the Sonovue® microbubbles. WGA Oregon green® showed a homogeneous binding to the microbubbles, however, background fluorescence was markedly present. When using NBD-PE, a clear, less homogeneous staining was observed, with less background fluorescence. Dextran appeared to bind selectively and homogeneously to the microbubbles, resulting in clear staining of microbubbles, with background fluorescence practically absent. In addition, we demonstrated that DNA can be successfully bound to microbubbles. Finally, we explored various possibilities to study microbubble-cell interactions using distinctly labeled microbubbles – with or without molecular cargo – using 4D-DIM.

Conclusion – The development of 4D-DIM in combination with various microbubble labeling techniques offers new possibilities to study the interaction between microbubbles and cells at the molecular level and in real-time.

INTRACELLULAR PRODUCTION OF REACTIVE OXYGEN SPECIES DURING SONOPORATION BY ULTRASOUND AND MICROBUBBLES

Lynda J.M. Juffermans, Pieter A. Dijkmans, René J.P. Musters and Otto Kamp

Laboratory for Physiology and Department of Cardiology (ICaR-VU),
VU University Medical Center (VUMC), Amsterdam, The Netherlands

Aim of the study – We evaluated the effects of intracellular reactive oxygen species (ROS) formation in an *in vitro* rat cardiomyoblast cell line after ultrasound exposure with variable acoustic powers, in the absence and presence of clinically available microbubbles.

Background – Ultrasound microbubbles are a promising technique for both local gene and drug delivery. Transient permeabilization of cell membranes by sonoporation is caused by acoustic cavitation, allowing the uptake of various macromolecules. However, the exact mechanism(s) underlying sonoporation are still unknown. One important intracellular implication may be the generation of ROS. Free radical formation by ultrasound is due to cavitation and depends strongly on its acoustic pressure threshold at specific frequencies. As microbubbles lower the threshold for cavitation, it is likely that in the presence of microbubbles more ROS are generated than when ultrasound alone is applied. ROS are crucial second messengers in normal cell function, however, dramatically elevated ROS levels may also become toxic and can cause significant damage to intracellular proteins, membranes and nucleic acids, leading to direct protein tyrosine nitrosylation, lipid peroxidation and chromosomal alterations, which may – in turn – trigger both necrosis and apoptosis.

Methods – Ultrasound, in the absence and presence of Sonovue™ microbubbles, was applied to atrial rat H9C2 cardiomyoblast cells, using a HP 5500 ultrasound system (Philips) at 1.8 MHz with a mechanical index (MI) of either 0.5 or 0.1 during ten seconds. This was repeated every minute for five times. Intracellular ROS production was measured with the fluorescent dye CM-H_2DCFDA, which is a cell-permeant indicator for ROS that is non-fluorescent until oxidation occurs within the cell. A 3D live-cell digital imaging fluorescence microscope (Marianas™, I.I.I.) was used to both qualitatively and quantitatively assess the formation of intracellular ROS. In addition, 24 hours after ultrasound exposure the cells were stained with Propidium Iodide (PI) and Hoechst 33342 for detection of necrosis and apoptosis, respectively. All probes and antibodies were purchased from Molecular Probes, Leiden, The Netherlands.

Results – Ultrasound alone, either at MI 0.1 or 0.5, did not provoke ROS generation. When microbubbles were present, however, there was a significant increase in intracellular ROS production at both MI 0.1 and 0.5. Interestingly, this ROS production was observed in the cytosol, mitochondria as well as in the nuclei. In addition, we detected a significant increase in both necrosis and apoptosis (as indicated by PI and Hoechst 33342 , respectively).

Conclusion – Microbubbles, cause a substancial increase in intracellular ROS production when ultrasound is applied. This increase is accompanied by morphological evidence of necrosis and apoptosis, especially when ultrasound is applied at MI 0.5. These are important bioeffects of ultrasound microbubbles at relatively low acoustic powers used for diagnostic imaging. Furthermore, even modest intracellular ROS production may contribute to the mechanism of sonoporation.

A MODEL OF NON LINEAR ATTENUATION FOR ULTRASOUND CONTRAST IMAGING

Meng-Xing Tang, Robert J. Eckersley**, J. Alison Noble**

*Medical Vision Laboratory, Department of Engineering Science, Oxford University, U.K.

**Ultrasound Group, Imaging Sciences Department, Imperial College London, U.K.

The attenuation of ultrasound by microbubble contrast agents during propagation is dependent on the acoustic pressure. This is a result of the non-linear acoustic behaviour of the bubbles and is a distinct feature from that of tissue. Modelling the pressure dependent behaviour is critical for ultrasound contrast imaging if accurate quantification of the bubble concentration in vivo is to be achieved. Previous studies have addressed this pressure-dependent attenuation of microbubbles through different models and experimental measurements. However, most of these models are either based on a single bubble or a small group of bubbles so that the acoustic path length is short and attenuation variation over the path length is ignored. In a typical in vivo contrast imaging situation the ultrasound propagates through a significant depth of tissue containing a varying concentration of microbubbles. As a result, the attenuation at a certain point in depth is not only a function of the attenuation properties of bubbles and tissue at this location, but is dependent on other bubbles/tissue along the acoustic path. Therefore it is necessary to take into account in the model not only the pressure-dependent behaviour of microbubbles but also the local variation of pressure dependent attenuation along the acoustic path. In this paper we propose such an attenuation model and provide preliminary validation of this model through single-element transducer experiments.

In this study the pressure-dependent attenuation resulting from a small unit of microbubble population is approximated with a simple relationship to the acoustic pressure. Based on this we develop an attenuation model for a volume of such microbubble population units with a local variation of concentration, in which the effect of the attenuation on the ultrasound propagation is considered. This gives a model of ordinary differential equation with three parameters, in which two parameters characterise the pressure-dependent attenuation for a unit of microbubble population and the third parameter is related to concentration. The model is further expanded to include linear attenuators such as tissue. This finally leads to a mathematical model that is sufficient to gain an understanding of the effects of pressure-dependent attenuation in a bulk volume of bubbles mixed with tissue. In vitro experiments were conducted to provide verification of the model. Dilute suspensions of the microbubble Sonovue™ were insonated using a laboratory ultrasound measurement system, consisting of a pair of broadband 3.5MHz single element transducers contained in a large water bath. Experiments were performed with three levels of bubble concentration and three sample chambers of different acoustic path length. Measurements were fitted to the proposed model to validate it. The results show good agreement between the model-predicted measurements and the real measurements.

The results also suggest that for a low acoustic pressure with little bubble destruction, attenuation of Sonovue™, measured in dB at 3MHz, is linearly related to both its concentration and the insonating acoustic pressure.

COMPARISON OF DIFFERENT MATHEMATICAL MODELS TO ANALYZE CONTRAST DIMINUTION KINETICS IN A FLOW PHANTOM

Karsten Meyer-Wiethe, Hakan Cangür and Günter Seidel

Department of Neurology, University Hospital Schleswig-Holstein, Campus Lübeck, Germany

Background. Ultrasound energy, applied to ultrasound contrast agent (UCA) microbubbles, leads to bubble destruction that can be detected as contrast diminution. Depending on the replenishment of UCA into the sample volume, contrast diminution kinetics is related to organ perfusion. Methods. We performed an in-vitro study with an open-circuit flow model and SonoVue® continuous infusion to analyze the contrast diminution kinetics after harmonic ultrasound application (SONOS 5500, 1.8/3.6 MHz, MI: 1.6) at three different frame rates (2, 4 and 6.67 Hz). Seven flow rates from 4.5 to 36 ml/min (flow velocities in the capillary 0.25 – 2.0 mm/s) were tested. Three mathematical models of the diminution kinetics were compared (linear intensity decrease, exponential decay and a destruction/reperfusion model). Results. In 113 of 126 trials (89.7 %), a signal decrease was observed after ultrasound application. Diminution failure occurred only at higher flow rates (18 – 36 ml/min). The *linear intensity* decrease depended significantly on the flow rate ($p = 0.005$, 0.0009 and 0.0008, respectively, $n = 7$). A sigmoid model could be fitted to the data, defining the slope in the dynamic range of linear dependence for the different frame rates as well as the inflection point. The faster the frame rate, the higher the flow rate at the point of inflection. For the *exponential model*, only the fastest frame rate of 6.67 Hz showed a dependence of contrast half life on the flow rate ($r = 0.94$ $p = 0.03$, $n = 6$). At 2 and 4 Hz, the data was insufficient for curve fitting. The perfusion coefficient derived from the *destruction/reperfusion* model was not related to the flow rate. Conclusion. The linear intensity decrease correlates well with the flow rate (i.e. flow velocity) and defines optimum frame rates for diminution imaging at different flow velocities. The more complicated models requiring curve fitting procedures were not feasible to describe flow in our phantom.

The Usefulness of Accumulated imaging and 3-D for Abdominal Contrast Examination

Hiroshi Hashimoto[1], Masahiro Ogawa[2]

1 Ultrasound Laboratory, GE Yokogawa Medical System, Ltd., Tokyo, Japan

2 The Third Department of Internal Medicine, Nihon University, Tokyo, Japan

HIROSHI.HASHIMOTO@med.ge.com

Purpose : Recently, wider and stronger enhancement is obtained by improved contrast application for high mechanical index (MI) contrast agents. Utilizing 3-D imaging provides information regarding the tumor position and the relationship between the tumor and vessels. However, it can't show the transition of the contrast agent during the examination. In this study, we tried several methods to visualize the transition of the contrast agent, such as inflow and perfusion.

Methods : All contrast images of Levovist were obtained using Coded Harmonic Angio (CHA) on the LOGIQ 7, GE Medical Systems. We tried the following two methods on the PC:

1) Fixed cross sectional images in the contrast examination were acquired for several seconds to the PC. These images were accumulated and displayed the resulting image in a step by step method.

2) Multiple images by sweep scan were acquired. The scanner swept from large vessel to the tumor. The rotational 3-D image (Maximum Intensity Projection; MIP) was reconstructed on the PC and displayed in a step by step method.

Results : We tried these methods for Hepato-Cellular Carcinoma (HCC) and Hemangioma. By the proposed image, the inflow to the tumor was clearly visualized. Of course, for the 3-D image, the scanner must know the flow direction before the contrast examination. However, this 3-D is very useful for comparison to angiography, information sharing, education and informed consent for patients.

Conclusions : New display methods for accumulated image and 3-D were developed for contrast examination to visualize the inflow to the tumor. Although only Levovist is approved in Japan at present, we expect our proposed methods can also be used with Low MI contrast agents as well.

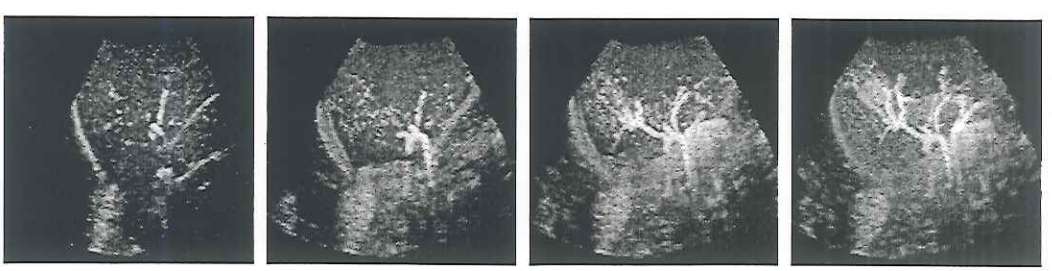

Fig. The inflow visualization to HCC by proposed 3-D (from left to right)

THE BEHAVIOUR OF MICROBUBBLE ULTRASOUND CONTRAST AGENTS IN WHOLE BLOOD

Eleanor Stride and Nader Saffari

Department of Mechanical Engineering, University College London

The size of a typical ultrasound contrast agent particle (CAP) is very similar to that of a human red blood cell (≈ 8 □m diameter). Hence, given the high concentration of cells in blood, the *in vivo* behaviour of CAPs subjected to an ultrasound field might be expected to involve significant CAP-cell interaction. Moreover, the presence of cells is known to be responsible for the non-Newtonian behaviour of blood observed in rheological experiments (Fung 1993). These observations would seem to imply that many of the standard models for contrast agent behaviour (e.g. de Jong 1992, Church 1995) are invalid, since the fluid surrounding the CAPs is almost invariably assumed to be Newtonian. Consequently a number of recent models have employed viscoelastic constitutive equations to describe the surrounding blood (e.g. Allen & Roy 2000, Khismatullin & Nadim 2003).

There are however, a number of physical reasons why the presence of blood cells is in fact less significant than might be expected intuitively. Firstly, the influence of the surrounding fluid upon CAP dynamics is small compared with that of the encapsulating shell (Stride & Saffari 2003). Secondly, cells are poor scatterers of ultrasound compared with CAPs. Thirdly, their physical properties are similar to those of the surrounding plasma; and finally the scale of the flow around an oscillating CAP is very different from that considered in rheological models. New modelling work by the authors indicates that the assumption of a Newtonian fluid can be justified for CAPs insonified in whole blood and may in fact be more appropriate than using non-Newtonian models derived for larger scale flows. These results are supported by the authors' experimental measurements of attenuation in CAP suspensions in plasma and whole blood which display no evidence of CAP/cell interaction (Stride & Saffari 2004).

References:

Allen, J.S., Roy, R.A. J. Acous. Soc. Am. 2000, 107 (6), 3167-3178.

Church, C. J. Acous. Soc. Am. 1995, 97 (3), 1510-1520.

de Jong, N., Hoff, L., Skotland, T., Bom, N. Ultrasonics 1992, 30, 95-103.

Fung Y. Biomechanics, Springer-Verlag, 1993.

Khismatullin, D., Nadim, A. Phys. Fluids 14 (10), 3543-3557.

Stride, E., Saffari, N. Ultrasound in Med. Biol. 29, 2003.

Stride, E., Saffari, N. Ultrasound in Med. Biol. 2004 (submitted).

QUANTIFICATION OF ABSOLUTE MYOCARDIAL, RENAL AND CEREBRAL PERFUSION IN HUMANS USING CONTRAST ENHANCED ULTRASOUND

Rolf Vogel & Christian Seiler

Cardiology, Swiss Cardiovascular Center Bern, University Hospital Bern, Switzerland

Background — Cardio-, neuro- and renovascular diseases cause organ dysfunction by impaired blood flow at the microcirculatory level. The gold standard for the functional assessment of the microcirculation is the quantification of absolute perfusion given in ml/min/g. To date, absolute perfusion in humans can only be obtained by PET (heart, kidney and brain) or MRI (kidney and brain).

Based on a novel volumetric model of ultrasound contrast agent (UCA) kinetics for the interpretation of UCA refill curves following ultrasound-induced microsphere destruction, we developed an algorithm for the measurement of absolute perfusion using contrast-enhanced ultrasound (CEU). Objectives of this study were to validate this algorithm in vitro (1) and in vivo (2) as well as to demonstrate its generalization (3).

Methods — The spatial form of the continuity equation yielded absolute perfusion: □=□·□/□□, where □□ is tissue density. Parameter □and □ indicate the rate constant of rise of the refill curve and the intravascular volume ratio (IVR) and were calculated from refill sequences recorded by real-time CEU during constant UCA infusion. (1) Two hemodialysis filters mimicking the microcirculation (IVR_1=0.327, IVR_2=0.213) were perfused with saline by a calibrated pump at flow rates between 10 and 230ml/min. (2) Regional myocardial perfusion of 15 healthy volunteers was studied by CEU and PET according to the 16 segment model. (3) Regional renal and cerebral perfusion of one healthy volunteer was studied by CEU.

Results — (1) For flow velocities from 0.4 – 8.6mm/s, mean (SD) $□_1$ and $□_2$ were 0.283 (0.028) and 0.219 (0.023) and □ parameters correlated linearly with pump flow Q_{pump} ($r_1^2 = r_2^2 = 0.98$). Spatial integration of □ yielded total phantom volume flow Q_{MCE} that served as an estimate of Q_{pump} (phantom1: $Q_{MCE} = 1.04 \cdot Q_{pump} + 0.56$ml/min, r^2=0.91; phantom2: $Q_{MCE} = 0.90 \cdot Q_{pump} + 0.45$ml/min, r^2=0.96). (2) Perfusion analysis by CEU was successful in 195 of 240 segments. Linear regression analysis showed good agreement between CEU and PET perfusion data ($□_{CEU} = 0.902 \cdot □_{PET} + 0.076$ml/min/g, r^2=0.88, SEE=0.130). (3) Renal cortical and cerebral perfusion was 2.91ml/min/g and 0.91ml/min/g, respectively. These data are in good agreement with published PET and MRI data.

Conclusion — The volumetric model of UCA kinetics provides the basis for absolute perfusion measurements in tissues accessible to ultrasound.

Vascular and Perfusion Imaging with Ultrasound Contrast Agents

Matthew Bruce[1,2], Mike Averkiou[2], Jeff Powers[2], Kirk Beach[1]
[1]University of Washington,[2] Philips Ultrasound

Introduction

Current techniques for imaging ultrasound contrast agents make no distinction between low velocity microbubbles in the microcirculation and higher velocity microbubbles in the larger vasculature. Since most of these contrast imaging techniques make use of multi-pulse acquisitions, Doppler information already exists that might be used to distinguish microbubbles in the larger vasculature from those in the microcirculation. This investigation focuses on a low-MI pulse inversion acquisition to determine if vascular flow can be detected and if this flow can add clinical value to a contrast exam for perfusion. A combination of RF and Doppler filtering on a low-MI pulse inversion acquisition is presented to differentiate higher velocity microbubbles in larger vessels from those in the microcirculation. *In-vitro* and *in-vivo* results are presented. Both fundamental and harmonic Doppler flow signals from microbubbles are compared against conventional power Doppler signals without contrast *in-vivo*.

Despite advances in sensitivity of color flow systems, clinical situations exist where the detection of blood flow in the vasculature is still challenged. Researchers have manipulated methods developed to detect perfusion with microbubbles in order to improve sensitivity to vascular flow. Two general methods have been used to visualize blood flow in larger vessels, using existing contrast agent imaging methods. Low mechanical index (MI<0.12) harmonic techniques have been devised to visualize nearly stationary microbubbles in the microcirculation in real time (frame rates>8Hz). Upon a bolus injection the larger feeding vessels of the vascular tree can be visualized until the microcirculation fills. This provides a momentary glimpse of the larger arterial vessels at the beginning of the bolus (~5-10 sec). Another approach has been to simply raise the MI such that the low velocity microbubbles are destroyed, leaving only microbubbles with high enough velocities in larger vessels to replenish sample volumes. This method destroys agent, relies on a delicate balance of signal and destruction, and is unable to display perfusion information.

Real-time visualization of vascular blood flow with contrast at a low-MI would:

1. enable simultaneous detection of perfusion,
2. simplify detection of vascular flow over current methods.

The display of larger vessels throughout a bolus or infusion would help serve as landmarks during a scan with contrast. Improved vascular visualization over color Doppler would have clinical impact on a number of applications: liver lesion detection and characterization, cancer therapy monitoring, and stroke management.

Theory and Design

A pulse inversion acquisition consists of transmitting N pulses down a ray, where each adjacent pulse is inverted. The resulting affect on the Doppler spectrum is that odd harmonic components are modulated to Nyquist and even harmonic components moving to DC.

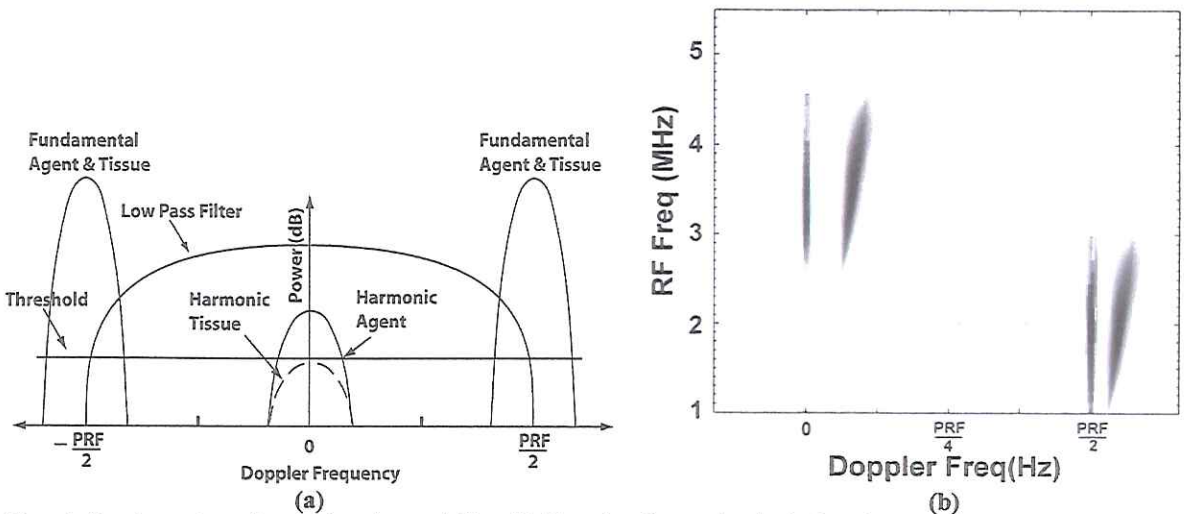

Figure 1. Doppler spectrum of a pulse inversion acquisition with illustration of conventional pulse inversion processing composed of a low pass filter to remove the fundamental and a threshold to remove harmonic tissue.

The detection of nearly stationary microbubbles in the microcirculation is accomplished by a low pass filter to remove the fundamental component (Figure 1(a)). The remaining harmonic tissue can be removed by a simple threshold. The two-dimensional (2D) Fourier transform shows the position of Doppler spectral components in the RF spectrum. Figure 1(b) illustrates the 2D power spectrum of a sample volume containing both stationary tissue with microbubbles and flowing microbubbles. The separation of harmonic and fundamental signals with and without Doppler shifts can be achieved as follows. To detect harmonic signals with Doppler shifts, a bandpass RF filter centered at the harmonic frequency attenuates the fundamental component. A bandpass filter in the Doppler domain removes the remaining stationary second harmonic and fundamental components at DC and Nyquist respectively. The same processing can be used to separate the fundamental vascular flow component.

Results

To test clinical feasibility, a normal volunteer was injected with a typical bolus 0.2 mL of Definity. RF data was collected using a Philips HDI 5000, using a C5-2 curvilinear transducer at a MI of 0.7. Figure 2 shows the perfusion image obtained through conventional pulse inversion processing. The portal vein is visible, but the rest of the larger vasculature is obscured due to microbubbles residing in the microcirculation. Figure 3(a) shows liver images of conventional power Doppler without contrast. Figure 3(b) shows the fundamental vascular flow signal from the same data with contrast used for the perfusion image of Figure 2. The maximum fundamental Doppler

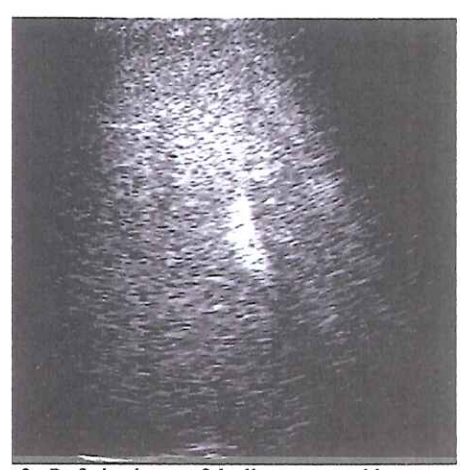

Figure 2. Perfusion image of the liver processed by conventional pulse inversion processing (top signal path of Figure 3) with a displayed dynamic range of 30 dB.

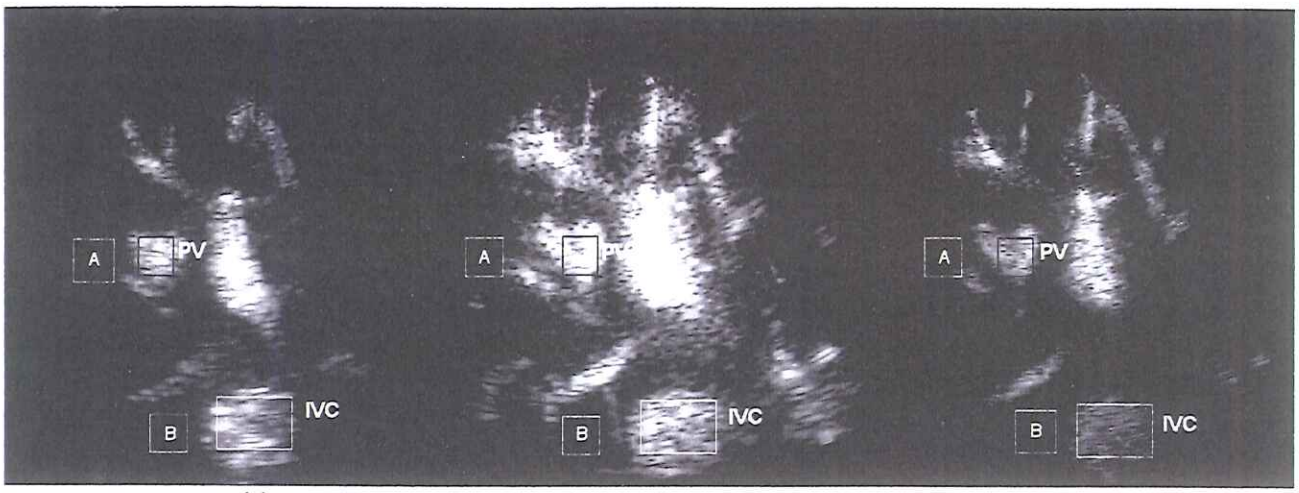

(a) (b) (c)

Figure3. Power Doppler Images of a liver with a dynamic range of 30 dB. The four marked regions are clutter (A) and (B), inferior vena cava (IVC), and portal vein branch (PV). a) Conventional color Doppler without contrast at MI 1.2, b) Fundamental vascular flow with contrast at MI 0.07, c) Harmonic vascular flow with contrast at MI 0.07.

signal is 12 dB higher, Figure 3(b), than the maximum power Doppler signal, Figure 3(a), but also exhibits pronounced blooming around the portal vein and other vessels. Figure 3(c) shows the result of processing for the harmonic flow signal with contrast. The maximum second harmonic Doppler signal is 20 dB below the maximum fundamental signal, but also exhibits less blooming. Table I lists the mean power of the Doppler signal for the regions illustrated in Figure 5. The clutter signals of ROI A and B in Figure 5 are the mean power of the pre-wall filtered signals. The harmonic signal has the lowest clutter levels, but also has the lowest power levels while experiencing the highest attenuation in depth. The fundamental flow signal has the highest signal to noise ratios (SNR) of the three methods, with 30dB less clutter relative to conventional power Doppler. At 9 minutes past injection 35dB and 25dB of fundamental and harmonic vascular signal respectively were seen in the portal vein (largest vessel in the center of images in Figure 3).

TABLE I
MEAN POWER OF THE DOPPLER SIGNAL IN THE FOUR REGIONS MARKED IN FIGURE 4.

Flow Signals	Portal Vein (dB)	Clutter(A) (dB)	IVC (dB)	Clutter(B) (dB)
Fundamental with UCA	29	40	24	30
Harmonic with UCA	18	22	9	12
Power Doppler without UCA	21	72	17	50

UCA-Ultrasound Contrast Agent.

Figure 4 shows the four pulse pulse-inversion acquisition discussed above processed three different ways. The background of Figure 4 in copper is conventional pulse inversion processing as seen in Figure 2. The foreground of Figure 4 in blue illustrates a combination of the fundamental and harmonic flow signals. The combination of the fundamental and harmonic flow signals of Figures 3(a) and 3(b) varies with depth. The second harmonic signal weighted more

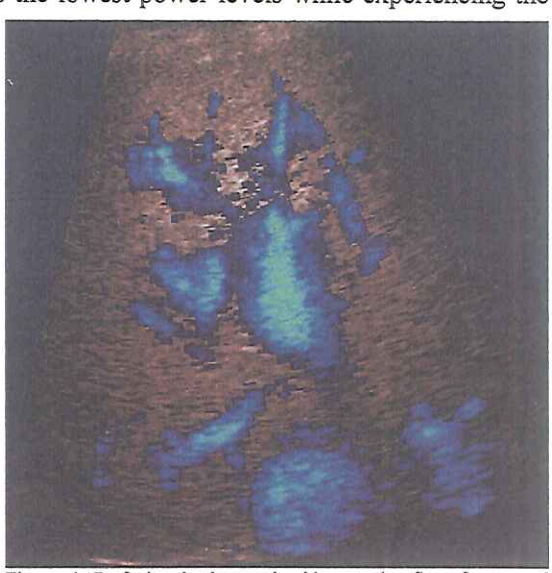

Figure 4. Perfusion background with vascular flow foreground image. Vascular flow component is a varying combination with depth of fundamental and second harmonic signals

at shallow depths with the fundamental flow signal weighted more at the deeper depths. The benefits of both harmonic, less blooming, and fundamental flow signals, better penetration, are utilized together.

Conclusion

Higher velocity microbubbles in the vasculature can be discriminated from the lower velocity microbubbles in the microcirculation, using the same acquisition used for estimating perfusion in real-time. The signal to clutter ratios for both the fundamental (-11 dB) and harmonic (-4 dB) vascular flow signals were greater than conventional power Doppler (-51 dB) without contrast agents (Table I). The fundamental Doppler signal from microbubbles exhibited the greatest SNR and penetration, but experienced blooming around large vessels not observed in the harmonic signal. A depth varying use of both components moderates the clutter and blooming artifacts of the fundamental Doppler signal at shallower depths and the penetration deficiencies of the harmonic Doppler signal at deeper depths. These favorable signal-to-clutter ratios and SNRs suggest that even at a low-MI, the performance of these vascular flow signals with contrast could be clinically superior to that of color flow without contrast. This method simplifies the visualization of vascular flow and adds additional information to a conventional contrast exam for perfusion.

QB-MODE ULTRASONIC IMAGING: A NEW METHOD FOR IMAGING QUADRATIC SIGNAL COMPONENTS

Pornchai Phukpattaranont and Emad S. Ebbini

Department of Electrical and Computer Engineering
University of Minnesota, Minneapolis, MN 55455, USA

We have recently validated the use of a second-order Volterra (SVF) model for separating the linear and quadratic components of the beamformed radio frequency (RF) data in pulse-echo ultrasonic imaging. The model separates the signal into its linear and quadratic components. The quadratic component captures the second order nonlinearities in the echo data. Grayscale images from the quadratic component, referred to as QB-mode images, typically have higher contrast and increased dynamic range than the standard B-mode images (without loss in spatial resolution). An algorithm for finding the coefficients of the SVF based on a linear plus quadratic prediction model of the RF data was developed and validated in a variety of imaging situations, including *in vivo*. The quadratic kernels used for filtering the RF data for producing QB-mode images can be derived to minimize the prediction error (in a least-squares sense) and/or to maximize the contrast of a perceived contrast target. The latter criterion is particularly useful for imaging with ultrasound contrast agents (UCAs). We describe a new approach to derive the coefficients of the quadratic kernel for maximum contrast and the application of this approach to imaging UCAs in a flow phantom and *in vivo*. In addition, the new approach allows for a computationally-efficient separable implementation of the 2D quadratic kernel, which leads to real-time implementation of QB-mode imaging on the current generation of ultrasonic scanners. Results from the real-time implementation of the separable form of the quadratic kernel have been obtained and will be shown.

This research is funded by a grant from Esaote, S.p.A., Genoa, Italy.

QUANTITATIVE CONTRAST ULTRASOUND TO MEASURE THE EFFECTS OF ANTI-ANGIOGENIC AND ANTI-VASCULAR THERAPIES FOR CANCER

Raffi Karshafian, Xiuling Qi, Peter N. Burns

Department of Medical Biophysics, University of Toronto, Sunnybrook & Women's College Health Sciences Centre, 2075 Bayview Avenue, S6 39, Toronto, Ontario, Canada, M4N-3M5

Objective: Imaging modalities that can measure blood flow in tumours and the changes resulting from treatment by anti-vascular agents will play a central role in the evaluation and assessment of a new generation of anti-angiogenic therapies for cancer. In this study, the effects of ZD6126 (AstraZeneca), a tubulin-binding agent that targets the endothelial cells of the neovasculature, are measured using ultrasound contrast microbubble perfusion imaging techniques.

Methods and Materials: Twenty New Zealand White rabbits, 3.5-4.5 kg in weight, were implanted with VX2 tumours within their thighs – 10 were treated with 30 mg/kg of ZD6126 and 10 were used as controls. Contrast imaging was performed using Definity (BMS, Boston MA) and HDI 5000 system (ATL Ultrasound, Bothell, WA). Microbubble disruption-reperfusion data were acquired in pulse inversion mode (L7-4 transducer) with high MI (MI > 0.9) intermittent triggered imaging at pretreatment baseline, then at 4, 24 and 72 hours following injection of the anti-vascular drug. The microbubbles were administered by steady infusion into the ear vein. Ultrasound induced disruption of contrast microbubbles and their replenishment were analyzed offline (HDI Lab, ATL/Phillips Ultrasound). Three regions of interest (ROI) were positioned within the tumour – the interior, the periphery and an ROI enclosing the whole tumour. The resulting reperfusion curve of each ROI was fitted to a mono-exponential function of the form $S(t) = A(1- e^{-\beta t})$, where A is the relative vascular volume, and β is the rate constant.

Results: Microbubble disruption-reperfusion imaging of VX2 tumours detected a significant reduction in blood volume and flow rate within 4-24 hours following injection of the anti-vascular drug ZD6126, followed by a recovery by 72 hours. The vascular volume and flow rate of the VX2 tumours treated with ZD6126 relatively decreased in the three ROIs compared to the control group. The interior vascular volume of the treated tumour decreased (-35% relative to baseline) compared to the control group (+75%), however, it recovered by 72 hours (+50%). The peripheral vascular volume of the treated tumour increased by 28% at the 4 hour point compared with 92% increase of the control tumour. At the 24 hour point, the peripheral vascular volume decreased (-28%) compared to the 4 hour point. The vascular volume of the whole tumour showed a similar response. The volumetric flow rate of the treated tumour decreased (-85%, -54% and –74%) at the 4 hour point in the interior, peripheral and whole tumour ROI. Within 72 hours, the flow rate recovered.

Conclusion: Pulse inversion contrast imaging with the microbubble agent Definity is capable of monitoring blood flow and blood volume of tumours undergoing anti-vascular therapy. The tubulin rounding agent ZD6126 causes an acute reduction in tumour blood flow and volume within 24-72 hours of a single bolus administration. This method may a suitable for use in clinical trials of anti-vascular and anti-angiogenic therapies, providing a unique method for the non-invasive monitoring of haemodynamic effect in superficial tumours such as those in breast cancer.

BUBBLE MICROSTREAMING NEAR A BOUNDARY, DIRECT OBSERVATION WITH BRANDARIS 128

Philippe Marmottant, Michel Versluis, Nico de Jong, Sascha Hilgenfeldt and Detlef Lohse*

Physics of Fluids group, University of Twente, The Netherlands
*Department of Experimental Echocardiography, Erasmus Medical Centre, Rotterdam, The Netherlands

Drug delivery and gene transfer into cells rely on the poration of the cells' lipid membranes. Efficient and localized poration has been achieved using the forces exerted on the cell wall by the oscillations of ultrasound-driven microbubbles. To elucidate the physics behind this phenomenon, we developed a setup for controlled study of the interaction of single microbubbles with other objects like cells or lipid bilayer vesicles of known mechanical properties.

Microscopic observations show vivid liquid motion near a bubble, due to acoustic streaming. The high shear rates in the flow lead to dramatic deformations of lipid vesicles, enough to obtain break-up. We study the motion in detail, both the non-linear, steady streaming flow component and the primary flow oscillating at the sound frequency. The latter is captured with the ultra high-speed camera Brandaris 128 at 4 million fps. We are able to distinguish two types of oscillations: the radius pulsation, and a periodic translation of the bubble center, slightly out of phase with the first one. The phase shift is a consequence a self-induced Bjerknes force, created by the presence of the wall. We show that the wall exerts a force identical to that exerted by an "image" bubble. The out-of phase superposition of these oscillations is essential for the observed efficient microstreaming.

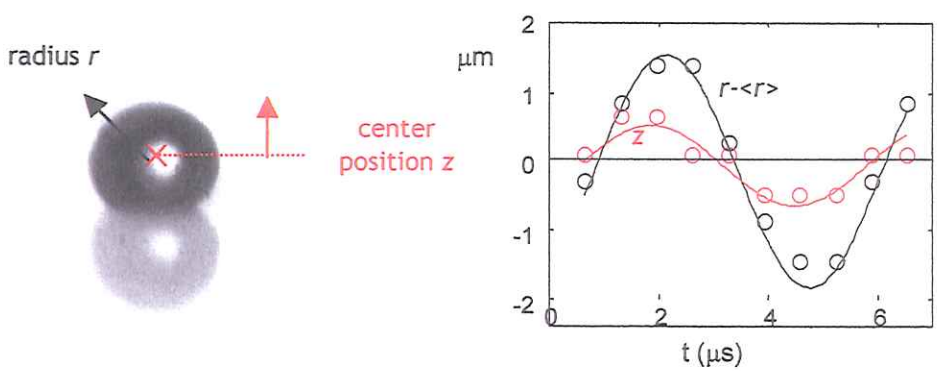

Bubble (and its image) on a glass wall:
pulsation of the radius and periodic translation of the bubble center.

Impulse Response Estimation of Ultrasound-Contrast-Agent Dilution Systems for Cardiac Parameter Measurements

M. Mischi[1], A.H.M. Jansen[2], A.A.C.M. Kalker[1], H.H.M. Korsten[1;3]

1- Technical University Eindhoven (The Netherlands) 2- Dept. of Cardiology and
3- Dept. of Anestesiology and Intesive-Care of the Chatharina Hospital Eindhoven (The Netherlands)

The dilution of Ultrasound Contrast Agents (UCA) is usually interpreted by means of indicator dilution models, such as gamma, lognormal, compartmental, or random walk models [3][8]. However, in the low contrast concentration range, the contrast dilution system is linear, therefore, it is characterized by its impulse response.

This study presents a new approach for the analysis of UCA dilution curves. A small dose of contrast is peripherally injected. Indicator Dilution Curves (IDCs) are measured by video or acoustic analysis of the B-mode output of an ultrasound scanner. The scanner is set in power modulation mode in order to enhance the signal backscattered by the contrast. Several IDCs are measured in different sites in the central circulation. A Wiener deconvolution technique is implemented to estimate the impulse response between the selected sites [2]. The choice for a least squared error deconvolution technique is due to the small signal-to-noise ratios (SNR) of UCA dilution curves. Specific models are then adopted to analyze the estimated impulse response. Many clinical parameters can be assessed by the estimation of impulse responses from different sites.

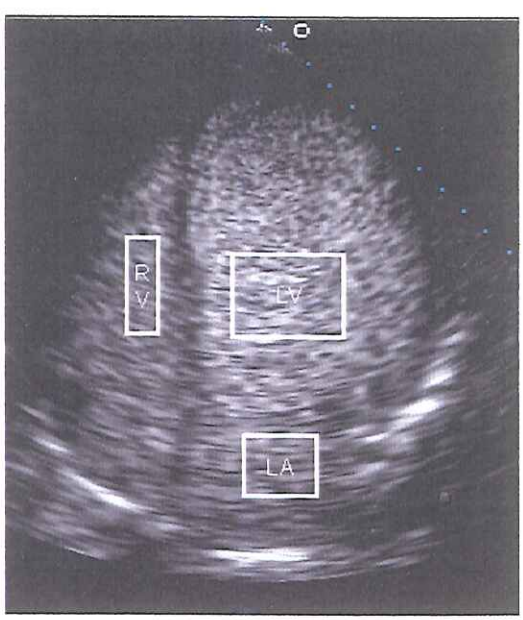

Fig. 1 – Trans-thoracic four chamber view of the heart after a SonoVue® (Bracco Diagnostic) 0.25mg bolus injection. Three regions of interest are placed on the RV, the LA, and the LV for the IDC measurements.

In this study we present two applications: the assessment of the Pulmonary Blood Volume (PBV) and the assessment of the Left Ventricle (LV) Ejection Fraction (EF).

For the PBV assessment, two IDCs are measured in the Right Ventricle (RV) and in the Left Atrium (LA) (see Fig. 1). As shown in Fig. 2 and Fig. 3, the implemented Wiener deconvolution algorithm is robust to small signal-to-noise ratios and identifies the impulse response of the system between RV and LA.

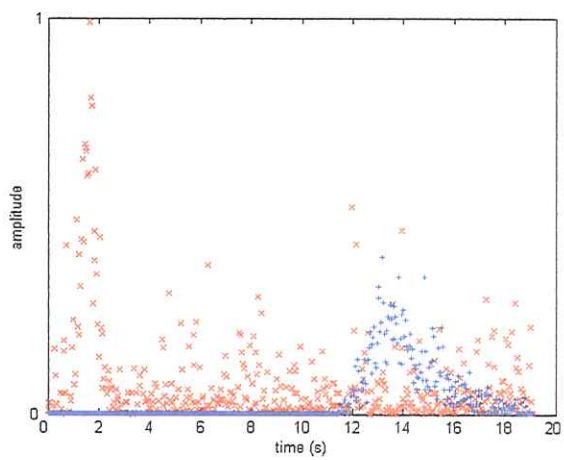

Fig. 2 – Two IDCs with small SNR are measured in the RV and the LA.

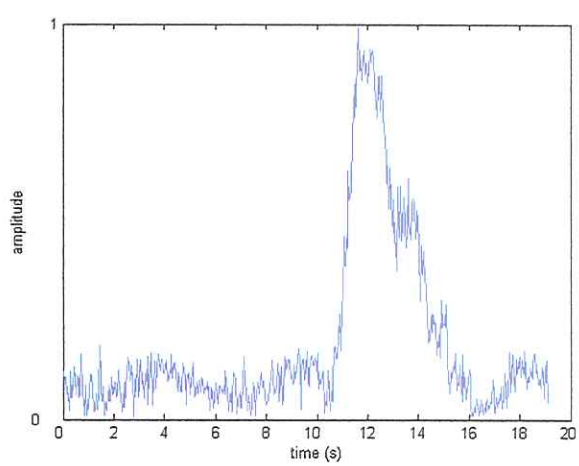

Fig. 3 – Estimated impulse response of the dilution system between the RV and the LA.

$C(t)$ is the IDC, M is the injected mass of contrast, Q is the volumetric flow of the carrier fluid, μ is the time that elapses at the carrier velocity to cover the distance between injection and detection site, and λ represents the skewness of the curve.

The use of a model is necessary to overcome the low signal-to-noise ratios (SNR) and contrast recirculation issues. A specific fast and accurate least-square fitting algorithm is adopted [4]. MTT, RV EF, and LV EF are derived from the fitted model.

The MTT is equal to the parameter μ of the fitted LDRW model.

The EF assessment can be derived from the fitted model too, resulting in an increase of accuracy with respect to the usual technique, which considers the contrast concentration C at two subsequent systoles as given in Eq. (2).

$$EF = 1 - \frac{C_{n+1}}{C_n} \tag{2}$$

In fact, this approach assumes a sudden injection of the complete contrast bolus in the ventricle, which is washed out by the cardiac action.

If the contrast is peripherally injected, such a hypothesis is true only after infinite time, i.e., when no more contrast enters the ventricle. The IDC fitting for large time values fails due to the extremely low SNR. The problem is overcome if the limit of the LDRW model fit for t going to infinite is considered. The result, which represents the EF when the contrast is injected all at once in the ventricle, is given as in Eq. (3), where Δt is heart beat period.

$$EF = 1 - \frac{C_{n+1}}{C_n} = \lim_{t\to\infty}\left\{1 - \sqrt{\frac{t_n}{t_{n+1}}}\, e^{\frac{\lambda}{2}\left[\left(\frac{t_n}{\mu}-\frac{\mu}{t_n}\right)-\left(\frac{t_{n+1}}{\mu}-\frac{\mu}{t_{n+1}}\right)\right]}\right\}$$

$$\Rightarrow EF = 1 - e^{-\frac{\lambda \Delta t}{2\mu}} \tag{3}$$

The volume measurement is validated by in-vitro experimentation [5]. A Sonos 5500 ultrasound scanner is used to detect SonoVue® contrast agent IDCs. The scanner is set in power modulation mode at 1.9MHz. The results in Fig. (3) show very accurate volume measurements with a determination coefficient larger than 0.999. The standard deviation is smaller than 1.8% of the volume for a wide range of flows (from 1L/min to 5L/min).

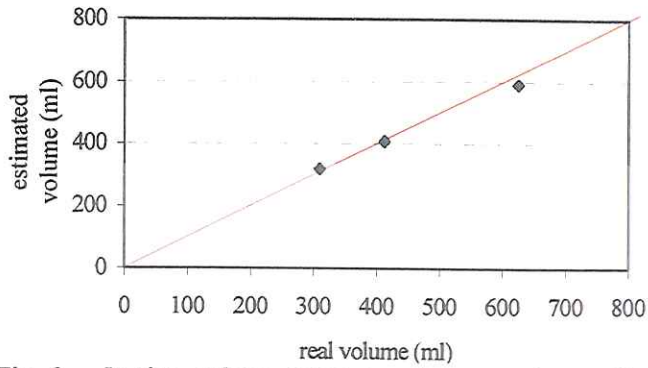

Fig. 3 – In-vitro volume measurements averaged over five flows from 1L/min to 5L/min.

The EF measurement is validated in patients. A small bolus of 0.25mg of SonoVue® is injected in an arm vein and detected in the LV by a trans-thoracic ultrasound transducer. The ultrasound scanner setting is the same as for the in-vitro volume measurements. The results are compared to those obtained by bi-plane Simpson integration. The results show a clear correlation between the two measurements with a correlation coefficient equal to 0.97 (see Fig. (4)).

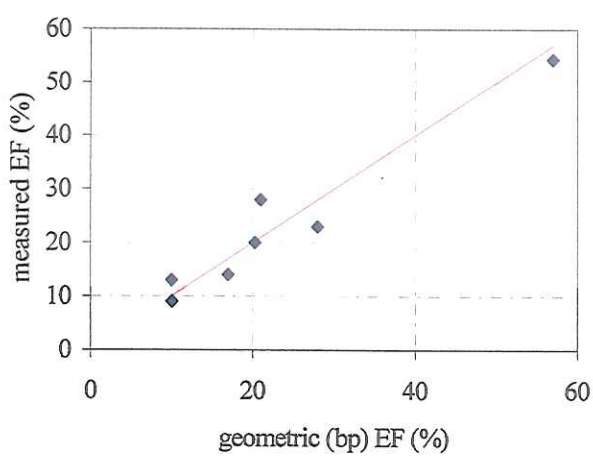

Fig. 4 – In-vivo LV EF measurements compared to bi-plane Simpson integration.

Also the PBV assessment system has been tested in patients with promising results. CO is measured by aortic echo-Doppler.

The Local Density Random Walk model is used to fit the impulse response [3][6][7]. The mean transit time of the contrast between the RV and the LA is derived from the fitted model and multiplied times the blood flow (cardiac output) [4][5]. The result is the PBV estimate. The cardiac output can be measured by echo-Doppler time integration in the aorta.

The volume measurements are validated in-vitro with excellent results. Fig. 4 shows the in-vitro measurement of three different volumes with a flow varying from 1L/min to 5L/min. The correlation coefficient is higher than 0.999 and the standard deviation of the measurements is smaller than 2.7% of the volume. The system has been also applied in patients with promising results.

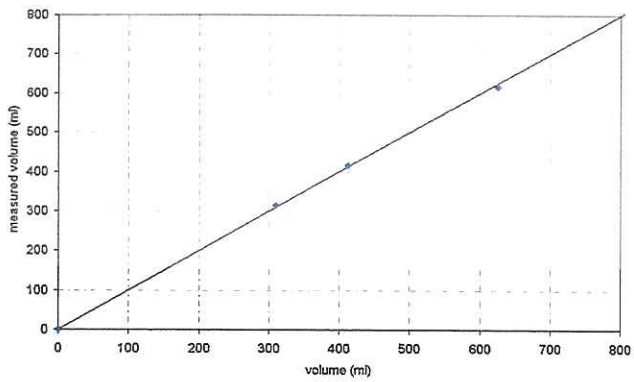

Fig. 4 – In-vitro volume measurement results. The average measurements over five different flows (from 1L/min to 5L/min) are shown.

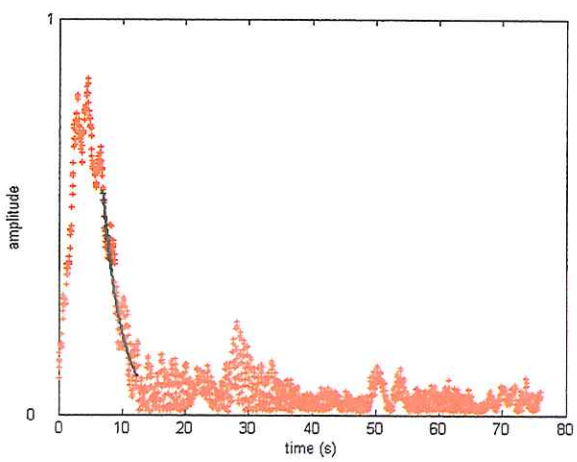

Fig. 5 – Impulse response estimate of the LV dilution system. An exponential curve is fitted for the EF measurement.

The EF measurement is tested in-vivo. Two IDCs are measured in the LA and the LV. The estimated impulse response corresponds to the LV IDC after a theoretical rapid injection of the contrast right in the LV. This allows measuring the EF by Eq. (1), which is derived when the contrast leaves the ventricle without being replaced [1].

$$EF = 1 - \frac{C_{n+1}}{C_n} \qquad (1)$$

C_n and C_{n+1} represent the concentration in the LV at two subsequent systoles. Since the impulse response of a one-compartment system is given by an exponential decay [7][8], C_n and C_{n+1} in Eq. (1) may be substituted by the exponential fit of the estimated impulse response of the LV. The EF is then measured as given in Eq. (2), where τ is the time constant of the fitted exponential curve and Δt is the cardiac cycle period.

$$EF = 1 - \frac{C_{n+1}}{C_n} = 1 - e^{-\frac{\Delta t}{\tau}} \qquad (2)$$

Fig. 5 shows the exponential fit of a LV impulse response. The EF measurements are compared to those measured by bi-plane Simpson integration from the echo videos. 12 validation measurements are performed and the resulting correlation coefficient equals 0.98.

In conclusion, impulse response estimations of the UCA concentration are feasible even for low SNR. Moreover, they allow a minimally invasive measurement of several parameters, such as the PBV and the LV EF. The results are promising and encourage further validation and investigation for new applications.

REFERENCES

[1] L. A. Geddes, "Cardiac Output Measurement," The biomedical engineering handbook: second edition, Ed. Joseph D. Bronzino, Boca Raton: CRC Press LLC, 2000

[2] Peter A. Jansson, "Deconvolution of images and spectra," Academic Press, 1997

[3] M. Mischi, A.C.C.M. Kalker, H.H.M. Korsten, "Videodensitometric Methods for Cardiac Output measurements," Eurasip Journal on Applied Signal Processing, vol. 2003, no. 5, April 2003

[4] M. Mischi, A.H.M. Jansen, A.A.C.M. Kalker, H.H.M. Korsten, "Intra-Thoracic Blood Volume Assessment by Dilution of Ultrasound Contrast Agents," IEEE-UFFC Proceedings on the IEEE International Ultrasonics Symposium, Honolulu (Hawaii), 5-8 Oct. 2003

[5] M. Mischi, A.A.C.M. Kalker, H.H.M. Korsten, "Blood Volume Measurements by Videodensitometric Analysis of Ultrasound-Contrast-Agent Dilution Curves," IEEE-EMBS Proceedings on the 25th Annual International Conference of the IEEE Engineering in Medicine and Biology Society, Cancun (Mexico), 17-21 Sept. 2003

[6] K.H. Norwich, "Molecular dynamics in biosystems," Pergamon Press, 1977

[7] E.A. Reth, J.M. Bogaard, "Comparison of a two-compartment model and distributed models for indicator dilution studies," Med. & Biol. Eng. and Comput., vol. 21, pp. 453-459, 1983

[8] C. Xucai, K.Q. Schwarz, D. Phillips, S.D. Steinmetz, R. Schlief, "A mathematical model for the assessment of hemodynamic parameters using quantitative contrast echocardiography", IEEE Trans. on Biom. Eng., vol. 45, no. 6, 1998

CAN COLOR DOPPLER BEFORE AND AFTER CONTRAST PREDICT THE QUALITY OF HIFU-INDUCED NECROSIS IN THE PROSTATE?

O. Rouvière, L. Curiel, J.Y. Chapelon, R. Ecochard, R. Bouvier, A. Gelet, D. Lyonnet

BACKGROUND: Tissue blood perfusion influences the results of some hyperthermia and thermotherapy procedures, but its role in the outcome of prostate cancer treatment by High Intensity Focused Ultrasound (HIFU) has not been evaluated yet. We evaluated preoperative prostate Color Doppler as a predictor of the efficacy of HIFU treatment.

METHODS: Thirty-five patients underwent pre- and post-contrast Color Doppler (CD) examination of the prostate before HIFU treatment. Specific software was used to calculate, on CD images, the Color Pixel Density (CPD) and the Specific Flow (SF, i.e. Mean velocity x CPD) in different regions of interest. Post-treatment sextant biopsies were obtained in 31 patients, 5.8 2.8 months after HIFU treatment.

RESULTS: No significant correlation was found between the quality of HIFU-induced necrosis observed on control biopsies and the pre-treatment CPD/SF values in any region of interest, either before or after contrast injection. On the other hand, history of radiation therapy was significantly associated with homogeneous necrosis and history of hormone therapy was significantly associated with incomplete necrosis.

CONCLUSION: Color Doppler cannot predict the quality of HIFU-induced necrosis. History of radiation therapy was found to be a factor of favourable prognosis and history of hormone therapy was found to be a factor of poor prognosis in our population.

Acknowledgment: This work was made in the scope of the concerted action contract no. QLK6-CT-2002-02174.

THREE DIMENSIONAL LEFT VENTRICULAR OPACIFICATION AND MYOCARDIAL CONTRAST ECHOCARDIOGRAPHY

Janice Frisa, McKee Poland, Karl Thiele, Pat Rafter

Philips Medical Systems, Andover, MA, United States

Myocardial Contrast Echo (MCE) has reached the critical threshold allowing for clinical validation against gold standards such as SPECT and angiography. The first ever Phase III trial for MCE is concluding and hopefully soon this will be followed by FDA approval and routine clinical adoption. Very recent advancements in transducer and system technology promise to open even more opportunities, as the possibility for 3D perfusion gets closer to reality.

We have reached a point where transducer and system technology have made real-time 3D beamforming and rendering a reality on standard ultrasound equipment. Last year, Philips Medical Systems introduced a fully sampled 2D array (the x4 Matrix transducer) and system (the SONOS 7500) that produces high quality volume rendered 3D images at a 20+Hz frame rate. This transducer has an interconnection scheme to connect ~3000 acoustic elements to ASICS within the transducer handle. The ASICS process the resulting acoustic signals funneling them down to a manageable 128 signals to be further processed by a standard ultrasound system.
Use of all elements leads to much improved 3D image quality compared to prior sparse matrix solutions. Philips' "x4" matrix transducer uses technology that offers extremely wide bandwidth and thus enables harmonic imaging. System improvements also allow real-time volume rendering and 3D images can be easily rotated and cropped to obtain different views from the same dataset.

3D Left Ventricular Opacification

This new 3D technology has many clinical possibilities, one of the most exciting of which is the combination with contrast. The ability to quickly acquire a full 3D volume or two planes simultaneously has great potential for quicker and more accurate stress echoes[1] as well as for more accurate LV volume calculations with echocardiography. Early results with harmonic imaging and contrast have shown that just like in 2D imaging contrast can help immensely in the discrimination of the border in 3D.

The recent addition of an LVO setting and new triggering capability in 3D on the SONOS 7500 allow for 3D LVO and 3D MCE research to begin. Dual triggering has been added to Full Volume mode. By adding a Dual trigger feature in Full Volume mode it is possible to get the end Diastolic and end

Systolic Image only. This helps eliminate apical destruction of contrast creating a better, more robust delineation of the border. This will help in any segmentation algorithm done later.

3D/Biplane Myocardial Contrast Echo

Not everything is known and understood in terms of the best way to use Matrix and Live 3D technology for perfusion imaging. There are questions to be answered regarding the replenishment kinetics when going from a plane of destruction to a volume of destruction. LV cavity destruction will be much greater with a volume of destruction and this will significantly decrease the concentration of microbubbles available for replenishment. Also, contrast destruction in larger intramyocardial arteries and epicardial coronary arteries that were previously out of the scan plane with conventional 2D imaging techniques will further "choke" off supply of microbubbles. These effects are expected to alter the observed velocity or "beta" term in a curve fit - a parameter that has yielded great success in terms of improving diagnostic accuracy of MCE studies.

The biplane feature allows simultaneous acquisition of two planes and offers a step between traditional 2D imaging and Live 3D. Biplane imaging also has triggering capabilities with manually adjustable rotation and tilt between the two intersecting planes. A recent enhancement to biplane imaging is the addition of an "elevation tilt" feature, to allow for acquisition of multiple non-intersecting planes of data. Some initial results using biplane triggered harmonic MCE imaging will be discussed.

Matrix technology offers the ability to transmit and receive data in arbitrary directions with arbitrary apertures and foci and has important implications for improving contrast detection techniques for MCE. This can lead to the creation of a more uniform power field including better penetration. This will not only lead to the ability to acquire views not traditionally acquired before but will allow data to be acquired more quickly. This promises to lead to shorter studies and potentially more accurate diagnosis. Although there are challenges to overcome in maintaining a high enough frame rate with multi-pulse techniques and large volumes, the ultimate goal of measurement of myocardial mass at risk is closer to becoming a reality.

1. Lissa Sugeng, MD, Jim Kirkpatrick, MD, Roberto M. Lang, MD, James E. Bednarz, BS, Jeanne M. DeCara, MD, Georgeanne Lammertin, RCVT, Kirk T. Spencer, MD.
Biplane stress echocardiography using a prototype matrix-array transducer.
Journal of the American Society of Echocardiography; Sept 2003 volume 16(# 9); pages 937-941.

NEW CONTRAST IMAGING METHOD BASED ON DOUBLE FREQUENCY INSONIFICATION: PRELIMINARY RESULTS

Ayache Bouakaz and Nico de Jong

Erasmus Medical Center, Exp Echo, Rotterdam The Netherlands and ICIN Utrecht The Netherlands

Introduction: Ultrasound contrast agents (UCA) are indicated for use for left ventricular opacification and for enhanced endocardial border delineation. However still substantial research efforts are undertaken to use UCA for assessment of myocardial perfusion. New contrast imaging methods such as Pulse inversion and power modulation are now effectively used for LVO but have shown limited success to detect myocardial perfusion during echocardiographic examinations. The ultimate perfusion technique should be able to ascertain the suppression of the strong (linear or nonlinear) tissue echoes while bringing more in front the bubbles' echoes.

We present in this study preliminary results of a new imaging technique, which is capable to detect echoes only from UCA and damp or eliminate those emanating from non-oscillating structures such as tissues. The method is based on blending two frequency components, a low frequency component signal called the conditioner or modulator signal and a high frequency component signal called the imaging or detection signal. The low frequency signal is used to modulate the size of the bubbles by making them vibrate. The high frequency signal, blended to the low frequency signal, is used to interrogate the modulated bubbles or in other terms to image the local oscillations of the gas bubbles as induced by the low frequency signal.

Method description: The advantage of mixing the LF signal to the HF signal resides in the fact that the LF signal will alter the properties of the gas bubble mainly its size between its compression (positive cycle of the pressure signal) and rarefaction (negative cycle of the pressure signal) phases. This change in bubble size is due to the bubble oscillations. The LF signal will make the bubble expand in the negative (rarefaction) phase of the signal and shrink in the positive (compression) phase of the low frequency signal. During these two phases of the LF signal where the bubble size has been modified, the HF signal is used to image the bubble. Hence, the HF signal will sense the same bubble but at two different stages: small and large size depending on the phase of the low frequency signal. During the expansion phase (rarefaction of the low frequency signal), a larger bubble is insonified with the high frequency signal and during the shrinkage phase (compression of the low frequency signal), a smaller bubble is insonified with the high frequency signal. Consequently the response of the gas bubble to the HF imaging signal will be different from the positive to negative cycles of the conditioning signal. However when non-oscillating scatterers (such as tissue) are present, the response will be identical in both phases of the conditioning LF signal since these scatterers do not oscillate.

This finding will increase the distinction between gas bubbles and tissue usually termed contrast to tissue ratio compared to other existing methods.

Experiments and simulations: Ultra-fast optical observations of bubbles insonified simultaneously at two different frequencies were carried out using the "becoming popular" Brandaris. To interrogate the bubbles at 2 different frequencies, two different transducers were used. The transducers had center frequencies of 0.5MHz and 3.5 MHz. The transducers were mounted in a Plexiglas container and positioned such that their focal distances coincide at a depth of 75mm. The optical observations were carried out at a frame rate of 14 millions frames per second and 128 successive frames were recorded. A bubble of 4mm diameter was observed oscillating under the effects of both 0.5 and 3.5MHz signals. Figure 1 shows the filtered radius-time curves around 0.5MHz and 3.5MHz frequencies. As the figure shows, up to 3□s, the 0.5MHz signal amplitude is low and therefore the vibration of the bubble during this period of time is weak. The compression and expansion phases of the bubble are small meaning that the bubble diameter did not change significantly between the compression and rarefaction phases. Consequently the vibrations of the bubble at 3.5MHz are about equal between the 2 phases. However beyond 3□s, the 0.5MHz signal amplitude has increased which is demonstrated by stronger vibrations of the bubble. The bubble radius compresses to about 3□m and expands up to 6 □m. During these oscillations, the 3.5 MHz imaging signal interrogates thus the same bubble but that has a variable size. This is clearly seen in the bubble vibrations at 3.5MHz during the positive and negative cycles of the 0.5 MHz conditioner signal. The decorrelation between the compression and expansion phases of the LF signal in the 3.5MHz bubble response is significantly high to be used as a parameter to detect gas bubbles and discriminate between oscillating structures (contrast bubbles) and non-oscillating structures (tissues).

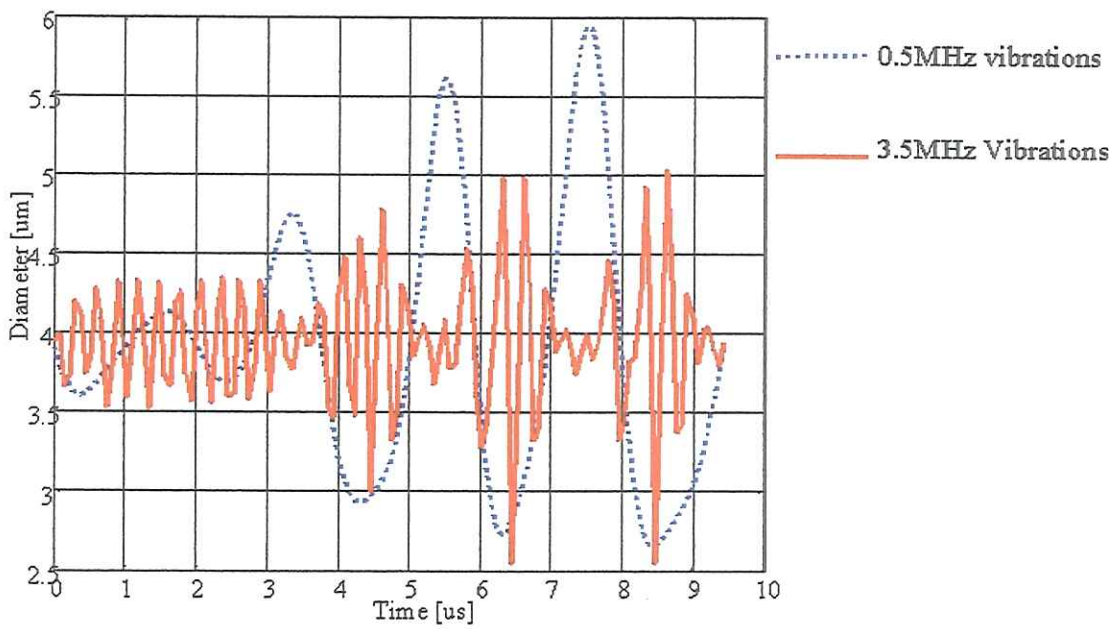

Figure 1: Brandaris observations of bubble vibrations with double frequency insonification; dashed: RT curve at 0.5MHz, solid: RT curve at 3.5MHz.

In addition, simulations were carried out using the modified Herring equation. The purpose was the evaluation and comparison of the performances of this new method against pulse inversion. The results showed that the double frequency insonification increases the contrast to tissue ratio by more than 10dB compared to pulse inversion.

Conclusions: The preliminary results demonstrate the feasibility of this approach in improving the contrast to tissue ratio compared to current contrast detection methods.

SURFACE MODES OF ULTRASOUND CONTRAST AGENTS

Michel Versluis, Sander van der Meer, and Detlef Lohse
Physics of Fluids, University of Twente, Enschede, The Netherlands

Chien Ting Chin, Dave Goertz, Peggy Palanchon, and Nico de Jong
Experimental Echocardiography, Erasmus MC, Rotterdam, The Netherlands

Bubbles insonified by ultrasound will generally exhibit a radial oscillation mode. In addition, surface waves can be generated through instabilities at the interface of the liquid medium and the gaseous content of the bubble. These so-called surface modes have been studied extensively for droplets and millimeter-sized bubbles generated through needle injection [1]. Here, we investigate surface waves generated by ultrasound excitation of individual unencapsulated micron-sized bubbles. In addition, we will present surface modes (n = 2 and 3) observed for phospholipid-coated ultrasound contrast agents excited through excitation of radial modes at frequencies between 1 and 4 MHz. Even higher modes of vibration (up to mode 6) are observed for coated microbubbles at insonation frequencies of 10 and 19 MHz. The potential relevance of surface modes for medical ultrasound will be discussed, including the possible implications for current theoretical models of ultrasound contrast agents.

Single air bubbles with diameters ranging from 30 μm to 120 μm were generated in a regulated co-flow micropipette injector [2]. The injector allowed for a controlled production of microbubbles, both in diameter and in separation distance. The bubbles were left to rise to the test section at a downstream distance of 4 cm from the injector. The bubbles were insonified with a pulse of ultrasound from a flat transducer consisting of a burst of 6 cycles at a frequency of 130 kHz. The dynamics of the free air bubbles was recorded with an ultra high-speed camera [3] at a frame rate of 1.25 million frames per second. Figure 1 shows a selection of the observed vibration modes for these bubbles.

Phospholipid-coated microbubbles contained in a 150 μm diameter fiber were subjected to ultrasound from a focused transducer at low (1-4 MHz) and high frequencies (10 and 19 MHz). The experiments were conducted with mechanical indices in the range of 0.1-0.6. The dynamics of the contrast agents were recorded with the Brandaris camera at a frame rate of 16 million frames per second for the low

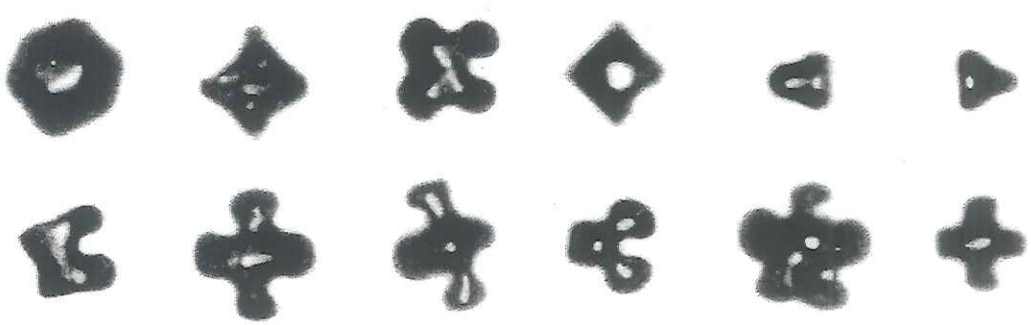

Figure 1. A selection of surface modes observed for free air bubbles with a diameter ranging from 30 to 120 μm. The preferred mode of vibration is linearly dependent on the initial radius R_0 and is independent of the applied pressure.

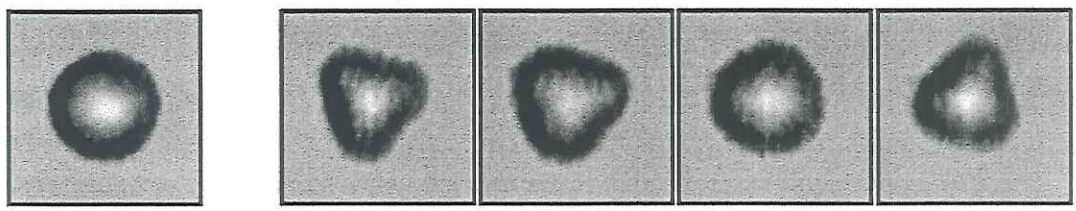

Figure 2. Mode vibrations for a Sonovue™ bubble with a diameter of 4 μm. Here a mode n = 3 is observed, however a range of modes is observed for a transmit frequency of 3.5 MHz.

frequency experiments. A strobe technique was used to record the vibration modes of the microbubbles in the high-frequency experiments, with sampling at an offset of 0.8 MHz with respect to the transmit frequency. Figure 2a shows a 4 μm diameter Sonovue™ bubble before the transmit pulse (burst of 10 cycles; f = 3.5 MHz) was applied. The figures 2b-2d show that the microbubble had developed a mode n = 3 vibration along the interface. Figure 3 shows a small microbubble (diameter 1.4 μm) of the experimental agent BR14 (Bracco Inc.) which was insonified with a transmit pulse (burst of 40 cycles) at a frequency of 19 MHz. The recorded images show a mode n = 4 vibration, while a second experiment (bottom of Fig. 3) clearly shows a mode of order 5. For both free and encapsulated microbubbles, we observed surface wave oscillations with a periodicity at the half subharmonic of the transmit frequency. This is consistent with previous theoretical and experimental investigations of free millimeter sized bubbles.

The relevance of the observation of surface modes of ultrasound contrast agents may extend in several directions. First, the ability to initiate active surface modes may have implications for imaging, particularly of subharmonics, though at present this remains unexplored. Further investigations will examine the conditions under which the surface modes are generated, the potential for coupling between these modes and monopolar radiated energy, and whether surface waves may play a role in the generation of acoustically observable subharmonic energy. Second, for modeling purposes, surface modes may provide more insights into the shell properties of contrast agents, leading to a better description of shell elasticity and friction. In addition, none of the current theoretical models for encapsulated microbubbles incorporate surface modes. Third, as known from the literature, surface modes can give rise to intense microstreaming very close to the bubble which may conceivably be exploited for local drug delivery in cell permeability studies [4]. Finally, as the surface vibrations are directly coupled to the fragmentation of the bubble (in fact the mode number is directly related to the number of fragments formed) these interesting observations of surface mode vibrations may lead to a better understanding of contrast agent break up and destruction.

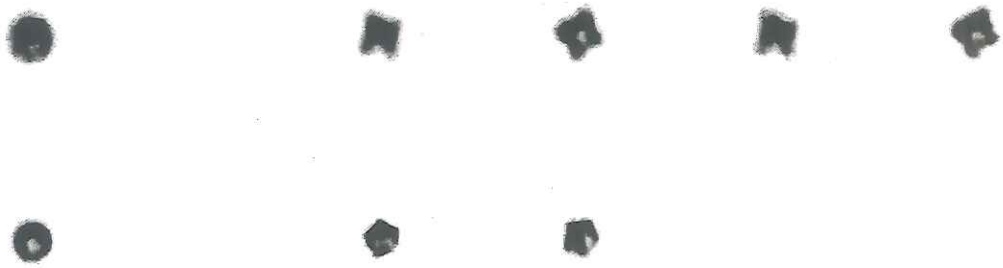

Figure 3. Mode n = 4 (top) and mode n = 5 (bottom) vibrations for small microbubbles of 1.4 μm diameter. The transmit frequency is 19 MHz. The images were recorded using a strobe technique on the Brandaris camera.

References

[1] Leighton T.G., Chapter 3, "The acoustic bubble", Academic Press, 1994.

[2] Palanchon P, Bouakaz A, Klein J, et al. "Subharmonic and ultraharmonic emissions for emboli detection and characterization", Ultrasound Med. Biol., 29, 417-425 2003.

[3] Chin CT, Lancee C, Borsboom J, et al. "Brandaris 128: A digital 25 million frames per second camera with 128 highly sensitive frames", Rev. Sci. Instrum., 74, 5026-5034, 2003.

[4] Marmottant, Ph. & Hilgenfeldt, S., "Controlled vesicle deformation and lysis by single oscillating bubbles", Nature, 423, 153-156 (May 8th 2003).

A NEW FORMALISM FOR THE DESTRUCTION-REPLENISHMENT PERFUSION ASSESSMENT TECHNIQUE BASED ON PHYSICAL CONSIDERATIONS

Marcel Arditi, Peter Frinking, Xiang Zhou, Nicolas Rognin, Tristan Messager

Bracco Research SA – Geneva / Switzerland

Since the introduction of the concept of the destruction-replenishment method by Kevin Wei *et al.*[1] in 1998, a number of pioneer investigators in contrast ultrasound have explored and demonstrated the potential of this elegant perfusion-quantification approach. The generally accepted method for the analysis of the replenishment signal recorded over time consists of fitting a so-called mono-exponential parametric function through the video echo-signal amplitude curve. By observing a correspondence between the parameters of this function and physiological perfusion parameters, such as blood flow velocity and blood volume, investigators found it a promising method for distinguishing healthy tissue from hypo-perfused areas, especially in the myocardium.

In the following years, the advent of sensitive contrast-specific detection methods, developed by equipment manufacturers, allowed lowering the driving ultrasound pulse pressures down to levels where the destruction of ultrasound contrast agent (UCA) microbubbles became minimal to negligible. This progress enabled "real-time" monitoring of the UCA during the replenishment phase after the destruction of the UCA by a short sequence of flash frames, transmitted at high a mechanical index (MI). It basically made the approach easier to implement in the clinical-research environment, compared to the destructive, intermittent-imaging method initially described by Wei *et al*[1]. However, since the method is based on the video echo-signal amplitude, and due to the assumptions made, it is system- and user-dependent and lacks a real physical foundation for a true quantitative analysis.

In this work, the destruction-replenishment method has been analysed from fundamental physical principles determining the imaging process during the UCA replenishment phase. Based on both transmit and receive diffraction characteristics of the imaging probe, it is shown how a simple closed-form parametric expression, different from the mono-exponential type, can be used for describing tissue perfusion characteristics. Using this approach, which is based on an analysis of echo-power or linearized video signals, estimates of perfusion are made independently of instrument settings, e.g. gain, log-compression, etc. (Figure 1).

1 Wei, K., Jayaweera, A. R., Firoozan, S., Linka, A., Skyhu, D. M., and Kaul, S., Quantification of Myocardial Blood Flow With Ultrasound-Induced Destruction of Microbubbles Administered as a Constant Venous Infusion, Circulation, vol. 97 1998.

Additionally, as a consequence of the physical foundation of the method, an analysis of the shape of the replenishment curve allows estimating parameters of lognormally distributed flow velocities. This may provide information about the organization of the microvascular network within the tissue under investigation, which is of importance for the characterisation of neovascular tissue in cancer and ischemic heart disease[2].

The concepts have been validated with *in-vitro* data, and are presently under investigation in the *in-vivo* context. Prospects will be presented for a truly quantitative perfusion assessment method using UCA such as SonoVue™.

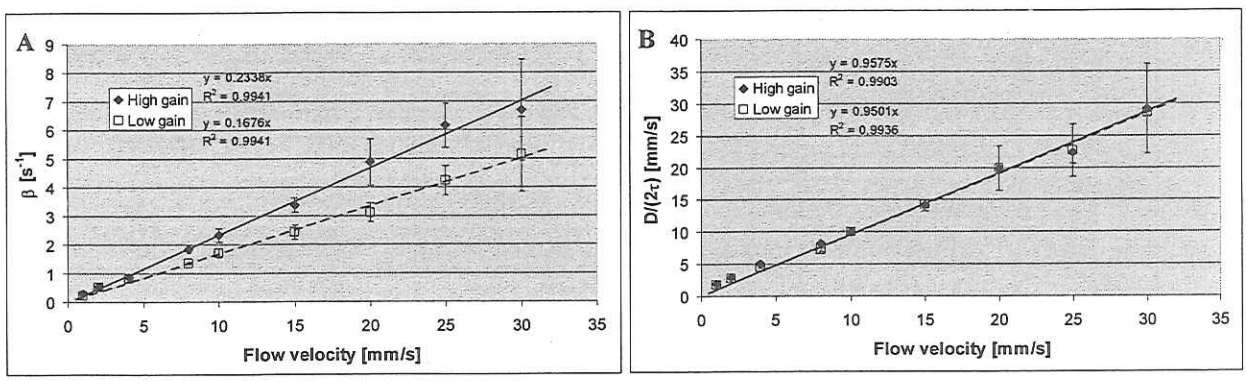

Figure 1. **Quantification results for different flow velocities obtained form *in vitro* experiments analyzed with the traditional mono-exponential function (A) and with the new method (B). The new method clearly shows the potential for true quantification because of its independency on gain settings.**

2 Kharchakdjian, R., Burns, P. N., and Henkelman, M. Fractal Modeling of Microbubble Destruction-Reperfusion in Unresolved Vessels. IEEE Ultrasonics Symposium, 2001.

NEW ULTRASOUND CONTRAST AGENT MODELS

J. Allen, Y. Kaneko, S. Yoshizawa, Y. Matsumoto

Dept. of Mechanical Engineering - University of Tokyo

The theory and experiments in the contrast agent field have not evolved in a simultaneous manner, as is the case with most interdisciplinary scientific disciplines. Initial models were developed with the agent Albunex™ in mind and have been subsequently generalized for newer agents due to the lack of better formulations. Currently, a wide variety of constructions and materials are being used for the contrast agent's shell. While current contrast agent models have provided some understanding and insight, many outstanding issues remain. Newer polymer shelled agents such as those developed by Point Biomedical and Acusphere have been introduced. Specific models for these types of agents are needed for their construction to be optimized for applications such as imaging, perfusion measurements and drug delivery. Likewise, the role of the shell in the destruction process is still not well understood. More theoretical investigation of contrast agent destruction is needed in order to assess the potential risk of bioeffects. Furthermore, evolving therapeutic applications, which include drug and gene delivery, are providing new directions and challenges for both the theory and modeling. These issues are discussed with respect to contrast agent models which rigorously take into account the large deformation of the shell, convective gas diffusion, and internal heating and phase transitions of the interior gas. The overall improvements and the remaining limitations of the new formulations are highlighted.

WILL COMBINATIONS OF MULTIPLE AGENTS PRODUCE MORE ROBUST CONTRAST IMAGING?
AN IN VITRO STUDY AND IN VIVO STUDIES IN DOGS

Xiaokui Li, Hui Jiang, Diane Paine, Zuhua Mao, Aarti Hejmadi Bhat, , Patrick von Behren, David Gustafson, Jonathan R. Lindner, Alexander L. Klibanov, David J. Sahn

Oregon Health & Science University, Portland, OR, University of Virginia Medical Center, Charlottesville, VA, Siemens Ultrasound, Issaquah Wa

Background: Very high-speed microscopic optical imaging of contrast microbubbles oscillating in an ultrasound field suggests complex bubble interactions. We tested whether mixtures of contrast agents could enhance myocardial perfusion imaging.

Methods: Four contrast agents [Sonovue (S), Definity (D), Optison (O) and MP 1950 (M) a decafluorobutane gas core and a lipid with PEG shell for improved longevity] were injected separately and in 2 triple-agent combinations in a flow phantom and in 6 closed chest dogs. Bolus injection of either S, D, O, or M was given at full dose, 1/3 dose of each agent for 2 mixtures of D + O + S or D + S + M were administered. We used a Siemens Antares^{TM} ultrasound system with a 3 MHz curved probe receiving at harmonic plus subharmonic frequencies for real time perfusion at 0.1 to 0.4 MI imaging with high MI burst every 40 sec.

Results: There were significant differences in vivo of peak temporal video intensity for triple-agent mixtures and the pooled mean of each single agent in LV cavity (222.80 ± 1.54 vs 203.45 ± 16.28, p = 0.003) and in myocardium (lateral wall) (136.28 ± 16.96 vs111.18 ± 14.83, p = 0.003). Perfusion was no longer well seen >1.5 minutes (p > 0.005) for the single agents, except for M which persisted >2.5 minutes; for both mixtures signals lasted 3-6 minutes (p > 0.05). The D + S + M mixture was most robust for time and intensity. In the water phantom study, the 2 combinations had higher signal strength and longevity than any single gent at full dose.

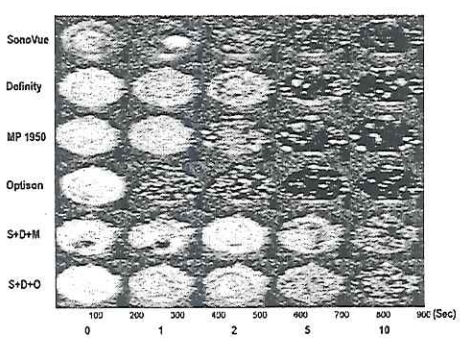

HIGH FREQUENCY CONTRAST AGENT IMAGING

Jim Chomas and Patrick Phillips

Siemens Ultrasound 1230 Shorebird Way, Mountain View, CA 94043

Introduction: Contrast Agent imaging is being adopted clinically as a tool to visualize perfusion kinetics in a range of applications from cardiology to radiology to scientific research on small animals. High frequency ultrasound imaging (i.e. up to 15MHz) offers spatial resolution on the order of several hundred microns which may be applied to areas such as the human breast, thyroid, testicle, or vascular structures like the carotid. The emerging field of small animal imaging for use in genomics, pharmaceutical, or other research studies can also benefit from improved resolution at high frequencies.

High frequency CPS:

Nonlinear signals created by contrast agents when they are insonified are the basis of many contrast agent imaging methods. Cadence™ CPS (Contrast Pulse Sequencing) utilizes nonlinear fundamental signals, which are generated by contrast agents in the fundamental frequency band. The unique aspect of detecting nonlinear fundamental signals is insignificant nonlinear fundamental signals exist in tissue, yielding high specificity to contrast agents compared to tissue. Furthermore, the detected nonlinear fundamental signals are centered on the same frequencies with similar bandwidth as the transmitted signals. This property is important with high frequency imaging where the relative bandwidth of transducers are limited and the effects of elevation diffraction and attenuation reduce sensitivity at higher frequencies.

In developing a high frequency contrast imaging method, both second harmonic imaging (HI) and nonlinear fundamental (NLFI) imaging were investigated. The specificity of HI was more limited than NLFI primarily because 2^{nd} harmonic energy is generated by tissue even with low MI imaging and second harmonic signals suffer more attenuation than fundamental signals. In fact, the relative amount of tissue 2^{nd} harmonic energy compared to tissue fundamental energy increases with increasing center frequency, making the specificity of HI worse at high frequencies than at low frequencies at a fixed depth [1].

Nonlinear fundamental imaging provides useful information over a wide range of applications for a single high frequency transducer. For human breast imaging, penetration is critical and therefore a design that adopts the lowest frequency edge of the transducer will be preferred [Figure 1a].

On the other hand, for small animal imaging, penetration is less demanding and broader band, higher frequency signals are preferred in order to achieve the fine spatial resolution required for visualizing mouse heart perfusion or for quantifying mouse tumor microvascular enhancement [Figure 1b].

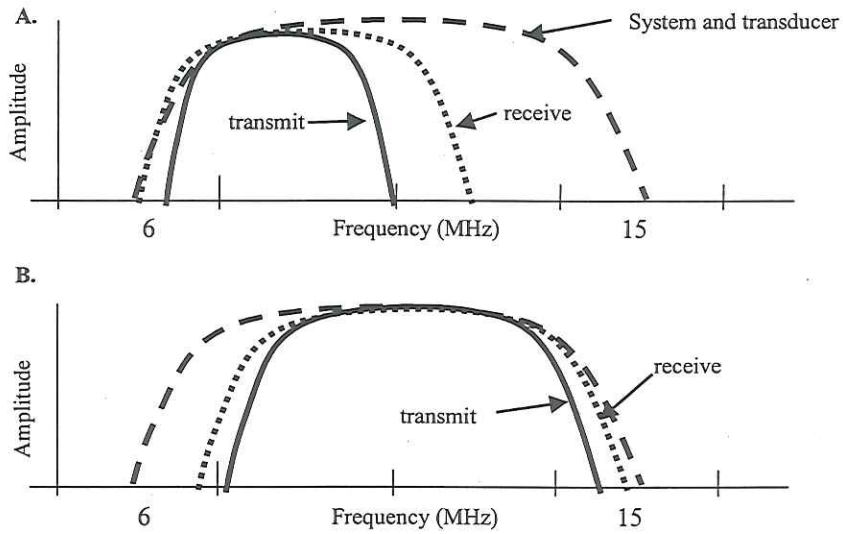

Figure 1. Nonlinear Fundamental Imaging frequency designs for high frequency contrast imaging on the 15L8 transducer. The dashed line represents the bandwidth of the transducer and system, the solid line represents transmit bandwidth, and the dotted line represents receive bandwidth. A. High sensitivity design to achieve maximum penetration. B. High bandwidth design, which exploits the maximum bandwidth of the transducer, to achieve maximum resolution.

Convergent CPS:

With highly sensitive contrast imaging modes, it has become increasingly difficult to discriminate between perfused tissue and larger feeder vessels after contrast agent has perfused the entire organ. An example of this phenomenon is seen during imaging of the liver, where it is difficult to distinguish the hepatic vein from fully perfused parenchyma in a low MI contrast exam. Convergent™ CPS was designed to address this problem by transmitting a sequence of pulses where sub-sequences are processed in parallel – with one sub-sequence used to determine the contrast agent perfusion signal, and a second sub-sequence is used to determine the energy signal from moving blood. The method is a convergence of the CPS technology with traditional Color Doppler Energy (CDE) imaging [Figure 2].

Convergent™ CPS is useful in detecting lesions within highly perfused organs by highlighting the feeder vessels to the lesion. The method gives the user control of both CPS-specific imaging parameters as well as CDE-specific imaging parameters.

The CDE scale key allows the user to observe signals from different vessel sizes (or flow rates) of interest, with high scale settings displaying only the largest vessels and low scale settings displaying smaller vessels.

Conclusion

Contrast agent imaging using Cadence™ CPS works well for high frequency applications such as small parts or small animal imaging. The advantages of CPS over second harmonic imaging are the superior agent-to-tissue specificity and the ability to use the entire bandwidth of the transducer on transmit *and* receive. For the best penetration, the transmit and receive signals are designed utilizing the lower edge of the transducer and system bandwidth which minimizes frequency dependent attenuation and drives the contrast agent bubble more effectively than higher frequencies. For small animal imaging, where penetration is less of a problem, a very wideband transmit and receive approach is taken, providing spatial resolution on the order of a few hundred microns.

A new mode is presented, called Convergent™ CPS, which merges the CPS technology with Doppler energy from motion and displays perfusion information as well as vascular morphology. This mode offers important vascular information that may otherwise be lost in a contrast exam after the organ of interest has become fully perfused.

[1] Hamilton, MF and Blackstock DT. Nonlinear Acoustics. Academic Press, San Diego, 1998, p. 239.

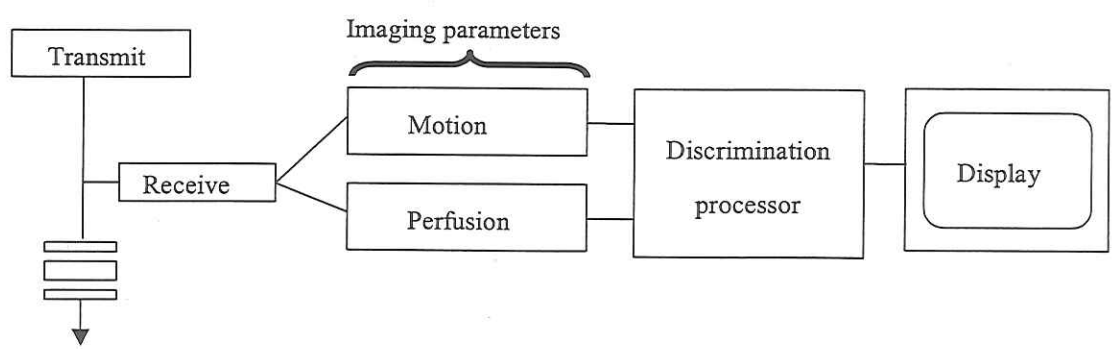

Figure 2. Schematic diagram of the Convergent CPS algorithm.

DO DIFFERENT FACTORS DETERMINE THE *IN VIVO AND IN VITRO* LONGEVITY OF PERFLUOROCARBON CONTRAST AGENTS?

Manabu Matsumura, Peter Bevan, Liis Lindvere, Raffi Karshafian, Fang-ming Wang, Hiroko Iijima and Peter N. Burns

Department of Medical Biophysics, University of Toronto, Sunnybrook & Women's College Health Science Centre, Toronto, ON, Canada

The concept of second generation of ultrasound contrast agents is to use low solubility (fluorinated) gas to improve stability in the blood stream. In contrast to non-ionic X-ray and Gd-chelate MR contrast agents, large differences in the *in vivo* longevity of blood pool enhancement are seen with various microbubble agents. In particular, the length of time that a suspension of the agent is effective *in vitro* does not necessarily predict the longevity of enhancement *in vivo*. In this study, we measure the longevity of contrast enhancement both *in vitro* and *in vivo* with several second-generation agents and investigate one origin of the observed discrepancies.

Methods

In Vitro: Scattering properties of the perfluorocarbon agents Definity (BMS), Optison and Sonazoid (Amersham), were measured by means of a two transducer, orthogonal scattering cell placed in a water tank. Agents were diluted to an approximately physiological concentration with deionized water exposed to the room air overnight prior to the experiment. The diluted agents were allowed to flow in the flow-cell in which was positioned the intersecting focal regions of a transmitting (2 MHz, Gaussian envelope) and receiving (centre frequency 3.5 MHz) transducer. The power of the scattered signal was measured with time after the dilution and at various incident ultrasound pressures. Signal intensity was calculated from the frequency spectrum of the scattered echoes by integrated power over a fixed range of frequencies.

In Vivo: Rabbits were anesthetized with intravenous ketamine/xylazine and allowed to breath room air. Doppler signals from the femoral artery were acquired transcutaneously using a 5MHz pulsed system with MI<0.01, so that no significant bubble disruption was induced by the measurement. Contrast agents were injected into an ear vein by bolus, and digitised quadrature Doppler signals analyzed for integrated power on-line and stored. In addition, the liver was scanned at MI<0.05 using pulse inversion imaging (L7-4 transducer, ATL Philips HDI 5000 and Q-Lab, Bothell WA), acquiring images from the main portal and hepatic veins. Following multiple bolus injections, regions of interest were positioned in these vessels and tracked during the wash-in and wash-out of the agents. Integrated power was estimated over the ROI using Q-Lab software.

Results

In Vitro: Scattering power gradually decreased with time for all agents. The time-to-half-maximum for Optison was about 20 minutes; for Definity about 60 minutes. No detectable change was observed in the Sonazoid echo after one hour. With Definity and Optison, the scattering signal increased with increasing incident ultrasound pressure. Sonazoid produced less scatter than the other agents at low incident pressure (MI < 0.1), but produced larger scattering signals at higher pressures (MI ~ 0.3-0.7). Power spectral measurements showed that the low MI harmonic-to-fundamental ratio was higher with Optison than Definity. Disruption was observed as a decrease in scatter following multiple high MI pulses in all agents. The disruption threshold was highest and the subsequent loss of signal lowest for Sonazoid.

In Vivo: The Doppler signal from the femoral artery immediately increased after bolus injection of each contrast agent, then decreased with time with an approximately monoexponential characteristic. The decay of the signal *in vivo* was more rapid than that seen *in vivo*, with approximate times-to-half-maximum-power of 2.5 minutes for Optison and Sonazoid and 6 minutes for Definity. Comparison of the portal and hepatic venous enhancement in the animals revealed substantial reduction in hepatic venous power for Optison – suggesting uptake by the liver - but almost no detectable difference for Definity.

Discussion

These experiments show that in spite of substantial variation in the longevity of contrast effect *in vitro*, all the perfluorocarbon gas agents tested showed enhancement for a comparable period of time *in vivo*. The exception was Definity, which in all experiments showed the longest duration *in vivo*. This was also the only agent which showed no significant liver uptake in the rabbit.

For these agents at least, different processes appear to determine the *in vitro* stability and the *in vivo* duration of enhancement. Given the similarity of the physical properties of the gases used in these agents, it seems reasonable to speculate that their stability *in vitro* is at least partly determined by their shell properties. The fact that Sonazoid, which displayed the most stable acoustic behaviour *in vitro*, was also the agent with the highest threshold for disruption and gave the lowest low-MI scattered echo *in vitro*, suggests that its shell may be stiffer than those of the other agents.

In vivo, however, organ uptake of the microbubbles during their systemic circulation influences their clearance rate. Sonazoid has been demonstrated to be captured by Kupffer cells in the liver (1) and shown to last longer in the blood stream when Kupffer cells were artificially depleted in rats (2). The albumin shell used in Albunex (similar to Optison) is known to accumulate in Kupffer cells and macrophages in the spleen (3). From this perspective, entrapment of the microbubbles by reticuloendothelial sytem (RES) seemed to have more significant influence on longevity than gas

diffusion from the microbubbles or exhalation via the lung. In contrast, one of the lipids used in Definity has a polyethyleneglycol (PEG) chain, a lipid well known to have "stealth" effect in RES system (4), suggesting an explanation for the longer duration of Definity in the blood stream. Thus, the RES is suggested to play an important role on clearance of the microbubbles from the blood stream. Does this uptake correlate to the appearance of postvascular enhancement in the liver? Whereas Sonazoid is known to exhibit a strong postvascular phase in the liver, Optison, SonoVue and Definity do not. However, the results of the imaging analysis show that Optison were substantially depleted by the liver, with a strong reduction in echo level from the portal to hepatic veins. Definity showed no such reduction. One explanation of the absence of a detectable postvascular phase with Optison is that the protein in the shell is degraded rapidly after the bubble's uptake by the Kupffer cells, whereas the lipid of the Sonazoid shell is not.

We therefore conclude:

1. ***In vitro*** stability of perfluorocarbon agents is correlated with their disruption threshold and may therefore be determined by shell composition, with more stiff shells providing greater stability.
2. ***In vivo*** duration of enhancement is affected significantly by microbubble interaction with the RES.
3. Optison and Sonazoid are more strongly cleared by the RES than Definity, and this accounts for Definity's greater duration of enhancement in this animal model.
4. Contrary to popular belief, the presence or absence of a detectable postvascular phase on contrast liver imaging does not predict whether there is RES uptake of an agent.

References

1. Watanabe R. et al. Behavior of US contrast agent in rat liver microcirculation. Ultrasound Med. Biol. 2003;29:S109
2. Watanabe R. et al. Contribution of Kupffer Cells on Liver Parenchymal Enhancement with Microbubble-based US Contrast Agent. RSNA 2001
3. Walday P. et al. Biodistribution of air-filled albumin microspheres in rat and pigs. Biochem J. 1994;299:437-443
4. Senior J. et al. Influence of surface hydrophilicity of liposomes on their interaction with plasma protein and clearance from the circulation: studies with poly(ethylene glycol)-coated vesicles. Biochim. Biophys. Acta. 1991;1062:77-82

DEVELOPMENT OF NOVEL MICROBUBBLES FOR TARGETED IMAGING AND THERAPY

Charles A. Sennoga†, Rebecca C. Campbell†, Robert J. Eckersley†, Stefanos Theoharis†[¶], Jennelle Francis‡, Yaohe Wang‡, Oliver Florey[§], James Yeh†, David O. Cosgrove†, Dorian O. Haskard[§], John M. Seddon*, Nicholas R. Lemoine‡, Andrew J. T. George[¶] and Martin J. Blomley†*

†Imaging Sciences Department; [¶]Department of Immunology; [§]British Heart Foundation Cardiovascular Medicine Unit; and ‡Cancer Research UK, Molecular Oncology Unit, Imperial College School of Medicine, Hammersmith Hospital Campus, London, UK; *Department of Chemistry, Imperial College, South Kensington Campus, London, UK

Targeting of ultrasound microbubble contrast agents to endothelial adhesion molecules could provide early diagnostic insights into various disorders. Microbubble ultrasound (i.e., ultrasound in the presence of microbubbles) shows promise as a method of improving the efficiency of site-specific gene therapy. The utilization of microbubbles, both in targeted imaging and/or therapy, necessitates the construction of microbubbles with targeted specificity. We have developed a number of strategies to complex antibodies and other moieties including viruses to microbubbles. As part of this development procedure, we have also evaluated the effect of these additions on the acoustic properties and stability of microbubbles.

In work aimed at targeted microbubbles for imaging of inflammation we have designed a series of microbubbles bearing a mouse anti-human monoclonal antibody (1.2B6) against E-selectin. Both direct incorporation and covalent approaches for coupling of 1.2B6 to microbubble contrast agents have been developed. Using Chinese Hamster Ovary cells expressing E-selectin (CHO-E) as the antigen, we have characterised the binding affinities of our microbubbles in static flow conditions. Binding assays showed significantly higher immunoreactivity with microbubbles bearing 1.2B6 (37.0 ± 4.0%) as compared with microbubbles bearing an antibody with the non-specific immunoglobulin, MOPC-21 (10.9 ± 6.4%) and, naked microbubbles without antibodies (3.1 ± 3.0%). While both albumin and phospholipid based microbubbles show similar trends, we found that there was greater control of the antibody population and targetability when phospholipid microbubbles were used. In all cases, naked microbubbles and those bearing the non-specific mouse IgG_1, MOPC-21, show insignificant binding to CHO and CHO-E cells. In contrast, a high level of binding was observed following incubation of either albumin or phospholipid microbubbles bearing 1.2B6 with CHO-E cells. We are currently investigating the capacity of targeting inflammation in an *ex vivo* model following activation in human saphenous veins.

In additional work in progress, we have investigated the capacity of conjugating adenoviruses, which show value in gene therapy, to microbubbles. We complexed adenoviruses labelled with an intercalating agent (YOYO-1) to albumin perflurocarbon microbubbles produced in our laboratories.

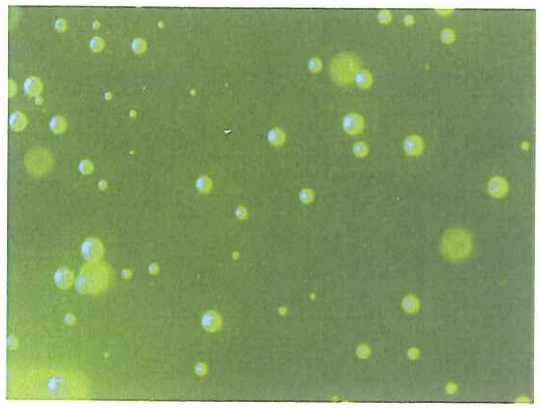

Figure shows albumin microbubbles at 200× magnification following complexation with adenoviral particles labelled with an intercalating agent (YOYO-1).

These show good adhesion of viral particles to albumin microbubble coat, even after repeated washing. In further work we are investigating the potential of our novel, virally loaded microbubbles to improve transfection efficiency. Preliminary work using Ad5-GFP virus (wildtype adenovirus expressing the green fluorescent protein from the Cytomegalovirus promoter) has shown encouraging results for the viral infectivity of microbubbles loaded with Ad5-GFP when tested on the A549 cell-line.

CHARACTERIZATION OF SIGNAL GENERATION FROM TARGETED MICROBUBBLES

James SM Yeh,[1] Jiri Sklenar,[2] Alexander L. Klibanov,[2] Christopher Lewis,[2] Joshua J Rychak,[2] Martin Blomley,[1] Robert Eckersley,[1] Jonathan R. Lindner.[2]

1. National Heart and Lung Institute and Department of Imaging Sciences, Faculty of Medicine, Imperial College of Science Technology and Medicine, Hammersmith Hospital, Du Cane Road, London, UK. 2. University of Virginia Medical Center, Charlottesville, Virginia, USA.

Targeted ultrasound contrast agents have recently been developed that are retained within tissue due to their adhesion to antigens expressed selectively within diseased tissue. Microbubbles bearing ligands for endothelial cell adhesion molecules have been used to image inflammatory processes and angiogenesis with contrast-enhanced ultrasound. Thus far, imaging of these pathophysiologic processes has been performed by detection of retention of microbubbles within the microcirculation in an organ of interest. There have been recent efforts to use microbubbles targeted to endothelial cell adhesion molecules to assess inflammation in large vessels in order to detect the presence of unstable or high-risk atherosclerotic phenotype. In order to assess the degree of vascular inflammation with this strategy, it must be possible to discriminate the extent of microbubble retention. The purpose of this study was to determine whether microbubble density on a relatively planar surface can be determined with state-of-the-art ultrasound imaging technology.

Lipid microbubbles containing decafluorobutane gas and bearing biotin at the end of a molecular tether were placed on polystyrene plates containing streptavidin, then washed. The density of microbubbles, assessed by light microscopy, was varied by changing microbubble concentration during their placement. Attached microbubbles were imaged using intermittement pulse-inversion imaging at a frequency of 3.5 MHz and a mechanical index (MI) of either 0.2 or 0.9 at a ~45 degree incident angle and fixed constant distance. Significant contrast enhancement over background on the first acoustic pulse could be detected for microbubbles at a concentration of approximately 5 mm^{-2} for both high- and low-power imaging. Signal intensity from attached microbubbles increased in proportion to their concentration until a concentration of approximately 300 mm^{-2} was reached, above which signal intensity remained unchanged but less than saturation level. For any concentration in this range, the signal from low-power imaging was approximately half that of high-power imaging. To further examine the mechanism for the flattening of the microbubble concentration vs. intensity curve, the rate of microbubble destruction with sequential pulses was determined by videocaliper measurements of microbubble diameter. At medium to high microbubble density, the rate of microbubble destruction at the high acoustic power was substantially reduced regardless of microbubble size, indicating local attenuation of the acoustic pressure. At lower acoustic pressures, the

rate of microbubble volume decay with sequential pulses was also inversely related to microbubble density but only for microbubbles with a small to medium diameter (<5 □m).

These data suggest that, for the purposes of imaging targeted microbubbles on planar surfaces such as large vessels, high-power pulse-inversion imaging provides greater discrimination between different degrees of retention, but is not more sensitive in terms of detecting low concentrations of microbubbles. At medium to high concentrations of microbubbles (beginning at approximately 0.5-1% surface coverage), acoustic attenuation can result in a limited upper dynamic range or signal enhancement, despite imaging single layers of microbubbles at a relatively steep incident angle.

THE ABILITY OF A DOBUTAMINE STRESS CONTRAST ENHANCED ECHOCARDIOGRAM TO IMPROVE THE DETECTION OF CORONARY ARTERY DISEASE RESULTS FROM THE *CADET* PILOT STUDY

Thomas R. Porter, Arthur J. Labovitz, Michael H. Picard, Bruno Cotter, Edward L. O'Leary, Harald Becher, Anna C. McGrain, Anthony N. DeMaria, Feng Xie

University of Nebraska Medical Center, Omaha, NE

Background. The Contrast Enhanced Dobutamine Echo Trial (CADET) is a prospective multi-center study designed to test the hypothesis that myocardial perfusion (MP) obtained with intravenous (IV) contrast and real time low mechanical index imaging (RTLMII) will improve test sensitivity when compared to wall motion (WM) analysis with or without contrast-enhanced border detection (CEBD).
Methods. This hypothesis was tested in 29 pilot patients presenting with chest pain and intermediate to high pre-test probability (mean age 57±11 years, 11 female). Patients with a previous myocardial infarction were excluded. Each patient underwent two dobutamine stress echo (DSE) studies: One with high mechanical index harmonic imaging to analyze WM without contrast, and one with RTLMII at frame rates >25 hertz and IV Optison to assess MP, and WM with CEBD. All patients underwent quantitative coronary angiography (QCA) within 96 hours of presentation. MP abnormalities were defined as a regional lack of myocardial opacification and assessed according to coronary artery territories (CAT). MP and WM during the DSE with contrast were examined at an intermediate stage (65-75% predicted heart rate), and again at peak stress (>85% predicted heart rate). All studies (with and without contrast) were read by two outside reviewers (R1 and R2) who were blinded to the results of QCA or clinical data. A coronary stenosis ≥70% was considered significant.
Results. Fourteen patients had no significant disease at QCA, 12 had one vessel, and three had multi-vessel disease. In the 15 patients with disease, 10 were detected by MP at peak stress, 8 were detected by WM with CEBD, and 6 were detected by WM without contrast. MP abnormalities in CAT supplied by >70% diameter stenosis were seen in an additional nine CAT by R1 and four CAT by R2 that were considered to have normal WM with or without CEBD. MP abnormalities were seen during the intermediate stage of the DSE in 9 of the 10 patients with disease at QCA and abnormal MP at peak stress.
Conclusions. These pilot data indicate that the addition of RTLMII following IV contrast during DSE improves test sensitivity because it detects MP abnormalities that occur in CAT with normal WM even with CEBD.

CONTRAST ENHANCED ECHOCARDIOGRAPHY IN PATIENTS WITH AN ABNORMAL ELECTROCARDIOGRAM

Dr O. Kamp

VU University Medical Center, Amsterdam

Two cases are described, in which the use of echocontrast resulted in the definite clinical diagnosis.

Case 1: Apical hypertrophic cardiomyopathy

Hypertrophic cardiomyopathy is a genetic cardiac disease in which a hypertrophied left ventricle, which is characterized by a wide variety of patterns of asymmetric wall thickening, is the morphologic hallmark. Distribution of hypertrophy is often diffuse, but may also be mild and localized. In particular, the apical form of hypertrophic cardiomyopathy, in which wall thickening is confined to the most distal portion of the left ventricular wall, is frequently underdiagnosed. Apical hypertrophic cardiomyopathy is expected when the striking electrocardiographic pattern of giant negative T waves are present. This case describes a patient with abnormal electrocardiogram but without abnormalities on the non-contrast enhanced two-dimensional echocardiogram. Using contrast, the echocardiographic study was conclusive for the diagnosis of apical hypertrophic cardiomyopathy.

Case 2: Anomalous apical insertion of a papillary muscle

Occurrence of structural mitral valve abnormalities due to anomalous insertion of the papillary muscle in e.g. hypertrophic cardiomyopathy and their significance in producing outflow obstruction (even in the absence of typical systolic anterior motion) has been described. However, we describe a case presenting with an abnormal electrocardiogram, whereby an anomalous apical insertion of the papillary muscle was found without left ventricular outflow obstruction using contrast-enhanced echocardiography.

A CASE OF HEART FAILURE

Petros Nihoyannopoulos, MD, FRCP

Hammersmith Hospital, NHLI, Imperial College London

London, UK

Hear failure requires precise diagnosis and assessment in order to plan the best therapeutic strategy. The vast majority (70%) of heart failure patients are secondary to coronary artery disease. while the next commonest is of dilated cardiomyopathy (20%). Treatment differs between the two diagnoses. While often the distinction is easy including history, ECG and echocardiography, frequently the two conditions are indistinguishable, particularly in the presence of left bundle branch block. This diagnostic difficulty will be highlighted by a case presentation where by contrast echocardiography will prove crucial in the differential diagnosis.

MRI PERFUSION VERSUS CONTRAST ECHO PERFUSION TO DETERMINE CONTRACTILE RESERVE AFTER PCI FOR ACUTE MYOCARDIAL INFARCTION

Folkert J. Ten Cate, MD

Eramus MC Rotterdam The Netherlands, Thoraxcentre, Department of Cardiology

MRI and contrast echo are both modalities to show function and perfusion of muscle. The case presented shows myocardial perfusion determined by MRI and contrast echo after PCI for acute myocardial infarction.

There is good agreement between both techniques for perfusion and function and for prediction of contractile recovery at follow up.

THE IDENTIFICATION OF NEOVASCULARIZATION IN HUMAN CAROTID ATHEROSCLEROTIC PLAQUE USING CONTRAST ENHANCED ULTRASOUND IMAGING AND HISTO-PATHOLOGIC VALIDATION: INITIAL OBSERVATIONS

Rachel Neems, Matt Feinstein, Marshall Goldin, John Dainauskas, Paul Espinoza, Mahala Johnson, Maria Daniels, Philip Liebson, James Macioch, and Steven B. Feinstein

Rush University Medical Center, Chicago, Illinois

Objectives: 1) To review contrast-enhanced ultrasound studies of human carotid arterial atherosclerosis and determine the incidence of neovascularization in plaque;

2) to correlate neovascularization observed in carotid plaque during non-invasive imaging to pathologic specimens obtained from carotid endarterectomy.

Background: Previous studies have demonstrated the existence of neovascularization in human atherosclerotic plaque and a far greater incidence of neovascularization from the adventitia relative to the lumen, and a correlation between plaque instability and carotid occlusive disease.

Methods: Patients were non-invasively imaged with an ATL HDI 5000 with a 7.4 MHz linear array probe using an intravenous ultrasound contrast agent (Optison^{Tm}). Twenty-one (21) carotid examinations were included in this review based upon the criteria that a >50% stenoisis was present in the carotid artery. In addition, 2 patients underwent surgical carotid endarectomies. Subsequently, the plaque specimens were analyzed for neovascularization by histology/pathology using Hematoxylin and Eosin staining.

Results: The review of 21 patients using contrast-enhanced ultrasound imaging revealed the visual presence of neovascularization in carotid arterial plaque in 20 patients. A visual grading system for the presence of neovascularization was applied (3=extensive, 1=minimal, and 2=moderate) . Of the 20 patients observed with plaque neovascularization, extensive neovasculature was observed in the plaque of 4 patients, moderate neovasculature was observed in the plaque of 5 patients, and minimal, sporadic vasculature was observed in the plaque of 11 patients. Of note, in the four patients with extensive neovascularization, 2 patients were known to not be on statins; whereas, in the limited neovascularization group, 5 of 8 with known treatment profiles were on statins.

Additionally, the mechanical index (MI) averaged the lowest value in the patients where extensive neovascularization was observed.

The histologic specimens of the 2 patients undergoing carotid endarterectomy revealed degrees of plaque neovascularization commensurate with the graded, non-invasive carotid ultrasound images.

Plaque neo-vascularization	patients	statin	no statin	unknown
Limited	11	5	3	3
Moderate	5	2	--	3
Extensive	4	1	2	1
None	1	--	--	--
Totals	21	8	5	7

Conclusion: This is the first report of direct, real-time, ultrasound contrast-enhanced visualization of the neovascularization contained within the human atherosclerotic carotid plaque. Of 21 patient carotid images, 20 revealed neovascularization (ranging from mild to extensive). Three patients subsequently underwent carotid endarectomy following the non-invasive imaging and the histologic review of the neovascular patterns was consistent with those observed at the time of the contrast-enhanced carotid ultrasound examination.

Figure A Patient P, patient with diabetes and not on statins. Note the marked neovascularization within the atherosclerotic plaque.

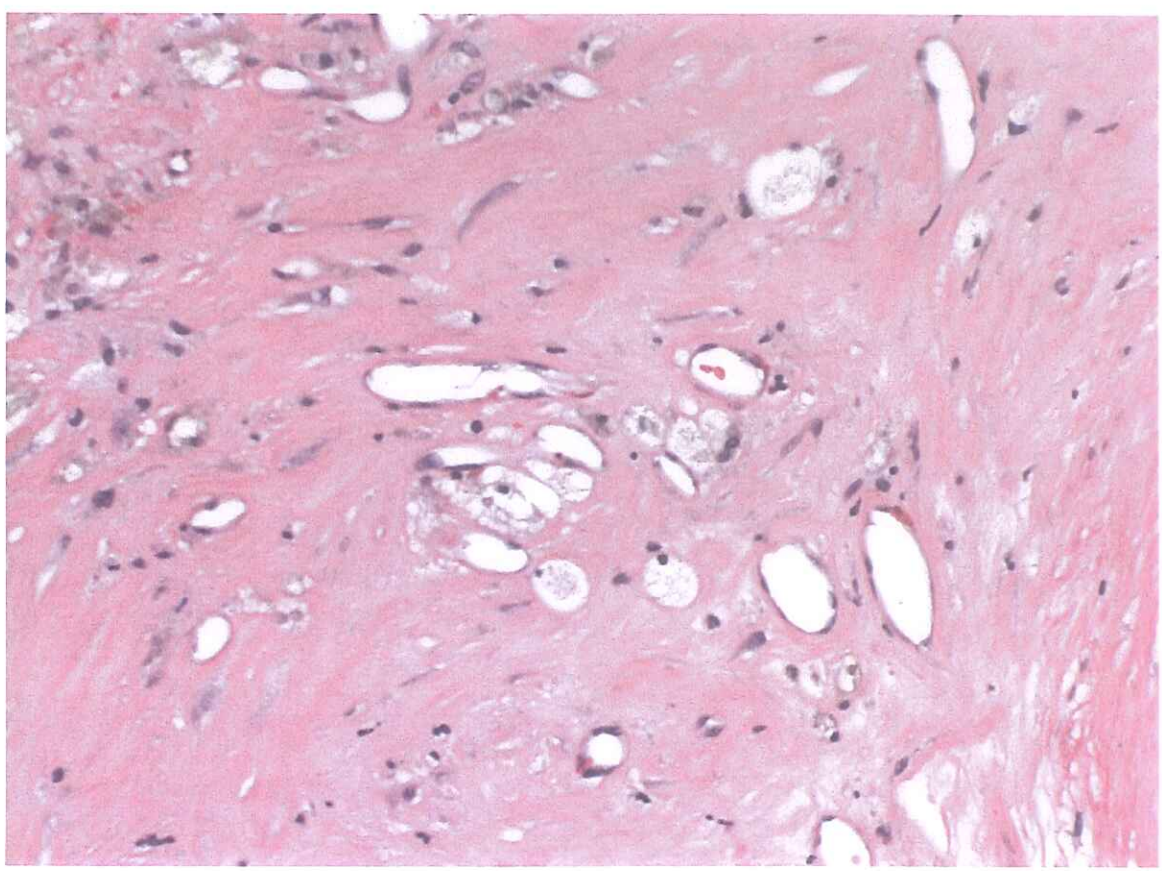

Figure B Patient G, statin usage for 3 years, no diabetes. Note the larger diameter of vessels. Also note the marked inflamatory cells.

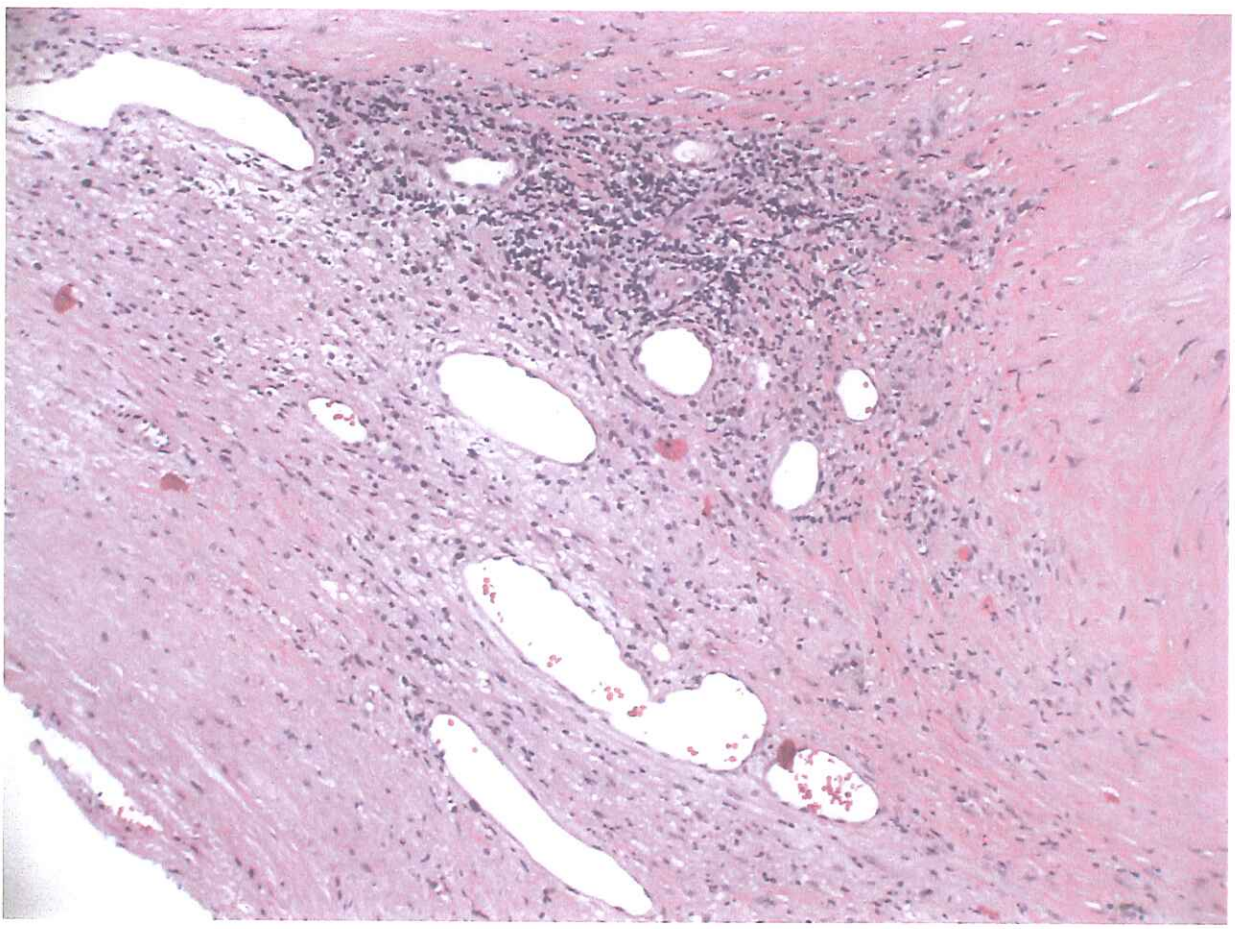

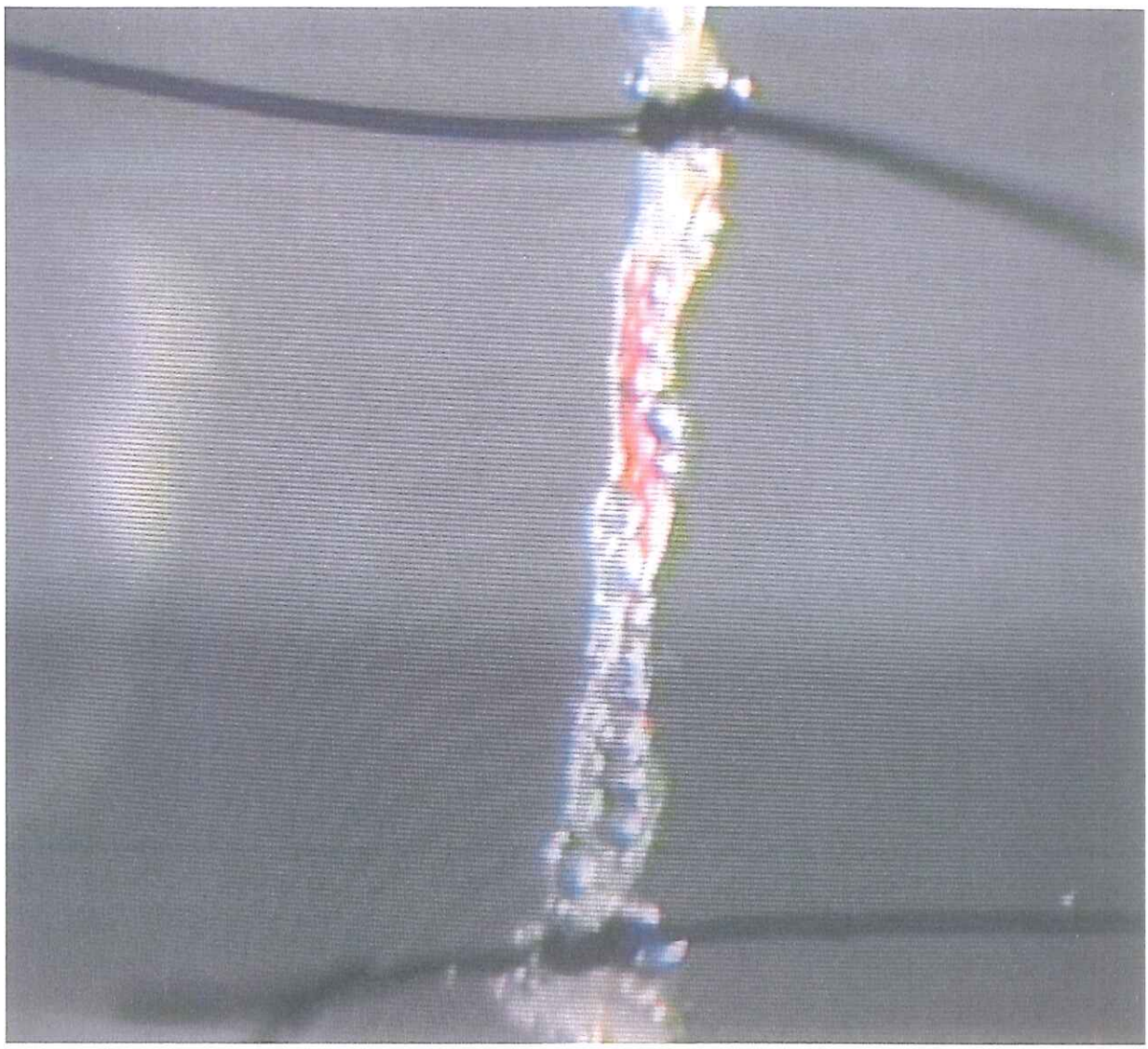

Thursday, January 22, 2004

Social Event
"Launching Solid Spheres"

Buffet and Bowling
at DOK '99
Straatweg 99
Rotterdam

Coaches will be leaving from the Inntel at 18:30 and will be back there around 22:30

The 9th ESUCI is sponsored by:

Bracco International
Mrs. M.C. Cedrini
Riva Caccia 1
6900 LUGANO
Switzerland

BMS-Medical Imaging
Mrs. Gail Ghiretti
331 Treble Cove Rd Bldg 600-2
North Billerica, Mass 01862
USA

Toshiba Medical Systems
Mrs. G. Mulders
Zilverstraat 1
2718 RP ZOETERMEER
The Netherlands

Oldelft B.V.
Ing. R. 't Hoen
Postbus 5082
2600 GB DELFT
The Netherlands

GE Medical Systems
Mr. Al Lojewski
4855 W. Electric Avenue
WI 53219-1628 Milwaukee
USA

Siemens Medical Solutions
Mrs. C. Marks
European Business Centre
126-135 Staines Road
HONSLOW, Middlesex TW3 3JF
UK

Philips Internationaal BV
Mr. F. Schuling
P.O. Box 10.000
5680 DA BEST
The Netherlands

Point Biomedical Corp.
Mrs. M. Kayan
887 L Industrial Road
SAN CARLOS, CA 94070
USA

SUGB
Prof.dr.ir. A.F.W. van der Steen
Thorax - Biomedical Engineering
ErasmusMC
P.O. Box 1738
3000 DR ROTTERDAM
The Netherlands

ICIN
Mrs. M. Helmers-Kersten
P.O. Box 19258
3501 DG UTRECHT
The Netherlands

FIRST ANNOUNCEMENT 2005

10th EUROPEAN SYMPOSIUM ON ULTRASOUND CONTRAST IMAGING 20-21 JANUARY 2005, ROTTERDAM, THE NETHERLANDS

Course Directors: Folkert ten Cate
Nico de Jong
David Cosgrove (Hammersmith – London)

Information on the 10th EUROPEAN SYMPOSIUM ON ULTRASOUND CONTRAST IMAGING: Mrs. Mieke Pruijsten
m.pruijsten@erasmusmc.nl

Erasmus MC
Universitair Medisch Centrum Rotterdam